

MASTER THESIS

**Multi-Band Side-Jump Scattering Contribution to
Anomalous Hall Conductivity from *Ab Initio***

Implementation and Application

From: Jürgen Weischenberg

Supervisor: Prof. Stefan Blügel,
Prof. Yuriy Mokrousov

Aachen and Jülich, November 17, 2011

Contents

Abstract	1
1 Introduction	3
1.1 What is the anomalous Hall effect?	3
1.2 AHE: More than 130 years of research	5
1.3 Analyzing the AHE into its parts	7
1.3.1 Skew scattering	7
1.3.2 Intrinsic contribution	8
1.3.3 Side jump contribution	9
1.4 Experimental studies on the AHE	9
1.4.1 Scaling relations	10
1.4.2 Crossover between AHE mechanisms	10
1.4.3 Sign of AHE	12
1.5 <i>Ab initio</i> computation of the AHE	12
1.5.1 Conventional approach: KKR and CPA	13
1.5.2 Novel approach: Universal side-jump contribution	14
1.6 Outline	14
2 Theory of the AHE	17
2.1 Definition of terms	17
2.1.1 Operators in real and reciprocal space	19
2.1.2 Equilibrium Hamiltonian	21
2.2 Linear response theory	22
2.2.1 Kubo formula for the conductivity	24
2.3 Correlation functions	26
2.3.1 Diagrammatic technique	30
2.3.2 Green's functions	32
2.4 Impurity averaging	33
2.4.1 Self-energy for Gaussian disorder	34
2.5 Kubo-Středa formula	35
2.5.1 Weak disorder limit	39
2.5.2 Eigenstate representation	40
2.5.3 Derivation of intrinsic contribution	41
2.5.4 Derivation of side jump contribution	43
2.5.5 Vertex corrections	45
3 <i>Ab initio</i> methods	49
3.1 Density functional theory	49
3.1.1 Kohn-Sham equations	49
3.1.2 Plane-wave basis set	52

3.1.3	FLAPW method	53
3.2	Basis sets	54
3.2.1	Bloch funtions	54
3.2.2	Wannier functions	55
4	Implementation	59
4.1	Required quantities	59
4.2	Wannier interpolation scheme	60
4.2.1	Interpolation of Hamiltonian	61
4.2.2	Interpolation of velocity	62
4.3	Adaptive broadening	62
5	Application and results	65
5.1	Iron and Cobalt	65
5.2	Ferromagnetic alloys FePd and FePt	66
5.3	Nickel	67
5.3.1	GGA+U/LDA+U approach	68
5.4	Fermi surface properties	70
5.4.1	Exchange splitting	71
5.4.2	Energy dependence	72
5.4.3	Band resolved conductivity	73
6	Conclusions	77
A	Appendix: Lattices	79
A.1	Internal coordinates	79
A.2	Brillouin Zones	79
	Bibliography	81

Abstract

This work describes the implementation of a method within density functional theory that allows to calculate the side-jump contribution to the transverse conductivity of the anomalous Hall effect from *ab initio*. Besides the Gaussian disorder model no additional assumptions are made.

The anomalous Hall effect is a very complicated phenomenon and no predictive theory that accounts for all its contributions exists so far. Until now, previous calculations of the anomalous Hall conductivity have mainly concentrated on the intrinsic contribution. The calculation of other contributions to the conductivity such as the side-jump contribution is very challenging, since no information about the impurity content and disorder type in the material considered is available from the outset.

In the present work it is explained that for a model of Gaussian disorder the side-jump contribution does neither depend on the impurity concentration nor the scattering strength and can be calculated directly from the electronic structure of the pure crystal alone. It is then described how the obtained quantities can be efficiently computed by employing the Wannier-interpolation scheme.

The procedure developed in this work is applied to a wide range of ferromagnetic materials such as elemental bcc Fe, hcp Co, fcc Ni, and L1₀ FePd and FePt alloys. It turns out that the inclusion of the side-jump contribution significantly improves upon the theoretical prediction of the anomalous Hall effect in these materials. Furthermore, it is illustrated that the side-jump contribution shows a strong anisotropy with respect to magnetization direction. The topological properties of the side-jump contribution in contrast to that of the intrinsic contribution are examined as well.

Introduction

At the beginning of this work it shall be explained in a few words what the anomalous Hall effect is and why it is such an interesting topic at all. We start with describing the empirical observations which are meant by the term "anomalous" and give a short overview of how the understanding of the anomalous Hall effect has evolved over time. Then we review the current state of the art of the field: We show what others have done, both experimentally and theoretically, and explain what the intended contributions of this work are, namely to derive a theory for the anomalous Hall effect which is in better agreement to the observed results than the existing one.

1.1 What is the anomalous Hall effect?

From now on, we will refer to the anomalous Hall effect as AHE for brevity. The discovery of the AHE by E. Hall in 1881 may be regarded as one of the earliest experiments in solid state physics and was a breakthrough at that time [1]. Fig. (1.1) shows a schematic experimental setup for measuring the AHE. The specimen is a ferromagnetic material to which some voltage is applied in the presence of an external magnetic field H_z . Due to the magnetic field the sample will be magnetized; we denote its magnetization by M_z . The applied voltage is associated with a current I_x and an electric field E_x . However, there also exists a transverse current j_y which originates from the AHE. The ratio between the induced current \mathbf{j} and the electric field \mathbf{E} is a measure of the conductivity σ ,

$$\mathbf{j} = \sigma \mathbf{E}, \quad (1.1)$$

or, written in its components,

$$j_\alpha = \sum_\beta \sigma_{\alpha\beta} E_\beta. \quad (1.2)$$

The resistivity tensor ρ is defined as the inverse of the conductivity tensor σ :

$$\rho = \sigma^{-1}. \quad (1.3)$$

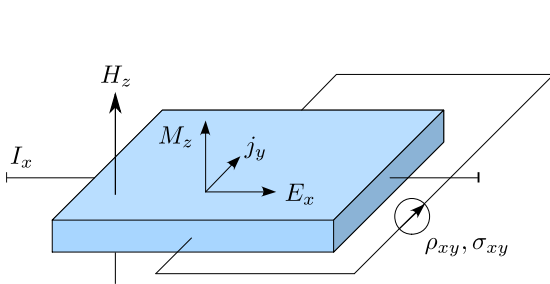


FIG. 1.1: Experimental setup for measuring the anomalous Hall effect (AHE).

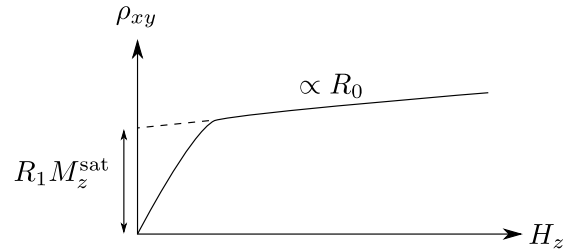


FIG. 1.2: Dependency of the Hall resistivity ρ_{xy} on the magnitude of the external magnetic field.

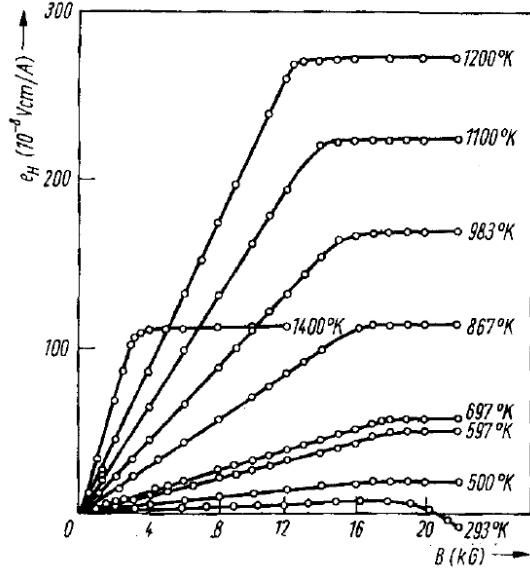


FIG. 1.3: (left) Hall resistivity in Co as a function of H_z at various temperatures [4].

TABLE I: Hall coefficients at room temperature in units of 10^{-12} Vcm/(AG) [5].

	Non-ferromagnets		Ferromagnets		
		R_H	R_0	R_1	
V		0.82	Fe	0.28	7.22
Mn		0.84	Ni	-0.46	-6.05
Cu		-0.50	Co	-0.84	0.60
			Ni ₃ Mn	-0.56	155
			Fe ₃ Al	0.00	470
			CrTe		-5000

The AHE shows itself as a strong signal in the off-diagonal elements of the resistivity tensor ρ . Already at an early stage in the history of the AHE a number of experimental studies had revealed that for a sample geometry as in Fig. (1.1) the off-diagonal element ρ_{xy} can be decomposed into two parts [2, 3]. The first, so-called ordinary contribution depends directly on the magnetic field H_z while the second, anomalous contribution is a function of the magnetization M_z :

$$\rho_{xy} = \rho_{xy}^{\text{ordinary}} + \rho_{xy}^{\text{AHE}} = R_0 H_z + R_1 M_z. \quad (1.4)$$

In this equation R_0 stands for the ordinary Hall coefficient and the anomalous Hall coefficient is denoted R_1 . While the ordinary contribution to the resistivity is due to the Lorentz force like in non-magnetic materials, the anomalous contribution to the resistivity arises from completely different physical mechanisms and is not easy to explain. Note that in ferromagnetic materials the magnetization is not a simple function of the magnetic field and in general \mathbf{H} and \mathbf{M} may even point into different directions. The dependency of the anomalous contribution ρ_{xy}^{AHE} on the magnetization direction in the sample leads to distinctive anisotropy effects.

The anomalous contribution differs from the ordinary contribution in several ways. First of all, ferromagnets might show a non-vanishing spontaneous magnetization even if the external magnetic field is zero. Therefore, it holds that $\rho_{xy}^{\text{AHE}} = R_1 M_z \neq 0$ if $M_z \neq 0$ and for that reason one can still measure a transverse current for the AHE if $H_z = 0$, whereas the ordinary Hall resistivity does not exist if $H_z = 0$. Second, the anomalous contribution is typically very large, i.e.:

$$R_1 \gg R_0. \quad (1.5)$$

In Fig. (1.2) the qualitative dependency of the Hall resistivity ρ_{xy} on the magnitude of the external magnetic field H_z is shown. On a phenomenological level such curves are easy to explain. Lets assume that the sample is not magnetized from the outset. Without a magnetic field random magnetic domains in the ferromagnet form and the net resistivity adds up to zero. When the magnetic field increases, the magnetization will increase as well until a certain saturation value M_z is reached. Beyond the saturation value only the ordinary contribution $R_0 H_z$ to the resistivity will increase any further which becomes noticeable as a kink in the course of ρ_{xy} . According to Eq. (1.4), from the slope of ρ_{xy} the ordinary Hall coefficient R_0 and from the offset the anomalous Hall coefficient R_1 can be determined if one extrapolates from the magnetically saturated state back to zero magnetic field.

In Fig. (1.3) the Hall resistivities in Co as a function of the external magnetic field for various temperatures are shown. The general course of ρ_{xy} pretty much resembles that of Fig. (1.2). It can be derived from the different slopes and offsets at different temperatures T that both R_0 and R_1 have a distinctive dependency on T . Depending on the material and temperature R_0 and R_1 may have either sign, positive or negative. For Co the anomalous Hall coefficient R_1 becomes positive at $T \approx 210^\circ\text{K}$ [5]. At room temperature R_0 is negative and its absolute value is greater than R_1 . However, at higher temperatures R_1 becomes much larger than R_0 .

In Tab. (I) the ordinary Hall constants R_H of some non-ferromagnetic materials and the Hall coefficients R_0 and R_1 of some ferromagnetic materials are summarized. We notice that the absolute values of R_0 are comparable in magnitude to the corresponding values of the ordinary Hall constants R_H in non-ferromagnets, but the anomalous contribution is typically very large as stated in Eq. (1.5). Since the resistivity is so much enhanced in ferromagnets, the AHE has also been called the extraordinary Hall effect in the older literature.

1.2 AHE: More than 130 years of research

Shortly after the AHE was discovered in 1881 it became apparent that its underlying physical mechanisms must clearly differ from the ordinary Hall effect. While the ordinary Hall effect in non-magnetic materials can easily be explained in terms of the Lorentz force, which is proportional to the strength of the external magnetic field \mathbf{H} , the AHE is approximately independent of \mathbf{H} and depends on a multitude of material specific parameters instead. Smith and Sears assumed that ρ_{xy} in ferromagnets should in particular be a function of the magnetization \mathbf{M} [6]. However, it were Pugh and Lippert who developed a method to measure \mathbf{H} and \mathbf{M} accurately and confirmed this assumption experimentally [2, 3].

It was not before 1954 that Karplus and Luttinger calculated for the first time the order of magnitude of ρ_{xy}^{AHE} in their seminal work on the Hall effect in ferromagnets [7]. Their idea was that spin-orbit interaction modifies the movement of electrons in the presence of an electric field and gives rise to the anomalous effects. Although their notion is correct from today's point of view and leads to the so-called intrinsic contribution of the AHE, it was not believed in their time. Especially Smit criticized that Karplus' and Luttinger's theory neglected the effects of scattering from impurities [8]. In that regard he argued that the momentum relaxation which is caused by scattering processes exactly compensates for the acceleration of electrons by the electric field and the intrinsic contribution should therefore vanish. Although his reasoning eventually turned out to be wrong, he nevertheless succeeded in deriving the skew-scattering mechanism which he considered the primary contribution to the AHE [9].

In response to Smit's criticism Luttinger devised a rigorous quantum mechanical theory of the AHE by expanding the conductivity in terms of the impurity scattering strength v [10]. With this approach he recovered the intrinsic contribution, which is of order $\mathcal{O}(v^0)$, and Smit's skew-scattering contribution, which is of order $\mathcal{O}(v^{-1})$. His solution for the AHE conductivity also contained some additional terms but his approach was too complicated and nontransparent so that he could not assign any physical meaning to them. For that reason Luttinger's theory did not find wide acceptance among his compatriots although it was utterly correct.

In search of an alternative and simpler formalism Berger found that some of the intriguing aspects of the AHE could intuitively be explained in terms of electron wave-packets that scatter from impurities [11]. He showed how the center of mass of a suitable wave packet experiences a small transverse displacement $\Delta\mathbf{r}$ on scattering from a single impurity. In the presence of spin-orbit interaction this leads to the so-called side-jump contribution to the AHE. Berger's theory built up on an earlier work by Adams and Blount. Since an electric field mixes Bloch states of different bands, parts of a wave packet would start fast oscillations if it was constructed from Bloch states of a single band alone. Adams and Blount

TABLE II: Selection of important contributions to the field of the AHE.

Author(s)	Year	Ref.	Findings
Hall	1881	[1]	Experimental discovery
Pugh and Lippert	1930	[2, 3]	Empirical relation: $\rho_{xy} = R_0 H_z + R_1 M_z$
Karplus and Luttinger	1954	[7]	Intrinsic contribution
Smit	1955	[8, 9]	Skew scattering
Luttinger	1958	[10]	Quantum theory of AHE
Berger	1970	[11]	Side-jump contribution
Onoda and Nagaosa	2002	[14]	Topological nature of AHE
Yao <i>et al.</i>	2004	[15]	First principles calculation of intrinsic AHE in bcc Fe
Sinitsyn <i>et al.</i>	2007	[16]	Semiclassical theory of AHE
Kovalev <i>et al.</i>	2010	[17]	Side-jump contribution from the electronic structure

demonstrated that the unwanted interband mixing can be eliminated if one chooses a basis in which the part of the Hamiltonian due to \mathbf{E} is diagonal [12, 13].

Confusingly, the side-jump contribution shows the same parametrical dependence on the impurity scattering strength v like the intrinsic contribution, i.e., it is of order $\mathcal{O}(v^0)$. This misled Berger to the assumption that the intrinsic contribution is "spurious" and, as a consequence, his work triggered a persistent debate on how the skew-scattering and the side-jump contribution relate to each other.

The discovery of the Berry phase has brought fresh impetus into the discussion of the AHE [18]. The Berry phase is a general quantum geometrical concept, which can readily be applied to the case of Bloch electrons in a solid, see Appendix (??). At first, topological arguments were utilized in the semiclassical theory of the AHE, which deals with the dynamics of wave packets moving in a weak electric field. The wave packets are composed of Bloch states $\psi_{n\mathbf{k}}(\mathbf{r})$ and subject to scattering due to disorder. Their dynamics is determined by the time dependent Schrödinger equation, which can be obtained from an effective Lagrangian with the help of a variational principle [19]. The advantage of this semiclassical approach is that the wave packet dynamics allows for an intuitive picture of the AHE mechanisms, although the side-jump contribution has to be treated separately [16, 20--22].

In the framework of semiclassical transport theory it is easy to distinguish between the different contributions to the AHE. It was found that the conventional decomposition of the AHE into only three parts may actually be misleading and the link to physical mechanisms should be established with care. Instead of identifying these physical mechanisms it has been suggested that a more natural classification of the contributions to the AHE consists in separating them according to their dependence on the Bloch-state transport lifetime τ , which is directly proportional to the inverse of the impurity concentration n_i [23]. This approach appears to be evident and is followed in the present work.

In the meantime, major theoretical efforts revealed that the Berry phase of Bloch wave-functions plays an important role in the field of the AHE. In particular, the intrinsic contribution can be understood as a realization of Berry-phase effects in momentum space [14, 24, 25]. Research on the topological properties of the AHE has also stimulated interest in its calculation from *ab initio*. For the first time this has been accomplished by Yao *et al.* [15]. Their work introduced the long sought possibility to quantitatively compare experiment with the theory of the AHE, but only for the intrinsic contribution.

A predictive theory of the other contributions to the AHE does not exist by now because of the difficulties in modeling impurity scattering from the outset. However, Kovalev *et al.* recently derived an expression for the side-jump contribution which is fully determined by the electronic structure of the material [17].

In the present work their ideas are applied to real materials, thereby predicting the values for the AHE with an accuracy unprecedented so far.

In Tab. (II) some of the important contributions to the field of the AHE are summarized. Considering the fact that only the theoretical efforts of over one century of intense research led to the understanding of the AHE on the level we currently have, such a summary must be rather incomplete. For a thorough review of the field of the AHE the reader is referred to the excellent article [23].

1.3 Analyzing the AHE into its parts

Conventionally, the AHE can be divided into three different contributions, namely the intrinsic contribution, the skew scattering and the side-jump contribution. These names were not chosen systematically, they rather reflect the physical understanding of the specific mechanism assigned to each contribution at that time. If these contributions are actually evaluated with modern Green's function techniques, they are interpreted in a different way. For example, from today's point of view the side-jump contribution is no longer just the sideways displacement of a wave packet scattering from impurities but it is made up of other contributions which were not taken into account previously.

The approach followed in the present work complies with the modern point of view and separates the contributions to the AHE according to their dependency on the impurity concentration n_i [23]. The contribution proportional to $\mathcal{O}(n_i^0)$ is separated further into the intrinsic contribution and the side-jump contribution, but we do not exclusively assign the particular physical mechanism found by Berger to the latter. A vocabulary mismatch can easily be avoided if the potential sources of confusion are known. For example, the intrinsic contribution should be understood as the contribution to the AHE which does not involve scattering from impurities. In this sense the other contributions can be considered extrinsic [20]. It turns out that the side-jump contribution is an extrinsic contribution but nevertheless independent of the impurity concentration n_i . Some authors use the term intrinsic contribution in a different sense and assign it to any contribution which is independent of n_i . This slightly different definition of the intrinsic contribution would then include the side-jump contribution as well [24]. In the following we will provide a proper definition of the various contributions to the AHE which occur in this work, see Fig. (1.4).

1.3.1 Skew scattering

Smit found out that the scattering of electrons from impurities becomes asymmetric if spin-orbit interaction is present [8, 9]. According to Fermi's golden rule, the transition probability $W_{i \rightarrow f}$ from a state i to a state f due to a perturbation normally equals the transition probability $W_{f \rightarrow i}$ of the inverse process. However, spin-orbit interaction, which is contained either in the scattering potential or in the Hamiltonian of the unperturbed crystal alone, introduces a chiral dependence which modifies the transition probability according to its right- or left-handedness with respect to the magnetization direction \hat{M} , i.e., $W_{i \rightarrow f} \neq W_{f \rightarrow i}$ for terms of higher order than in Fermi's rule. Smit coined the term skew scattering for these asymmetric scattering contributions to the AHE and demonstrated that the skew-scattering mechanism is inversely proportional to the impurity concentration n_i ,

$$\sigma_{xy}^{\text{sk}} \propto \frac{1}{n_i}. \quad (1.6)$$

For our purposes we define the contribution to the AHE conductivity which satisfies $\sigma_{xy} \propto n_i^{-1}$ as the skew scattering contribution. Skew scattering is the dominating contribution in the super-clean regime where the impurity concentration goes to zero. It appears that the diagonal conductivity σ_{xx} is inversely proportional to the impurity concentration n_i as well, for the more dirt in the sample is, the less free will

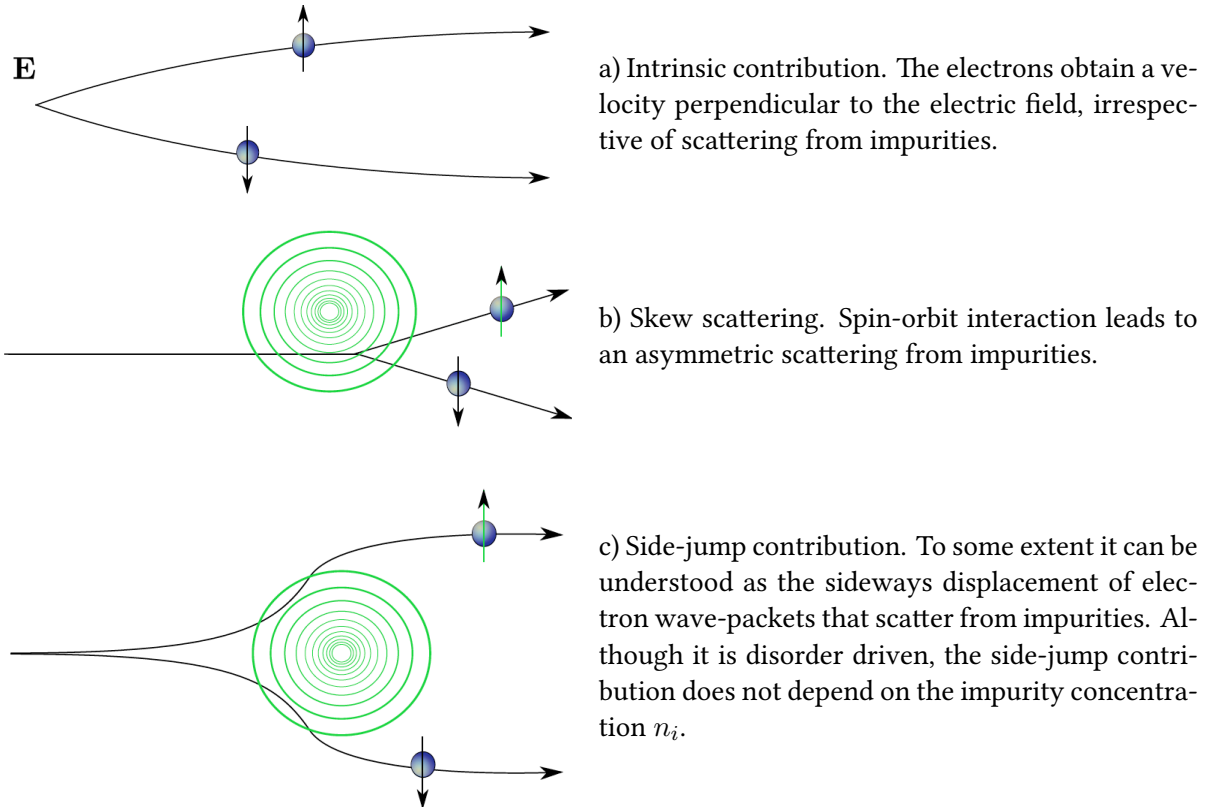


FIG. 1.4: Illustration of main mechanisms to the AHE according to [23].

the current flow. This means that the skew-scattering is also proportional to the diagonal conductivity σ_{xx} and the constant of proportionality is denoted by S :

$$\left. \begin{array}{l} \sigma_{xy}^{\text{sk}} \propto \frac{1}{n_i} \\ \sigma_{xx} \propto \frac{1}{n_i} \end{array} \right\} \Rightarrow \sigma_{xy}^{\text{sk}} \propto S \sigma_{xx}. \quad (1.7)$$

S is often called the skewness factor. The difficulty in calculating the skew-scattering contribution to the AHE consists in creating a realistic model which describes the disorder.

1.3.2 Intrinsic contribution

The first theoretical work which dealt with the AHE in detail was published by Karplus and Luttinger in 1954 [7]. They discovered the intrinsic contribution and showed that electrons moving in the presence of an electric field experience a deflection which is perpendicular both to the field and to the direction of their spin. In non-ferromagnetic materials, the number of electrons with spin up is equal to the number of electrons with spin down and the contributions from both kinds of spin cancel each other out if no external magnetic field is applied. In ferromagnets this symmetry is broken by the spontaneous magnetization which these materials show and the intrinsic contribution does not sum to zero.

The intrinsic contribution depends only on the electronic structure governed by the Bloch functions $\psi_{n\mathbf{k}}(\mathbf{r})$, i.e., it occurs regardless of any scattering mechanism. This characteristic feature can be explained in terms of the Berry phase of Bloch electrons. We will see later that the intrinsic contribution

may be identified with the expression

$$\sigma_{xy}^{\text{int}} \equiv e^2 \hbar \int \frac{d^3 k}{(2\pi)^3} \text{Im} \sum_{n \neq m} \frac{\langle \psi_{n\mathbf{k}} | \hat{v}_x | \psi_{m\mathbf{k}} \rangle \langle \psi_{m\mathbf{k}} | \hat{v}_y | \psi_{n\mathbf{k}} \rangle}{(\varepsilon_{n\mathbf{k}} - \varepsilon_{m\mathbf{k}})^2}, \quad (1.8)$$

where \hat{v} is the velocity operator and $\varepsilon_{n\mathbf{k}}$ is the band energy. Written in this form the intrinsic contribution is directly accessible to *ab initio* calculations. As can be seen from inspection, it is truly independent from the impurity concentration n_i :

$$\sigma_{xy}^{\text{int}} \propto n_i^0. \quad (1.9)$$

The intrinsic contribution has large values at avoided band crossings in the electronic structure, where the energy values $\varepsilon_{n\mathbf{k}}$ and $\varepsilon_{m\mathbf{k}}$ are close together. This divergent behavior makes its calculation computationally demanding.

1.3.3 Side jump contribution

The side-jump contribution has already been found by Smit, but it was Berger who revised this concept and analyzed it thoroughly. Berger considered the scattering of an electron wave packet from a spherical impurity in the presence of spin-orbit interaction and showed that it experiences a sideways displacement transverse to its incident wave vector \mathbf{k} . For a single scattering process this displacement is extremely small. Berger argued that the accumulation of side-jumps in dilute alloys is the main reason for the AHE [11].

However, if we actually compute the AHE with rigorous quantum mechanical techniques, we inevitably find ourselves confronted with expressions that lack an identification in simple semiclassical terms. By the very nature of things the AHE is rich in its possible shapes and we generally refrain from establishing links to a semiclassical picture that might prove deceptive in the end. The semiclassical theory is certainly more transparent, but on the other hand many aspects of the AHE cannot be treated systematically [20]. In the light of this fact it is convenient to define the side-jump contribution as the disorder driven contribution to the AHE which is independent of the impurity concentration n_i^0 , or equivalently

$$\sigma_{xy}^{\text{AHE}} = \underbrace{\sigma_{xy}^{\text{sk}}}_{\mathcal{O}(n_i^{-1})} + \underbrace{(\sigma_{xy}^{\text{int}} + \sigma_{xy}^{\text{sj}})}_{\mathcal{O}(n_i^0)} \Leftrightarrow \sigma_{xy}^{\text{sj}} \equiv \sigma_{xy}^{\text{AHE}} - \sigma_{xy}^{\text{sk}} - \sigma_{xy}^{\text{int}}. \quad (1.10)$$

This definition does not rely on the identification of the semiclassical processes that constitute the side jump. Naturally, the physical mechanisms which lead to Berger's original side-jump contribution are declaredly contained in σ_{xy}^{sj} .

1.4 Experimental studies on the AHE

Since both the side-jump and the intrinsic contribution are independent of n_i , it is difficult to separate them in dc experiments. In this section it will be explained how the AHE can be decomposed in spite of this difficulty, since the anomalous Hall coefficient R_1 turns out to depend quite sensitively on a number of parameters, most notably on the longitudinal resistivity ρ_{xx} . Experimental evidence is provided that the scattering independent contributions to the AHE, i.e., the intrinsic and side-jump contribution, are generally important.

1.4.1 Scaling relations

Due to symmetry reasons, only three components of the conductivity tensor $\sigma = \rho^{-1}$ are independent from each other for a sample geometry as depicted in Fig. (1.1). Therefore, if the sample is spatially uniform, we can write:

$$\sigma = \begin{pmatrix} \sigma_{xx} & \sigma_{xy} & 0 \\ -\sigma_{xy} & \sigma_{xx} & 0 \\ 0 & 0 & \sigma_{zz} \end{pmatrix}, \quad \rho = \begin{pmatrix} \rho_{xx} & \rho_{xy} & 0 \\ -\rho_{xy} & \rho_{xx} & 0 \\ 0 & 0 & \rho_{zz} \end{pmatrix} = \frac{1}{\sigma_{xx}^2 + \sigma_{xy}^2} \begin{pmatrix} \sigma_{xx} & -\sigma_{xy} & 0 \\ \sigma_{xy} & \sigma_{xx} & 0 \\ 0 & 0 & \frac{\sigma_{xx}^2 + \sigma_{xy}^2}{\sigma_{zz}} \end{pmatrix}. \quad (1.11)$$

It may be expected that the off-diagonal conductivity σ_{xy} is much smaller than the diagonal conductivity σ_{xx} . This permits the approximation

$$\rho_{xx} = \frac{\sigma_{xx}}{\sigma_{xx}^2 + \sigma_{xy}^2} \approx \frac{1}{\sigma_{xx}}, \quad (1.12)$$

$$\rho_{xy} = \frac{-\sigma_{xy}}{\sigma_{xx}^2 + \sigma_{xy}^2} \approx -\frac{\sigma_{xy}}{\sigma_{xx}^2} = -\sigma_{xy}\rho_{xx}^2. \quad (1.13)$$

The parametrical dependence of the off-diagonal resistivity $\rho_{xy} = \rho_{xy}^{\text{ordinary}} + \rho_{xy}^{\text{AHE}}$ on the longitudinal resistivity ρ_{xx} is a suitable means to distinguish between the several contributions of the AHE. The ordinary contribution $\rho_{xy}^{\text{ordinary}}$ to the off-diagonal resistivity ρ_{xy} is only proportional to the magnetic field and thus independent from ρ_{xx} :

$$\rho_{xy}^{\text{ordinary}} \propto H_z, \mathcal{O}(\rho_{xx}^0). \quad (1.14)$$

On the other hand, the anomalous contribution ρ_{xy}^{AHE} is proportional to the magnetization M_z according to Eq. (1.4). Since the criterion Eq. (1.13) has to be fulfilled, the relation $\rho_{xy}^{\text{AHE}} \propto \rho_{xx}^2$ implies that σ_{xy} is constant. This is the case for the intrinsic and side jump contributions. If $\rho_{xy}^{\text{AHE}} \propto \rho_{xx}$ instead, this relation implies $\sigma_{xy} \propto 1/\rho_{xx}$, or equivalently $\sigma_{xy} \propto \sigma_{xx}$, which is the case for the skew-scattering mechanism:

$$\rho_{xy}^{\text{AHE}} \propto M, \begin{cases} \mathcal{O}(\rho_{xx}^2) \Rightarrow \sigma_{xy} = \text{const.}, & \text{Intrinsic contribution and side jump,} \\ \mathcal{O}(\rho_{xx}) \Rightarrow \sigma_{xy} \propto \sigma_{xx}, & \text{Skew scattering.} \end{cases} \quad (1.15)$$

If the experimental measured off-diagonal resistivity ρ_{xy} is plotted against ρ_{xx} , the exponent β in the scaling relation

$$\rho_{xy} \propto \rho_{xx}^\beta \quad (1.16)$$

reveals which contribution to the AHE is important. In order to find the correct scaling behavior the longitudinal resistivity ρ_{xx} has to be varied appropriately.

1.4.2 Crossover between AHE mechanisms

Fig. (1.5) is extracted from a recent publication by Miyasato *et al.* where ρ_{xx} and consequently σ_{xx} has been varied with temperature in the range from a few °K up to room temperature [28]. In the so-called good metal regime, where $\sigma_{xx} \propto 10^4 - 10^6 (\Omega\text{cm})^{-1}$, the conductivity σ_{xy} was found to be insensitive to σ_{xx} for Fe, Co and Ni. According to Eq. (1.15) this suggests that the intrinsic contribution and side jump dominate in this regime. Generally, experiments in which the temperature T has been varied in

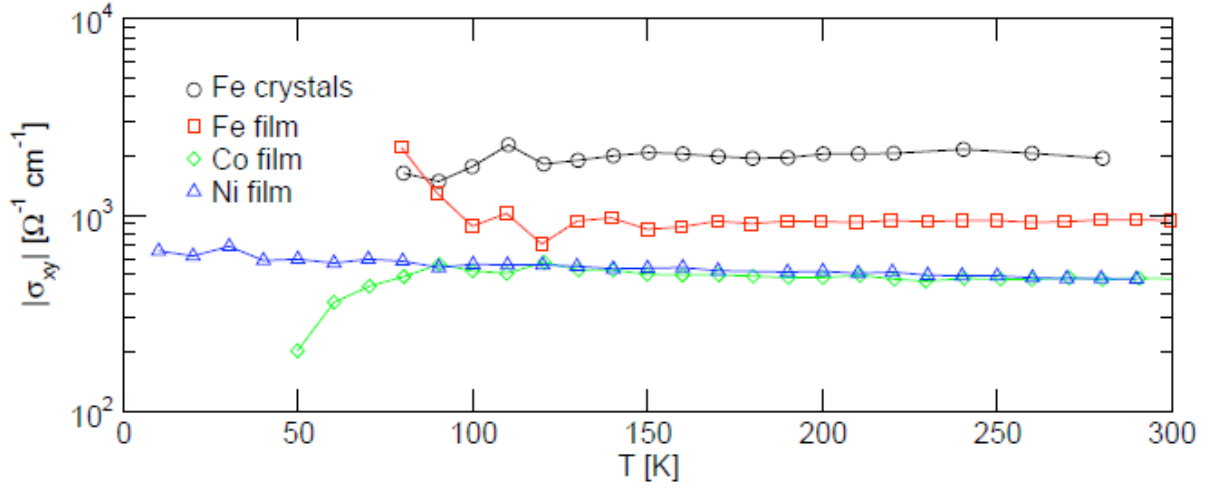


FIG. 1.5: Temperature dependence of the anomalous Hall conductivity for Fe, Co and Ni [23].

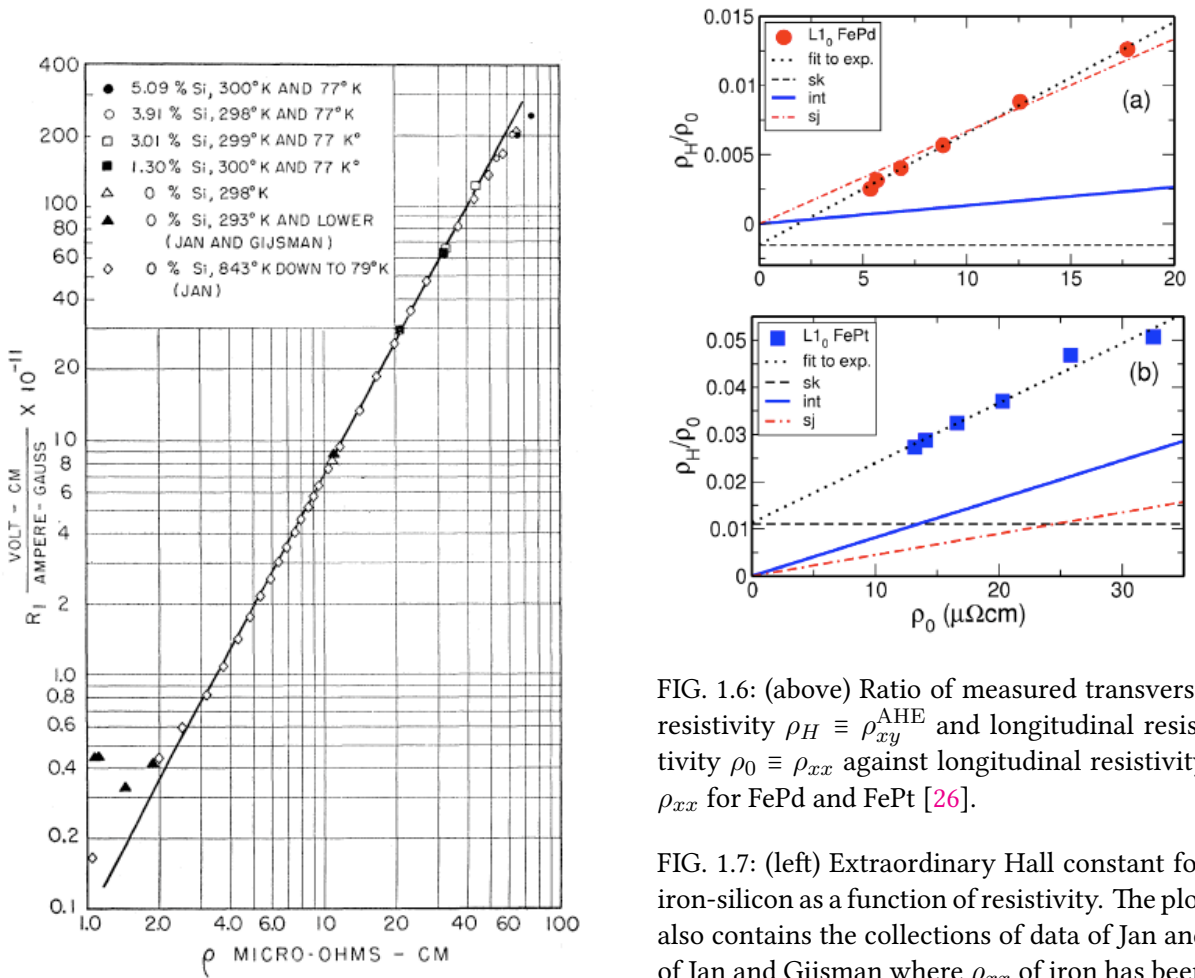


FIG. 1.6: (above) Ratio of measured transverse resistivity $\rho_H \equiv \rho_{xy}^{AHE}$ and longitudinal resistivity $\rho_0 \equiv \rho_{xx}$ against longitudinal resistivity ρ_{xx} for FePd and FePt [26].

FIG. 1.7: (left) Extraordinary Hall constant for iron-silicon as a function of resistivity. The plot also contains the collections of data of Jan and of Jan and Gijmsan where ρ_{xx} of iron has been varied with temperature [27].

order to change the resistivity ρ_{xx} have the disadvantage that they do not tell whether T or ρ_{xx} is the significant quantity. For example, at finite T inelastic scattering processes caused by phonons or spin-waves might occur which are not taken into account in the scaling relations Eq. (1.15). Besides ρ_{xx} the temperature might effect other parameters of the system such as the magnetization or the distribution of states as well. However, in an earlier measurement of the anomalous Hall coefficient $R_1 = \rho_{xy}^{\text{AHE}}/M_z$ in iron by Jan and Gijsman the resistivity had also been varied by changing the temperature T . These measurements have been checked by Kooi who had varied the resistivity in iron-silicon alloys $\text{Fe}_{1-x}\text{Si}_x$ by changing the impurity concentration x , i.e., the content of Si. His overall result $R_1 \propto \rho_{xx}^{1.9}$ from Fig. (1.7) suggests that either the intrinsic contribution or the side-jump prevails in Fe, too.

All mechanisms of the AHE can be treated on an equal footing if the anomalous Hall resistivity is fitted against the longitudinal resistivity according to

$$\rho_{xy}^{\text{AHE}} = a\rho_{xx} + b\rho_{xx}^2 \quad \Leftrightarrow \quad \rho_{xy}^{\text{AHE}}/\rho_{xx} = a + b\rho_{xx}, \quad (1.17)$$

where a and b are assumed to be constant and do not depend on temperature T if ρ_{xx} is tuned by T . While the parameter a is a measure of the strength of skew-scattering contribution to the AHE, the parameter b is a measure of the strength of the scattering independent contributions to the AHE, i.e., of the intrinsic contribution and side jump. Fig. (1.6) shows the linear fit of the ratio $\rho_{xy}^{\text{AHE}}/\rho_{xx}$ against ρ_{xx} for the ferromagnetic alloys FePd and FePt. The skew-scattering contribution can be read off directly from the offset a while the side-jump contribution $(b - b^{\text{int}})\rho_{xx} = b^{\text{sj}}\rho_{xx}$ can be obtained from the slope b provided that the intrinsic contribution $b^{\text{int}}\rho_{xx}$ is computed from first principles techniques. Seemann *et al.* adopted this approach and found that in FePt the intrinsic contribution is the dominant source of the AHE but in FePd the side-jump contribution is of equal importance. On the other hand, the skew-scattering seems to play only a minor role in these alloys [26].

1.4.3 Sign of AHE

The AHE has been studied most intensively in transition metals, i.e., including the ferromagnetic materials Fe, Co and Ni. The ordinary Hall coefficient R_0 depends mainly on the density of charge carriers in the sample and can be used as a means to distinguish between electron and hole conduction. For Fe the number of unoccupied states in the $3d$ atomic orbital is larger than the number of occupied states in the $4s$ atomic orbital and for this reason one expects hole conduction [29]. In analogy to the ordinary Hall effect, where the Hall constant is given by the density of charge carriers n and the elementary charge e ,

$$R_H = -\frac{1}{ne} = +\frac{1}{n|e|}, \quad (1.18)$$

a positive sign of the Hall coefficient R_0 in ferromagnets suggests that hole conduction is dominant. This presumption is confirmed by the fact that the sign of R_0 in Fe is actually positive, see Fig. (1.8). Hence, a negative sign of the Hall coefficient R_0 suggests that electron conduction prevails. This seems to be the case in Ni or Co. In contrast, the interpretation of the sign of R_1 is not clear. At low temperatures a highly nonlinear behavior of R_1 can be observed, even going through a sign change as in the case of Co, see Fig. (1.9). This phenomenon has been lacking a satisfactory explanation until now.

1.5 *Ab initio* computation of the AHE

Until recently calculations of the AHE conductivity for ferromagnetic materials such as Fe, Co and Ni have mainly focussed on the intrinsic contribution. The practical reason for this is that no information about the impurity potential is available from the outset and because of that scattering effects are difficult

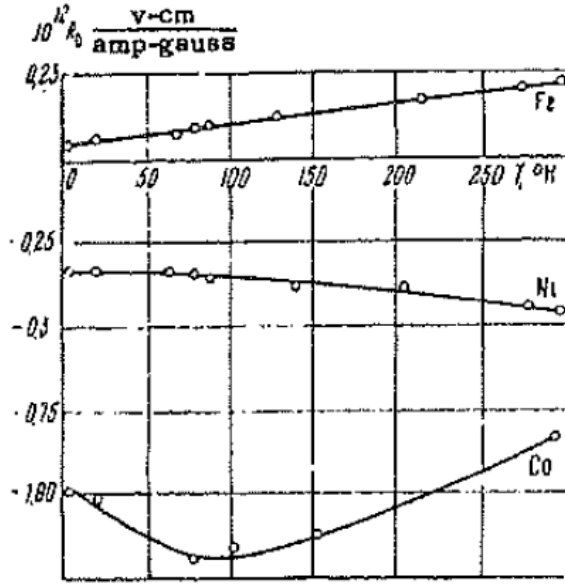


FIG. 1.8: (above) Temperature dependence of the ordinary Hall coefficient R_0 in Fe, Co and Ni [5].

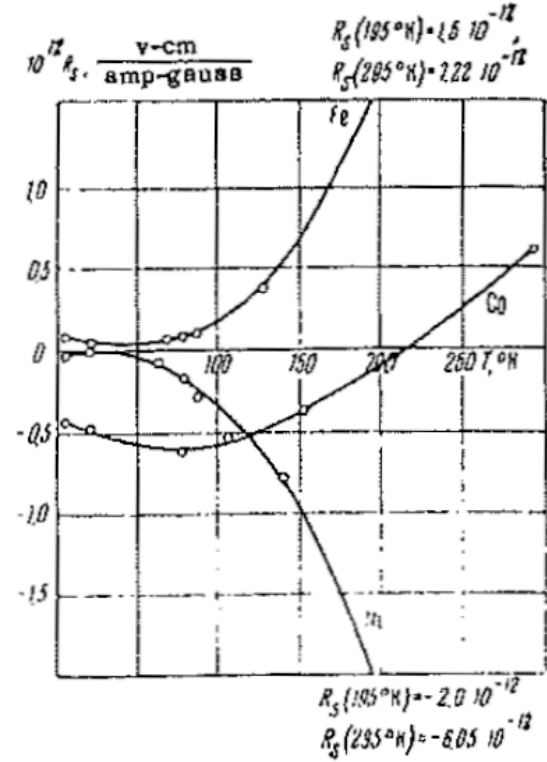


FIG. 1.9: (left) Temperature dependence of the anomalous Hall coefficient $R_S \equiv R_1$ in Fe, Co and Ni [5].

to deal with. In many materials the intrinsic contribution is the dominant contribution to the transverse conductivity σ_{xy}^{AHE} , see Tab. (III). Then it is possible to predict the AHE on the level of general trends and signs with the intrinsic contribution alone. For example, in Fe the intrinsic contribution can be accounted for about 75% of the total AHE conductivity. On the other hand, in materials such as FePd or Ni one fails to describe the AHE based on the intrinsic contribution alone and a considerable deviation from the calculated intrinsic contribution can be observed. However, some disagreement is also due to the confusing experimental situation. For example in Ni, the complicated temperature dependence of the AHE makes it very difficult to identify the intrinsic contribution and the values for the measured conductivity range from -1100 S/cm at 5 °K to -637 S/cm at room temperature [30, 31].

1.5.1 Conventional approach: KKR and CPA

The conventional approach to deal with disorder in the computation of the AHE consists in using the Korringa-Kohn-Rostoker method (KKR) in combination with the coherent potential approximation (CPA) [32]. According to Eq. (1.7) the contribution σ_{xy}^{sk} is proportional to the longitudinal conductivity σ_{xx} so that the overall conductivity can be decomposed into

$$\sigma_{xy}^{\text{AHE}} = \sigma_{xy}^{\text{int}} + \sigma_{xy}^{\text{sj}} + \sigma_{xy}^{\text{sj}} = (\sigma_{xy}^{\text{int}} + \sigma_{xy}^{\text{sj}}) + S\sigma_{xx}. \quad (1.19)$$

Eq. (1.19) yields a linear dependence of σ_{xy}^{AHE} on σ_{xx} if the impurity concentration is regarded as an implicit parameter to vary the latter.

In Fig. (1.10), the Hall conductivity $\sigma_{xy}^{\text{extr}} \equiv \sigma_{xy}^{\text{AHE}} - \sigma_{xy}^{\text{int}}$ has been calculated in the ferromagnetic alloys $\text{Fe}_x\text{Pd}_{1-x}$ and $\text{Ni}_x\text{Pd}_{1-x}$ for several values of the impurity concentration x . By extrapolation to $\sigma_{xx} = 0$ the side-jump contribution in the dilute regime can then be obtained from the offset of $\sigma_{xy}^{\text{extr}}$ for these materials. However, such an indirect computation of the contributions to the AHE represents a sig-

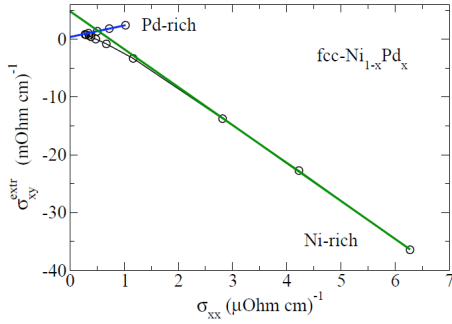


FIG. 1.10: $\sigma_{xy}^{\text{extr}} \equiv \sigma_{xy}^{\text{AHE}} - \sigma_{xy}^{\text{int}}$ vs. σ_{xx} for $\text{Fe}_x\text{Pd}_{1-x}$ and $\text{Ni}_x\text{Pd}_{1-x}$ [33].

TABLE III: Calculated σ^{int} compared with experimental values for the scattering independent conductivity.

	σ^{int} [S/cm]	Exp. [S/cm]	$\sigma^{\text{int}}/\text{Exp.}$
Fe	751 [15]	1032 [34]	73%
Co	481 [35]	813 [36]	59%
Co	116 [35]	150 [36]	77%
FePt	818 [26]	1267 [26]	65%
FePd	133 [26]	806 [26]	17%
Ni	-2203 [37]	-1100 ÷ -637 [30, 31]	>200%

nificant computational challenge since the exact knowledge of the disorder potential in the system is necessary in order to compute σ_{xy}^{AHE} , but precisely this information is usually not known.

1.5.2 Novel approach: Universal side-jump contribution

Clearly the overall theoretical prediction and understanding of the AHE is not satisfactory at this point and is in fact the motivation of the present work, namely to improve the prediction of the AHE conductivity from *ab initio* by taking the side-jump contribution into account. The experimental and theoretical data presented above suggests that the side-jump contribution constitutes a significant part of the AHE, but so far the calculation of the AHE mainly concentrated on the intrinsic contribution. Previous attempts to include disorder employed either fitting procedures or extrapolation techniques but were not capable to directly derive the side jump.

However, Kovalev *et al.* have recently shown that for a model of Gaussian disorder a universal side-jump contribution to the AHE exists which can be calculated directly from the electronic structure of the pure crystal alone [17]. It is universal in the sense that it depends neither on the impurity concentration nor the scattering strength, so that the difficulties of incorporating scattering effects into *ab initio* techniques disappear. Of course, the Gaussian disorder model gives only a very rough description of the physical scattering processes that are taking place. Nevertheless, as the present work demonstrates the universal side-jump contribution appears to reproduce large portions of the disorder driven part of AHE conductivity astonishingly well. Until now, calculations of the universal side-jump contribution have been performed only for simple model Hamiltonians. The present work takes the concept of the universal side-jump contribution a step further and applies it to real ferromagnetic materials and ferromagnetic alloys using the full-potential linearized augmented plane-wave method for electronic structure calculations.

1.6 Outline

In Fig. (1.11) the organizing principle of the present work is shown. The content is subdivided into three domains, namely the theory domain (Chap. 2), the computing domain (Chap. 3) and the research domain (Chap. 4 and Chap. 5). In the theory domain the Kubo-Středa formula is derived which constitutes the starting point of the calculation of the scattering independent contributions to the AHE conductivity afterwards. These contributions are the intrinsic contribution and the universal side-jump contribution. On the basis of their analytical properties their symmetry relations are studied that make the physical

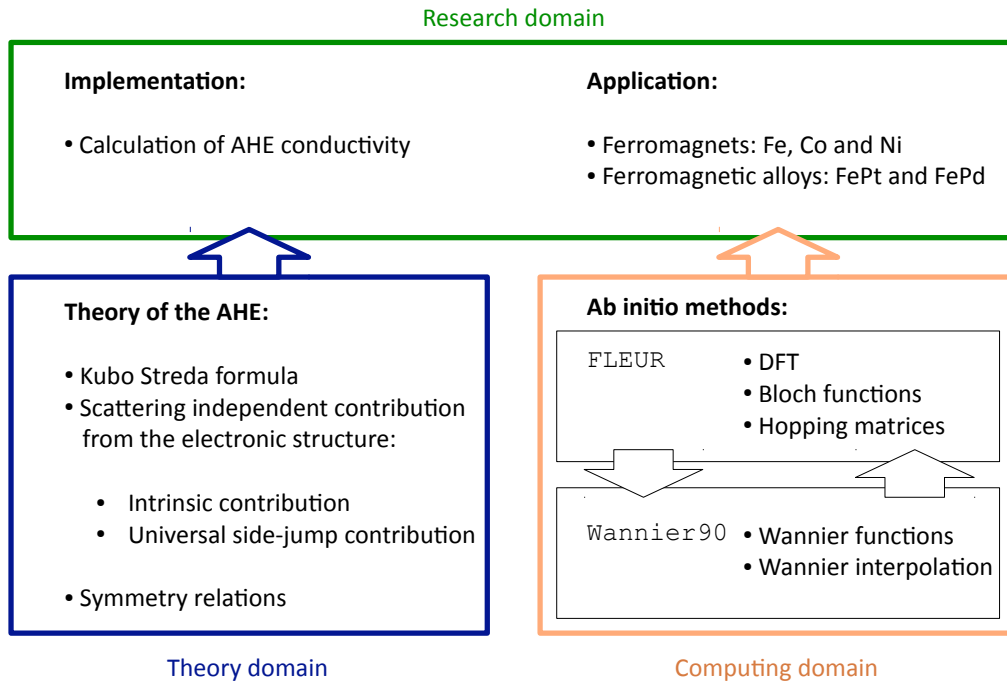


FIG. 1.11: Organizing principle of the present work.

understanding of these contributions easier. Other contributions like the skew-scattering mechanism are not discussed in this work.

In the computing domain the principles of density functional theory (DFT) are explained which is the method of choice to compute the AHE. The Jülich DFT code FLEUR is employed to provide the electronic structure of ferromagnetic materials in the basis of Bloch functions $|\psi_{n\mathbf{k}}\rangle$. In order to reduce the computational cost, a set of Wannier functions is constructed with the program Wannier90. The Wannier functions allow for a Wannier interpolation scheme in which the Bloch Hamiltonian can be written in terms of hopping matrices using Wannier90 and the interface between Wannier90 and FLEUR.

In the research domain the implementation of a new program to calculate the AHE conductivity and its application to ferromagnetic materials is described. The aspects of implementation include how the formulae from the theory domain can be evaluated in practice with the *ab initio* methods from the computing domain, e.g., how the convergence of a Brillouin-zone integration can be secured, how \mathbf{k} -derivatives can be evaluated and how to deal with degeneracies that lead to numerical instabilities. The topics about application include not only the results of the side-jump contribution for the ferromagnetic materials Fe, Co, Ni, FePt and FePd and its anisotropy for different magnetization directions, but also an analysis of the Fermi-surface properties of the side-jump contribution in comparison with the intrinsic contribution.

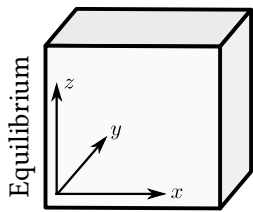
Theory of the AHE

IN this chapter the theory of the AHE is presented. Unless specified otherwise, the system of units is chosen in such a way that $\hbar = 1$. We describe the impurity scattering by a scalar delta-correlated Gaussian disorder model and show that within this model the conductivity depends neither on the impurity concentration nor the scattering strength. In other words, for a scalar delta-correlated Gaussian disorder model any reference to the scattering potential cancels out in the end and allows for the calculation of disorder driven contributions to the AHE conductivity from the electronic structure of the pure system alone.

The appropriate formulae for the AHE were originally obtained in the framework of the Keldysh formalism [38]. The Keldysh formalism is especially applicable to a quantum mechanical system in non-equilibrium state and is surely a perfectly valid and elegant approach to the physics of the AHE [39--41]. However, in the present work it shall be demonstrated that the same formulae can also be derived from the somewhat more conventional linear response theory. The virtue of the linear response theory is that it relates the conductivity of a quantum mechanical system which is not in equilibrium to its equilibrium current-current correlation function, which can be obtained from the familiar thermal Matsubara Green's functions.

2.1 Definition of terms

Before we engage in the physics of the AHE it is necessary to specify which information about the system is known and which quantities we are interested in. If the system is in equilibrium, i.e. no external fields are present, what we know are its thermodynamic state variables \mathcal{V} , T and N and the quantities μ , \hat{H} and $\hat{\rho}_{\text{eq}}$:



- \mathcal{V} Volume,
- T Temperature,
- N Particle number,
- μ Chemical potential,
- \hat{H} Equilibrium Hamiltonian,
- $\hat{\rho}_{\text{eq}}$ Equilibrium density matrix.

Let $|\psi_n\rangle$ be an eigenstate of the Hamiltonian,

$$\hat{H}|\psi_n\rangle = E_n|\psi_n\rangle, \quad (2.1)$$

which means that $|\psi_n\rangle$ is a N -particle wave function of the many particle system. Then the equilibrium density matrix can be defined as

$$\hat{\rho}_{\text{eq}} = \sum_n p_n |\psi_n\rangle \langle \psi_n|, \quad (2.2)$$

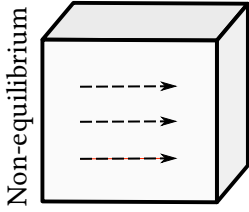
where the p_n are the statistical probabilities to find the state $|\psi_n\rangle$ in the equilibrium quantum ensemble. At temperature T the p_n are the usual Boltzmann factors $\exp[-\beta(E_n - \mu N)]$, where $\beta = 1/(k_B T)$ and E_n is the energy eigenvalue associated with the eigenstate $|\psi_n\rangle$:

$$p_n = \langle \psi_n | \hat{\rho}_{\text{eq}} | \psi_n \rangle = e^{-\beta(E_n - \mu N)} \Rightarrow \begin{cases} \hat{\rho}_{\text{eq}} = \frac{1}{Z} e^{-\beta(\hat{H} - \mu N)}, \\ Z = \text{Tr} e^{-\beta(\hat{H} - \mu N)}. \end{cases} \quad (2.3)$$

The partition function Z is a normalization factor which serves to normalize the trace over the density matrix to unity, $\text{Tr} \hat{\rho}_{\text{eq}} = 1$. In our case the trace includes states with any number of particles. Via the density matrix the expectation value of an operator \hat{O} in equilibrium can conveniently be written as

$$\langle \hat{O} \rangle_{\text{eq}} = \frac{1}{Z} \sum_n e^{-\beta(E_n - \mu N_n)} \langle \psi_n | \hat{O} | \psi_n \rangle = \text{Tr} \hat{\rho}_{\text{eq}} \hat{O}. \quad (2.4)$$

Now we adiabatically switch on a perturbation $\hat{H}_{\text{ext}}(t)$ as the system evolves in time from $t = -\infty$, when it is in equilibrium, to the present. In the context of the AHE the perturbation consists of a time dependent electric field \mathbf{E} which, according to Maxwell's equations, can be written as the time derivative of a vector potential \mathbf{A} and the gradient of a scalar potential ϕ . The electric field will generate a time-dependent current which is the expectation value of the current density operator $\hat{\mathbf{J}}$:



- $\hat{H}'(t) = \hat{H} + \hat{H}_{\text{ext}}(t),$
- $\mathbf{E}(\mathbf{r}, t) = -\frac{1}{c} \dot{\mathbf{A}}(\mathbf{r}, t) - \nabla \phi(\mathbf{r}, t),$
- $\langle \hat{O} \rangle_t \equiv \text{Tr} \hat{\rho}(t) \hat{O} \Rightarrow \langle \hat{\mathbf{J}} \rangle_t = \text{Tr} \hat{\rho}(t) \hat{\mathbf{J}}.$

For convenience Gaussian units are used. For the calculation of the expectation value $\langle \hat{O} \rangle_t$ at time t we need the density matrix $\hat{\rho}(t)$ of the system in non-equilibrium. Although the eigenstates evolve according to the Schrödinger equation

$$i \partial_t |\psi_n(t)\rangle = \hat{H}'(t) |\psi_n(t)\rangle, \quad (2.5)$$

the distribution of states does not change with time and is described by the same p_n as in equilibrium. With the help of the Schrödinger equation the von Neumann equation can be derived which yields the time evolution of the density matrix:

$$\begin{aligned} \dot{\hat{\rho}}(t) &= \sum_n p_n \{ -i \hat{H}'(t) |\psi_n(t)\rangle \langle \psi_n(t)| + i |\psi_n(t)\rangle \langle \psi_n(t)| \hat{H}'(t) \} \\ &= -i [\hat{H}'(t), \hat{\rho}(t)]. \end{aligned} \quad (2.6)$$

In the next section it will be demonstrated that $\hat{\rho}(t)$ can be expressed in terms of $\hat{\rho}_{\text{eq}}$ in linear response theory. By the response $\langle \delta \hat{O} \rangle_t$ of an operator \hat{O} we mean the change of its expectation value when the perturbation is switched on,

$$\langle \delta \hat{O} \rangle_t \equiv \langle \hat{O} \rangle_t - \langle \hat{O} \rangle_{\text{eq}}, \quad \Leftrightarrow \quad \langle \hat{O} \rangle_t = \langle \hat{O} \rangle_{\text{eq}} + \langle \delta \hat{O} \rangle_t. \quad (2.7)$$

However, before we proceed we discuss the representation of the operators we need in real and reciprocal space. The latter representation is particularly useful for translation invariant systems. For example, consider a function $f(\mathbf{r}, \mathbf{r}')$ which has the property that it is translation invariant, i.e., which only depends on the difference between its position arguments, $f(\mathbf{r}, \mathbf{r}') \equiv f(\mathbf{r} - \mathbf{r}')$. Remember the well-known

formulae for Dirac's δ -distribution and the Kronecker- δ [42]:

$$\frac{1}{\mathcal{V}} \sum_{\mathbf{k}} e^{i\mathbf{k}\cdot\mathbf{r}} = \delta(\mathbf{r}), \quad \frac{1}{\mathcal{V}} \int d^3r e^{-i\mathbf{k}\cdot\mathbf{r}} = \delta_{\mathbf{k},\mathbf{0}}. \quad (2.8)$$

We wish to evaluate the integral $C(\mathbf{r}) = \int d^3r' f(\mathbf{r}, \mathbf{r}')g(\mathbf{r}')$ of the function $f(\mathbf{r}, \mathbf{r}')$ with another function $g(\mathbf{r})$. The function $C(\mathbf{r})$ is precisely of the form of correlation functions we encounter in linear response theory. Using Eq. (2.8), the integral $C(\mathbf{r})$ and its Fourier transform $C_{\mathbf{k}}$ can be calculated in the following way:

$$\begin{aligned} C(\mathbf{r}) &= \int d^3r' f(\mathbf{r} - \mathbf{r}')g(\mathbf{r}') = \frac{1}{\mathcal{V}^2} \sum_{\mathbf{k}\mathbf{k}'} \int d^3r' f_{\mathbf{k}} e^{i\mathbf{k}\cdot(\mathbf{r}-\mathbf{r}')} g_{\mathbf{k}'} e^{i\mathbf{k}'\cdot\mathbf{r}'} = \frac{1}{\mathcal{V}} \sum_{\mathbf{k}} f_{\mathbf{k}} g_{\mathbf{k}} e^{i\mathbf{k}\cdot\mathbf{r}}, \\ C_{\mathbf{k}} &= \int d^3r e^{-i\mathbf{k}\cdot\mathbf{r}} C(\mathbf{r}) = \frac{1}{\mathcal{V}} \sum_{\mathbf{k}'} \int d^3r e^{-i(\mathbf{k}-\mathbf{k}')\cdot\mathbf{r}} f_{\mathbf{k}'} g_{\mathbf{k}'} = f_{\mathbf{k}} g_{\mathbf{k}}. \end{aligned} \quad (2.9)$$

We notice that due to the symmetry property of translation invariance $C(\mathbf{r})$ has the form of a convolution integral. In Fourier space the corresponding function $C_{\mathbf{k}}$ is simply the product of the Fourier transforms of $f(\mathbf{r})$ and $g(\mathbf{r})$.

2.1.1 Operators in real and reciprocal space

Of major importance is the Hamiltonian of the system, which is assumed to be of the form:

$$\hat{H}'(t) = \hat{H} + \hat{H}_{\text{ext}}(t). \quad (2.10)$$

At time $t \rightarrow -\infty$ no external fields are present and $\hat{H}'(-\infty) = \hat{H}$ is the Hamiltonian of the unperturbed system in equilibrium. The part $\hat{H}_{\text{ext}}(t)$ of the Hamiltonian which drives the system out of equilibrium contains all the effects of the electric field $\mathbf{E}(\mathbf{r}, t) = -\frac{1}{c} \dot{\mathbf{A}}(\mathbf{r}, t) - \nabla\phi(\mathbf{r}, t)$. For convenience we choose a gauge in which the scalar potential is zero, $\phi \equiv 0$. Such a choice is always possible if we redefine the vector potential \mathbf{A} appropriately. The constraint that the electric field shall vanish in equilibrium leads to the following equations:

$$\begin{aligned} \lim_{t \rightarrow -\infty} \mathbf{A}(\mathbf{r}, t) &= 0, \\ \mathbf{E}(\mathbf{r}, t) &= -\frac{1}{c} \dot{\mathbf{A}}(\mathbf{r}, t). \end{aligned} \quad (2.11)$$

The electric field induces an electric current in the system. The current density is the velocity of the N electrons in the system with charge $e = -|e|$ at a given position \mathbf{r} :

$$\hat{\mathbf{J}}(\mathbf{r}, t) = \frac{e}{2} \sum_{i=1}^N \hat{\mathbf{v}}_i(\mathbf{r}) \delta(\mathbf{r} - \hat{\mathbf{r}}_i) + \delta(\mathbf{r} - \hat{\mathbf{r}}_i) \hat{\mathbf{v}}_i(\mathbf{r}). \quad (2.12)$$

If we write the current density operator in this form it can be readily seen that it is manifestly hermitian. However, if an electric field is applied, the velocity of the i -th particle is its momentum minus the local vector potential:

$$\hat{\mathbf{v}}_i(\mathbf{r}) = \frac{1}{m} \left(\hat{\mathbf{p}}_i - \frac{e}{c} \mathbf{A}(\mathbf{r}, t) \delta(\mathbf{r} - \hat{\mathbf{r}}_i) \right). \quad (2.13)$$

In the presence of \mathbf{A} the current density operator consists of two terms, the so-called paramagnetic term $\hat{\mathbf{J}}_{\text{para}}$ and the diamagnetic term $\hat{\mathbf{J}}_{\text{dia}}$. The paramagnetic term is independent of the vector potential and

usually denoted the current operator $\hat{\mathbf{j}}$. Time dependency enters through the diamagnetic term which originates from \mathbf{A} :

$$\begin{aligned}\hat{\mathbf{J}} &= \hat{\mathbf{J}}_{\text{para}} + \hat{\mathbf{J}}_{\text{dia}}, \\ \hat{\mathbf{J}}_{\text{para}}(\mathbf{r}) &= \frac{e}{2m} \sum_{i=1}^N \{ \hat{\mathbf{p}}_i \delta(\mathbf{r} - \hat{\mathbf{r}}_i) + \delta(\mathbf{r} - \hat{\mathbf{r}}_i) \hat{\mathbf{p}}_i \} \equiv \hat{\mathbf{j}}(\mathbf{r}), \\ \hat{\mathbf{J}}_{\text{dia}}(\mathbf{r}, t) &= -\frac{e^2}{mc} \sum_{i=1}^N \mathbf{A}(\mathbf{r}, t) \delta(\mathbf{r} - \hat{\mathbf{r}}_i) \equiv -\frac{e^2}{mc} \mathbf{A}(\mathbf{r}, t) \hat{n}(\mathbf{r}).\end{aligned}\tag{2.14}$$

In the last line the particle density operator was introduced:

$$\hat{n}(\mathbf{r}) = \sum_{i=1}^N \delta(\mathbf{r} - \hat{\mathbf{r}}_i).\tag{2.15}$$

In the following we will need the paramagnetic part $\hat{\mathbf{j}}$ more often in the momentum representation rather than in the position representation. The change of basis from $\{|\mathbf{r}\rangle\}$ to $\{|\mathbf{k}\rangle\}$ is performed by a Fourier transform. We stick to the usual definition

$$\langle \mathbf{r} | \mathbf{k} \rangle = \frac{1}{\sqrt{\mathcal{V}}} e^{i\mathbf{k}\cdot\mathbf{r}},\tag{2.16}$$

where the normalization factor $1/\sqrt{\mathcal{V}}$ was chosen so that $\langle \mathbf{r}' | \mathbf{r} \rangle = \delta(\mathbf{r} - \mathbf{r}')$ is normalized in the continuum while $\langle \mathbf{k}' | \mathbf{k} \rangle = \delta_{\mathbf{k}\mathbf{k}'}$ is normalized as a discrete set of states. The completeness relation is $\mathbf{1} = \int d^3r |\mathbf{r}\rangle \langle \mathbf{r}| = \sum_{\mathbf{k}} |\mathbf{k}\rangle \langle \mathbf{k}|$. The matrix elements we have to compute for $\hat{\mathbf{j}}$ are

$$\begin{aligned}\langle \mathbf{k}' | \delta(\mathbf{r} - \hat{\mathbf{r}}) | \mathbf{k} \rangle &= \int d^3r' \int d^3r'' \langle \mathbf{k}' | \mathbf{r}' \rangle \langle \mathbf{r}' | \delta(\mathbf{r} - \hat{\mathbf{r}}) | \mathbf{r}'' \rangle \langle \mathbf{r}'' | \mathbf{k} \rangle \\ &= \int d^3r' \int d^3r'' \langle \mathbf{k}' | \mathbf{r}' \rangle \delta(\mathbf{r} - \mathbf{r}'') \delta(\mathbf{r}' - \mathbf{r}'') \langle \mathbf{r}'' | \mathbf{k} \rangle \\ &= \langle \mathbf{k}' | \mathbf{r} \rangle \langle \mathbf{r} | \mathbf{k} \rangle = \frac{1}{\mathcal{V}} e^{i(\mathbf{k} - \mathbf{k}')\cdot\mathbf{r}}\end{aligned}\tag{2.17}$$

and accordingly

$$\langle \mathbf{k}' | \hat{\mathbf{p}} \delta(\mathbf{r} - \hat{\mathbf{r}}) + \delta(\mathbf{r} - \hat{\mathbf{r}}) \hat{\mathbf{p}} | \mathbf{k} \rangle = (\mathbf{k}' + \mathbf{k}) \langle \mathbf{k}' | \delta(\mathbf{r} - \hat{\mathbf{r}}) | \mathbf{k} \rangle = \frac{1}{\mathcal{V}} (\mathbf{k}' + \mathbf{k}) e^{i(\mathbf{k} - \mathbf{k}')\cdot\mathbf{r}}.\tag{2.18}$$

Let $a_{\mathbf{k}}$ and $a_{\mathbf{k}}^\dagger$ be the corresponding creation and annihilation operators in momentum representation. The current operator does not depend on spin and is therefore diagonal in the spin index σ . In the context of second quantization $\hat{\mathbf{j}}$ is a single particle operator and assumes the form:

$$\begin{aligned}\hat{\mathbf{j}}(\mathbf{r}) &= \frac{e}{2m} \sum_{\sigma} \sum_{\mathbf{k}\mathbf{k}'} \langle \mathbf{k}' | \hat{\mathbf{p}} \delta(\mathbf{r} - \hat{\mathbf{r}}) + \delta(\mathbf{r} - \hat{\mathbf{r}}) \hat{\mathbf{p}} | \mathbf{k} \rangle a_{\mathbf{k}'\sigma}^\dagger a_{\mathbf{k}\sigma} \\ &= \frac{e}{2m\mathcal{V}} \sum_{\sigma} \sum_{\mathbf{k}\mathbf{k}'} (\mathbf{k} + \mathbf{k}') e^{i(\mathbf{k} - \mathbf{k}')\cdot\mathbf{r}} a_{\mathbf{k}'\sigma}^\dagger a_{\mathbf{k}\sigma} \\ &= \frac{e}{2m\mathcal{V}} \sum_{\sigma} \sum_{\mathbf{k}\mathbf{q}} (2\mathbf{k} - \mathbf{q}) e^{i\mathbf{q}\cdot\mathbf{r}} a_{\mathbf{k}-\mathbf{q},\sigma}^\dagger a_{\mathbf{k}\sigma} \\ &= \frac{1}{\mathcal{V}} \sum_{\mathbf{q}} e^{i\mathbf{q}\cdot\mathbf{r}} \hat{\mathbf{j}}_{\mathbf{q}},\end{aligned}\tag{2.19}$$

from which the Fourier transform of $\hat{\mathbf{j}}(\mathbf{r})$ can easily be identified as

$$\hat{\mathbf{j}}_{\mathbf{q}} = \frac{e}{2m} \sum_{\mathbf{k}\sigma} (2\mathbf{k} - \mathbf{q}) a_{\mathbf{k}-\mathbf{q},\sigma}^{\dagger} a_{\mathbf{k}\sigma}. \quad (2.20)$$

In the limit $\mathbf{q} \rightarrow 0$ the current operator is still well defined. Since the factor \mathbf{k} is the matrix element of the momentum operator, $\langle \mathbf{k}' | \hat{\mathbf{p}} | \mathbf{k} \rangle = \mathbf{k} \delta_{\mathbf{k},\mathbf{k}'}$, the current operator for $\mathbf{q} = 0$ can be substituted with the velocity $\hat{\mathbf{v}} = \hat{\mathbf{p}}/m$:

$$\lim_{\mathbf{q} \rightarrow 0} \hat{\mathbf{j}}_{\mathbf{q}} = e\hat{\mathbf{v}} = \frac{e}{m} \sum_{\mathbf{k}\sigma} \mathbf{k} a_{\mathbf{k}\sigma}^{\dagger} a_{\mathbf{k}\sigma}. \quad (2.21)$$

It can be shown by analytical mechanics and the correspondence principle that the perturbation \hat{H}_{ext} can be written in terms of $\hat{\mathbf{J}}$ in the following way [42]:

$$\begin{aligned} \hat{H}_{\text{ext}}(t) &= -\frac{1}{c} \int d^3r \hat{\mathbf{J}}(\mathbf{r}, t) \mathbf{A}(\mathbf{r}, t) \\ &= -\frac{1}{c} \int d^3r \hat{\mathbf{j}}(\mathbf{r}) \mathbf{A}(\mathbf{r}, t) + \frac{e^2}{mc^2} \int d^3r \mathbf{A}(\mathbf{r}, t) \hat{n}(\mathbf{r}) \mathbf{A}(\mathbf{r}, t). \end{aligned} \quad (2.22)$$

For each value of \mathbf{r} and up to linear order in \mathbf{A} the perturbation is of the form $\hat{H}_{\text{ext}}(t) = F(t)\hat{B}$ with a time dependent function $F(t)$ and an operator \hat{B} which does not explicitly depend on time. This is a very useful fact because it allows us to move time dependent factors back and forth without consideration of commutation relations. Via Fourier transform the integral in Eq. (2.22) can be performed to yield:

$$\begin{aligned} \hat{H}_{\text{ext}}(t) &= -\frac{1}{c} \frac{1}{\mathcal{V}^2} \int d^3r \sum_{\mathbf{k}\mathbf{k}'} e^{i(\mathbf{k}+\mathbf{k}')\cdot\mathbf{r}} \hat{\mathbf{J}}_{\mathbf{k}}(t) \mathbf{A}_{\mathbf{k}'}(t) \\ &= -\frac{1}{c\mathcal{V}} \sum_{\mathbf{k}} \hat{\mathbf{J}}_{\mathbf{k}}(t) \mathbf{A}_{-\mathbf{k}}(t). \end{aligned} \quad (2.23)$$

We can also employ Fourier transform to change from the time variable t to frequency ω . In the frequency domain the electric field and vector potential are proportional to each other:

$$\begin{aligned} \mathbf{E}_{\mathbf{k}}(\omega) &= \int_{-\infty}^{\infty} dt e^{i(\omega+i\eta)t} \int d^3r e^{-i\mathbf{k}\cdot\mathbf{r}} \mathbf{E}(\mathbf{x}, t) \\ &= -\frac{1}{c} \int_{-\infty}^{\infty} dt e^{i(\omega+i\eta)t} \dot{\mathbf{A}}_{\mathbf{k}}(t) \\ &= -\frac{1}{c} e^{i(\omega+i\eta)t} \mathbf{A}_{\mathbf{k}}(t) \Big|_{-\infty}^{\infty} + \frac{i\omega}{c} \int_{-\infty}^{\infty} dt e^{i(\omega+i\eta)t} \mathbf{A}_{\mathbf{k}}(t) \\ &= \frac{i\omega}{c} \mathbf{A}_{\mathbf{k}}(\omega). \end{aligned} \quad (2.24)$$

An infinitesimal small positive imaginary part η was added to the frequency in order to make the integral converge in the limit $t \rightarrow +\infty$. For $t \rightarrow -\infty$ the integrand vanishes because of the constraint that there should be no electric field in equilibrium according to Eq. (2.11).

2.1.2 Equilibrium Hamiltonian

The Hamiltonian of the system in equilibrium should contain all the interactions of the particles with each other and the interactions with impurities. However, our primary aim is to calculate the electric conductivity for metallic systems. In metallic systems the free electron model is applicable, which treats the electrons as a gas of non-interacting particles that move in the background of positively charged

ions. This is often a very good approximation and simplifies the calculations to a great extent [42]. For non-interacting electrons, which undergo impurity scattering, the equilibrium Hamiltonian assumes the form

$$\hat{H} = \hat{H}_0 + \hat{V}, \quad (2.25)$$

where $\hat{H}_0 = \sum_{\mathbf{k}\sigma} \varepsilon_{\mathbf{k}} a_{\mathbf{k}\sigma}^\dagger a_{\mathbf{k}\sigma}$ and \hat{V} is a single particle potential term. We consider the elastic scattering of electrons from N_i identical but randomly distributed impurities at positions \mathbf{R}_j :

$$\hat{V} = \sum_{j=1}^{N_i} v(\hat{\mathbf{r}} - \mathbf{R}_j). \quad (2.26)$$

For translation invariant systems it is most natural to express \hat{V} in momentum representation:

$$\begin{aligned} \langle \mathbf{k}' | \hat{V} | \mathbf{k} \rangle &= \int d^3r \int d^3r' \langle \mathbf{k}' | \mathbf{r} \rangle \langle \mathbf{r} | \hat{V} | \mathbf{r}' \rangle \langle \mathbf{r}' | \mathbf{k} \rangle \\ &= \frac{1}{\mathcal{V}} \int d^3r e^{-i(\mathbf{k}' - \mathbf{k}) \cdot \mathbf{r}} \sum_{j=1}^{N_i} v(\mathbf{r} - \mathbf{R}_j) \\ &= \frac{1}{\mathcal{V}} \sum_{j=1}^{N_i} \int d^3r e^{-i(\mathbf{k}' - \mathbf{k}) \cdot \mathbf{R}_j} e^{-i(\mathbf{k}' - \mathbf{k}) \cdot (\mathbf{r} - \mathbf{R}_j)} v(\mathbf{r} - \mathbf{R}_j) \\ &= \sum_{j=1}^{N_i} e^{-i(\mathbf{k}' - \mathbf{k}) \cdot \mathbf{R}_j} v_{\mathbf{k}' - \mathbf{k}}, \end{aligned} \quad (2.27)$$

and with this matrix element the potential can be written as:

$$\hat{V} = \sum_{\sigma} \sum_{\mathbf{k}\mathbf{k}'} \langle \mathbf{k}' | \hat{V} | \mathbf{k} \rangle a_{\mathbf{k}'\sigma}^\dagger a_{\mathbf{k}\sigma} = \sum_{\sigma} \sum_{\mathbf{k}\mathbf{k}'} \sum_{j=1}^{N_i} e^{-i(\mathbf{k}' - \mathbf{k}) \cdot \mathbf{R}_j} v_{\mathbf{k}' - \mathbf{k}} a_{\mathbf{k}'\sigma}^\dagger a_{\mathbf{k}\sigma}. \quad (2.28)$$

In summary, the system in equilibrium is described by the Hamiltonian

$$\hat{H} = \hat{H}_0 + \hat{V} = \sum_{\mathbf{k}\sigma} \varepsilon_{\mathbf{k}} a_{\mathbf{k}\sigma}^\dagger a_{\mathbf{k}\sigma} + \sum_{\sigma} \sum_{\mathbf{k}\mathbf{q}} \sum_{j=1}^{N_i} e^{-i\mathbf{q} \cdot \mathbf{R}_j} v_{\mathbf{q}} a_{\mathbf{k}+\mathbf{q},\sigma}^\dagger a_{\mathbf{k}\sigma}. \quad (2.29)$$

The equilibrium Hamiltonian \hat{H} cannot be solved easily although it is only bilinear in the operators $a_{\mathbf{k}\sigma}^\dagger$ and $a_{\mathbf{k}\sigma}$. The reason is that due to the random distribution of impurities the translation invariance of the system is broken. However, we have to average over all the possible microscopic different impurity configurations for practical calculations of macroscopic observables. The correct method of impurity averaging will be explained later in this chapter. By means of impurity averaging translational invariance will be recovered.

2.2 Linear response theory

In linear response theory one wishes to calculate the expectation value of an operator in non-equilibrium up to the first order in the perturbational field. For our purposes the perturbation can assumed to be of the following form:

$$\hat{H}_{\text{ext}}(t) = F(t) \hat{B}, \quad (2.30)$$

i.e., of the same form as in Eq. (2.22) up to linear order in the perturbation \mathbf{A} . In a preliminary step the density matrix $\hat{\rho}(t)$ has to be expressed in terms of the equilibrium density matrix $\hat{\rho}_{\text{eq}}$. This can be achieved by changing into the Heisenberg picture of the unperturbed system:

$$\hat{O}(t)_H = e^{i\hat{H}t} \hat{O} e^{-i\hat{H}t}. \quad (2.31)$$

The original operator \hat{O} is allowed to depend explicitly on time. Using the von Neumann equation Eq. (2.6) the time derivative of $\hat{\rho}(t)_H$ in the Heisenberg picture is

$$\begin{aligned} \dot{\hat{\rho}}(t)_H &= \frac{\partial}{\partial t} \left\{ e^{i\hat{H}t} \hat{\rho}(t) e^{-i\hat{H}t} \right\} \\ &= e^{i\hat{H}t} \left\{ i\hat{H} \hat{\rho}(t) + \dot{\hat{\rho}}(t) - i\hat{\rho}(t) \hat{H} \right\} e^{-i\hat{H}t} \\ &= e^{i\hat{H}t} \left\{ i\hat{H} \hat{\rho}(t) - i\hat{H}'(t) \hat{\rho}(t) + i\hat{H}'(t) \hat{\rho}(t) - i\hat{\rho}(t) \hat{H} \right\} e^{-i\hat{H}t} \\ &= -ie^{i\hat{H}t} [F(t) \hat{B}, \hat{\rho}(t)] e^{-i\hat{H}t} \\ &= -iF(t) [\hat{B}(t)_H, \hat{\rho}(t)_H]. \end{aligned} \quad (2.32)$$

This equation can be integrated and then iterated to yield:

$$\begin{aligned} \hat{\rho}(t)_H &= \rho(-\infty)_H + \int_{-\infty}^t dt' \dot{\hat{\rho}}(t')_H \\ &= \hat{\rho}_{\text{eq}} - i \int_{-\infty}^t dt' [\hat{B}(t')_H, \hat{\rho}(t')_H] F(t') \\ &\approx \hat{\rho}_{\text{eq}} - i \int_{-\infty}^t dt' [\hat{B}(t')_H, \hat{\rho}_{\text{eq}}] F(t') + \mathcal{O}(F). \end{aligned} \quad (2.34)$$

This expression for the density matrix is exact up to the linear order in $F(t)$, which is satisfactory for a weak perturbation or weak external fields. The preliminary aim to express the density matrix in terms of $\hat{\rho}_{\text{eq}}$ has been accomplished by changing into the Heisenberg picture. If we now change back into the original Schrödinger picture we obtain:

$$\begin{aligned} \hat{\rho}(t) &= e^{-i\hat{H}t} \hat{\rho}_{\text{eq}} e^{i\hat{H}t} - ie^{-i\hat{H}t} \int_{-\infty}^t dt' [\hat{B}(t')_H, \hat{\rho}_{\text{eq}}] F(t') e^{i\hat{H}t} \\ &= \hat{\rho}_{\text{eq}} - i \int_{-\infty}^t dt' [\hat{B}(t' - t)_H, \hat{\rho}_{\text{eq}}] F(t'), \end{aligned} \quad (2.35)$$

and the expectation value of an operator \hat{A} in non-equilibrium can be calculated via

$$\begin{aligned} \langle \hat{A} \rangle_t &= \text{Tr} \hat{\rho}(t) \hat{A} \\ &= \langle \hat{A} \rangle_{\text{eq}} - i \int_{-\infty}^t dt' \text{Tr} \hat{A} [\hat{B}(t' - t)_H, \hat{\rho}_{\text{eq}}] F(t'). \end{aligned} \quad (2.36)$$

This is already the so-called Kubo formula for linear response, but it is not in the form it is usually written. Using the cyclic invariance of the trace, the following identity

$$\begin{aligned} \text{Tr} \hat{A} [\hat{B}, \hat{C}] &= \text{Tr} \hat{A} (\hat{B} \hat{C} - \hat{C} \hat{B}) = \text{Tr} (\hat{A} \hat{B} \hat{C} - \hat{B} \hat{A} \hat{C}) \\ &= \text{Tr} [\hat{A}, \hat{B}] \hat{C} \end{aligned} \quad (2.37)$$

and the fact that $\hat{\rho}_{\text{eq}}$ commutes with \hat{H} ,

$$\begin{aligned}\text{Tr } \hat{A}\hat{B}(t-t)_H \hat{\rho}_{\text{eq}} &= \text{Tr } \hat{A} e^{i\hat{H}(t-t)} \hat{B} e^{-i\hat{H}(t-t)} \hat{\rho}_{\text{eq}} \\ &= \text{Tr } e^{-i\hat{H}(t-t)} \hat{A} e^{i\hat{H}(t-t)} \hat{B} \hat{\rho}_{\text{eq}} = \text{Tr } \hat{A}(t-t')_H \hat{B} \hat{\rho}_{\text{eq}},\end{aligned}\quad (2.38)$$

the expectation value from equation Eq. (2.36) can be manipulated to read

$$\begin{aligned}\langle \hat{A} \rangle_t &= \langle \hat{A} \rangle_{\text{eq}} - i \int_{-\infty}^t dt' \text{Tr}[\hat{A}(t-t')_H, \hat{B}] \hat{\rho}_{\text{eq}} F(t') \\ &= \langle \hat{A} \rangle_{\text{eq}} - i \int_{-\infty}^{\infty} dt' \Theta(t-t') \langle [\hat{A}(t-t')_H, \hat{B}] \rangle_{\text{eq}} F(t').\end{aligned}\quad (2.39)$$

In the last equation the step function $\Theta(t-t')$ was introduced,

$$\Theta(t-t') = \begin{cases} 1 & \text{for } t' < t, \\ 0 & \text{for } t' > t. \end{cases}\quad (2.40)$$

We notice that the linear response $\langle \delta \hat{A} \rangle_t = \langle \hat{A} \rangle_t - \langle \hat{A} \rangle_{\text{eq}}$ is a convolution integral in time for a perturbation of the form Eq. (2.30). Thus, it is natural to define the following correlation function:

$$\langle\langle \hat{A}\hat{B} \rangle\rangle(t) \equiv -i\Theta(t)\langle [\hat{A}(t)_H, \hat{B}] \rangle_{\text{eq}}, \quad \Leftrightarrow \quad \langle \delta \hat{A} \rangle_t = \int_{-\infty}^{\infty} dt' \langle\langle \hat{A}\hat{B} \rangle\rangle(t-t') F(t').\quad (2.41)$$

Via Fourier transform the convolution integral can be written as a product like in Eq. (2.9):

$$\langle \delta \hat{A} \rangle(\omega) = \langle\langle \hat{A}\hat{B} \rangle\rangle(\omega) F(\omega),\quad (2.42)$$

and accordingly

$$\langle \hat{A} \rangle(\omega) = \langle \hat{A} \rangle_{\text{eq}}(\omega) + \langle \delta \hat{A} \rangle(\omega) = \langle \hat{A} \rangle_{\text{eq}}(\omega) + \langle\langle \hat{A}\hat{B} \rangle\rangle(\omega) F(\omega).\quad (2.43)$$

This equation is the Kubo formula in the frequency domain. It provides the correct expectation value in non-equilibrium up to linear order $\mathcal{O}(F)$.

2.2.1 Kubo formula for the conductivity

In the context of the AHE the observable of interest is the current density operator $\hat{\mathbf{J}}$. According to Eq. (2.14) it can be written as

$$\hat{\mathbf{J}}(\mathbf{r}, t) = \hat{\mathbf{j}}(\mathbf{r}) - \frac{e^2}{mc} \mathbf{A}(\mathbf{r}, t) \hat{n}(\mathbf{r}).\quad (2.44)$$

In equilibrium the net charge current $\hat{\mathbf{j}}$ vanishes whereas the expectation value of the density operator \hat{n} is the electron density n :

$$\begin{aligned}\langle \hat{\mathbf{J}}(\mathbf{r}, t) \rangle_{\text{eq}} &= \langle \hat{\mathbf{j}}(\mathbf{r}) \rangle_{\text{eq}} - \frac{e^2}{mc} \mathbf{A}(\mathbf{r}, t) \langle \hat{n}(\mathbf{r}) \rangle_{\text{eq}} = -\frac{ne^2}{mc} \mathbf{A}(\mathbf{r}, t), \\ \langle \hat{\mathbf{J}}_{\mathbf{k}} \rangle_{\text{eq}}(\omega) &= \int_{-\infty}^{\infty} dt e^{i\omega t} \int d^3r e^{-i\mathbf{k}\cdot\mathbf{r}} \langle \hat{\mathbf{J}}(\mathbf{r}, t) \rangle_{\text{eq}} = -\frac{ne^2}{mc} \mathbf{A}_{\mathbf{k}}(\omega).\end{aligned}\quad (2.45)$$

From the perturbation \hat{H}_{ext} Eq. (2.23) we may consider only those terms which contain a single \mathbf{A} since the Kubo formula is exact just to the linear order in the perturbing field:

$$\hat{H}_{\text{ext}}(\omega) = -\frac{1}{c\mathcal{V}} \sum_{\mathbf{k}'} \hat{\mathbf{j}}_{\mathbf{k}'} \mathbf{A}_{-\mathbf{k}'}(\omega) + \mathcal{O}(\mathbf{A}^2). \quad (2.46)$$

$\hat{H}_{\text{ext}}(\omega)$ is of the form $\hat{H}_{\text{ext}}(\omega) = \sum_{\mathbf{k}'} F_{\mathbf{k}'}(\omega) \hat{B}_{\mathbf{k}'}$. Obviously the previous result Eq. (2.43) can be easily generalized to this kind of perturbation if we carry out the replacements $F(\omega) \rightarrow F_{\mathbf{k}'}(\omega)$, $\hat{B} \rightarrow \hat{B}_{\mathbf{k}'}$ and sum over the indices \mathbf{k}' . For the calculation of the expectation value of $\hat{\mathbf{J}}$ in momentum space we substitute $\hat{A} \rightarrow \hat{\mathbf{J}}_{\mathbf{k}}$, $\hat{B} \rightarrow \hat{\mathbf{j}}_{\mathbf{k}'}$ and $F(\omega) \rightarrow -1/(c\mathcal{V}) \mathbf{A}_{-\mathbf{k}'}(\omega)$ in Eq. (2.43) and keep only terms up to linear order in the vector potential $\mathbf{A}_{\mathbf{k}}$. The current operator enters twice since it is an integral part of both the current density operator $\hat{\mathbf{J}}_{\mathbf{k}}$ and the perturbation $\hat{H}_{\text{ext}}(\omega)$:

$$\langle \hat{\mathbf{J}}_{\mathbf{k}} \rangle(\omega) = -\frac{ne^2}{m\omega} \mathbf{A}_{\mathbf{k}}(\omega) - \frac{1}{c\mathcal{V}} \sum_{\mathbf{k}'} \langle \langle \hat{\mathbf{j}}_{\mathbf{k}} \hat{\mathbf{j}}_{\mathbf{k}'} \rangle \rangle(\omega) \mathbf{A}_{-\mathbf{k}'}(\omega) + \mathcal{O}(\mathbf{A}^2). \quad (2.47)$$

For the evaluation of the second term we make use of the symmetry properties of the system. Because of translational invariance the current-current correlation function depends only on the distance $\mathbf{r} - \mathbf{r}'$:

$$\begin{aligned} \langle \langle \mathbf{j}(\mathbf{r}) \mathbf{j}(\mathbf{r}') \rangle \rangle &= \frac{1}{\mathcal{V}^2} \sum_{\mathbf{k}\mathbf{k}'} e^{i\mathbf{k}\cdot\mathbf{r}} e^{i\mathbf{k}'\cdot\mathbf{r}'} \langle \langle \hat{\mathbf{j}}_{\mathbf{k}} \hat{\mathbf{j}}_{\mathbf{k}'} \rangle \rangle \\ &= \frac{1}{\mathcal{V}^2} \sum_{\mathbf{k}\mathbf{k}'} e^{i\mathbf{k}\cdot(\mathbf{r}-\mathbf{r}')} e^{i(\mathbf{k}'+\mathbf{k})\cdot\mathbf{r}'} \langle \langle \hat{\mathbf{j}}_{\mathbf{k}} \hat{\mathbf{j}}_{\mathbf{k}'} \rangle \rangle. \end{aligned} \quad (2.48)$$

Due to the exponential factors this is a function of $\mathbf{r} - \mathbf{r}'$ only if $\mathbf{k} = -\mathbf{k}'$, since then any reference to the absolute value of position \mathbf{r}' vanishes [42]:

$$\langle \langle \hat{\mathbf{j}}_{\mathbf{k}} \hat{\mathbf{j}}_{\mathbf{k}'} \rangle \rangle \propto \delta_{\mathbf{k},-\mathbf{k}'}. \quad (2.49)$$

Since the current-current correlation function $f(\mathbf{r}, \mathbf{r}') = \langle \langle \mathbf{j}(\mathbf{r}) \mathbf{j}(\mathbf{r}') \rangle \rangle$ shall depend only on the distance $\mathbf{r} - \mathbf{r}'$, the constant of proportionality in Eq. (2.49) can be directly obtained from the corresponding expressions of the Fourier transform:

$$\begin{aligned} f(\mathbf{r}, \mathbf{r}') &= \frac{1}{\mathcal{V}^2} \sum_{\mathbf{k}\mathbf{k}'} e^{i\mathbf{k}\cdot\mathbf{r}} e^{i\mathbf{k}'\cdot\mathbf{r}'} f_{\mathbf{k},\mathbf{k}'} \stackrel{!}{=} \tilde{f}(\mathbf{r} - \mathbf{r}') = \frac{1}{\mathcal{V}} \sum_{\mathbf{k}} e^{i\mathbf{k}\cdot(\mathbf{r}-\mathbf{r}')} \tilde{f}_{\mathbf{k}}, \\ \Rightarrow f_{\mathbf{k},\mathbf{k}'} &= \langle \langle \hat{\mathbf{j}}_{\mathbf{k}} \hat{\mathbf{j}}_{\mathbf{k}'} \rangle \rangle = \mathcal{V} \delta_{\mathbf{k},-\mathbf{k}'} \tilde{f}_{\mathbf{k}} = \mathcal{V} \delta_{\mathbf{k},-\mathbf{k}'} \langle \langle \hat{\mathbf{j}}_{\mathbf{k}} \hat{\mathbf{j}}_{-\mathbf{k}} \rangle \rangle. \end{aligned} \quad (2.50)$$

Furthermore, if we use the relation Eq. (2.24) between the vector potential \mathbf{A} and the electric field \mathbf{E} the formula Eq. (2.47) for the expectation value of the current density operator becomes:

$$\langle \hat{\mathbf{J}}_{\mathbf{k}} \rangle(\omega) = i \frac{ne^2}{m\omega} \mathbf{E}_{\mathbf{k}}(\omega) - \frac{1}{i\omega} \langle \langle \hat{\mathbf{j}}_{\mathbf{k}} \hat{\mathbf{j}}_{-\mathbf{k}} \rangle \rangle(\omega) \mathbf{E}_{\mathbf{k}}(\omega). \quad (2.51)$$

The constant of proportionality between the electric field and the current is defined to be the conductivity:

$$\begin{aligned} \langle \hat{J}_{\alpha} \rangle(\omega) &= \sum_{\beta} \sigma_{\alpha\beta}(\omega) E_{\beta}(\omega), \\ \sigma_{\alpha\beta}(\mathbf{k}, \omega) &= i \frac{ne^2}{m\omega} \delta_{\alpha\beta} - \frac{1}{i\omega} \langle \langle \hat{j}_{\alpha}(\mathbf{k}) \hat{j}_{\beta}(-\mathbf{k}) \rangle \rangle(\omega). \end{aligned} \quad (2.52)$$

Thus, the conductivity can be directly determined from the current-current correlation function. In the limit of a static, homogenous field one obtains the dc conductivity:

$$\sigma_{\alpha\beta} = \lim_{\omega \rightarrow 0} \lim_{\mathbf{k} \rightarrow 0} \sigma_{\alpha\beta}(\mathbf{k}, \omega). \quad (2.53)$$

The two limiting processes may not be interchanged because the limit $\omega \rightarrow 0$, $\mathbf{k} \neq 0$ describes a static but periodic electric field which would give rise to an unphysical charge build-up. In the limit $\mathbf{k} \rightarrow 0$ the operator $\hat{\mathbf{j}}$ is well defined. In the limit $\omega \rightarrow 0$ the divergent term $ine^2/(m\omega)$ is cancelled by an equally divergent $\hat{\mathbf{j}}$ term from the current-current correlation function. The current-current correlation function is commonly denoted $\Pi_{\alpha\beta}(\mathbf{k}, t)$:

$$\Pi_{\alpha\beta}(\mathbf{k}, t) = \langle\langle \hat{j}_\alpha(\mathbf{k}) \hat{j}_\beta(-\mathbf{k}) \rangle\rangle(t) = -i\Theta(t) \langle [\hat{j}_\alpha(\mathbf{k}, t)_H, \hat{j}_\beta(-\mathbf{k}, 0)] \rangle_{\text{eq}}, \quad (2.54)$$

and its Fourier transform is defined by

$$\Pi_{\alpha\beta}(\mathbf{k}, \omega) = \int_{-\infty}^{\infty} dt e^{i\omega t} \Pi_{\alpha\beta}(\mathbf{k}, t). \quad (2.55)$$

Since the dc conductivity $\sigma_{\alpha\beta}$ is a real quantity, it can be obtained from the current-current correlation function via

$$\sigma_{\alpha\beta} = \text{Re} \left[\lim_{\omega \rightarrow 0} \lim_{\mathbf{k} \rightarrow 0} \sigma_{\alpha\beta}(\mathbf{k}, \omega) \right] = -\text{Re} \left[\lim_{\omega \rightarrow 0} \lim_{\mathbf{k} \rightarrow 0} \frac{1}{i\omega} \Pi_{\alpha\beta}(\mathbf{k}, \omega) \right] = -\lim_{\omega \rightarrow 0} \lim_{\mathbf{k} \rightarrow 0} \frac{1}{\omega} \text{Im} \Pi_{\alpha\beta}(\mathbf{k}, \omega). \quad (2.56)$$

The remainder of this chapter addresses the question how $\Pi_{\alpha\beta}(\mathbf{k}, \omega)$ and consequently the AHE conductivity can be evaluated.

2.3 Correlation functions

It has been shown that for the calculation of the conductivity the current-current correlation function is of central importance. In general, one can define two different types of correlation functions, the so-called retarded and advanced correlation function:

$$\begin{aligned} C_{AB}^R(t) &= -i\Theta(t) \langle [\hat{A}(t)_H, \hat{B}]_{\mp} \rangle_{\text{eq}}, \\ C_{AB}^A(t) &= i\Theta(-t) \langle [\hat{A}(t)_H, \hat{B}]_{\mp} \rangle_{\text{eq}}. \end{aligned} \quad (2.57)$$

The sign convention is as follows: If \hat{A}, \hat{B} are bosonic operators choose the upper sign (-), if \hat{A}, \hat{B} are fermionic operators choose the lower sign (+):

$$\begin{aligned} c, c^\dagger, c^\dagger c c, c c c, \dots & \quad \text{fermionic operators,} \\ c^\dagger c, c^\dagger c^\dagger, c c c c, \dots & \quad \text{bosonic operators,} \\ [\hat{A}, \hat{B}]_- = [\hat{A}, \hat{B}] = \hat{A}\hat{B} - \hat{B}\hat{A} & \quad \text{commutator,} \\ [\hat{A}, \hat{B}]_+ = \{\hat{A}, \hat{B}\} = \hat{A}\hat{B} + \hat{B}\hat{A} & \quad \text{anticommutator.} \end{aligned} \quad (2.58)$$

Since the expectation value $\langle \dots \rangle_{\text{eq}}$ in the correlation functions is always meant to be taken with respect to equilibrium the subscript $_{\text{eq}}$ is henceforth omitted:

$$\langle \hat{A} \rangle \equiv \langle \hat{A} \rangle_{\text{eq}}. \quad (2.59)$$

From now on we measure single particle energies with respect to the chemical potential, i.e.:

$$\hat{H} \rightarrow \hat{H} - \mu N, \quad \hat{\rho}_{\text{eq}} \rightarrow \frac{1}{Z} e^{-\beta \hat{H}}. \quad (2.60)$$

For the investigation of the analytical properties of the correlation functions it is useful to introduce the Lehmann representation. In the Lehmann representation one uses the eigenstates $\{|n\rangle\}$ of the Hamiltonian \hat{H} as a basis set:

$$\hat{H}|n\rangle = E_n|n\rangle, \quad \rho_n \equiv \hat{\rho}_{\text{eq}}|n\rangle = \frac{1}{Z} e^{-\beta E_n}, \quad A_{nm} = \langle n|\hat{A}|m\rangle. \quad (2.61)$$

Inserting a unity matrix $\mathbf{1} = \sum_n |n\rangle\langle n|$ in the expectation value one obtains:

$$\begin{aligned} \langle [\hat{A}(t)_H, \hat{B}]_{\mp} \rangle &= \frac{1}{Z} \text{Tr} \left\{ e^{-\beta \hat{H}} e^{i\hat{H}t} \hat{A} e^{-i\hat{H}t} \hat{B} \mp e^{-\beta \hat{H}} \hat{B} e^{i\hat{H}t} \hat{A} e^{-i\hat{H}t} \right\} \\ &= \frac{1}{Z} \sum_{nm} \left\{ e^{-\beta E_n} A_{nm} B_{mn} e^{i(E_n - E_m)t} \mp e^{-\beta E_n} B_{nm} A_{mn} e^{i(E_m - E_n)t} \right\} \\ &= \sum_{nm} \rho_n \left\{ A_{nm} B_{mn} e^{i(E_n - E_m)t} \mp B_{nm} A_{mn} e^{i(E_m - E_n)t} \right\}, \end{aligned} \quad (2.62)$$

and the Fourier transform reads:

$$\begin{aligned} C_{AB}^R(\omega) &= -i \int_{-\infty}^{\infty} dt e^{i(\omega+i\eta)t} \Theta(t) \langle [\hat{A}(t)_H, \hat{B}]_{\mp} \rangle = -i \int_0^{\infty} dt e^{i(\omega+i\eta)t} \langle [\hat{A}(t)_H, \hat{B}]_{\mp} \rangle \\ &= \sum_{nm} \rho_n \left\{ \frac{A_{nm} B_{mn}}{E_n - E_m + \omega + i\eta} \mp \frac{B_{nm} A_{mn}}{E_m - E_n + \omega + i\eta} \right\}, \\ C_{AB}^A(\omega) &= i \int_{-\infty}^{\infty} dt e^{i(\omega-i\eta)t} \Theta(-t) \langle [\hat{A}(t)_H, \hat{B}]_{\mp} \rangle = i \int_{-\infty}^0 dt e^{i(\omega-i\eta)t} \langle [\hat{A}(t)_H, \hat{B}]_{\mp} \rangle \\ &= \sum_{nm} \rho_n \left\{ \frac{A_{nm} B_{mn}}{E_n - E_m + \omega - i\eta} \mp \frac{B_{nm} A_{mn}}{E_m - E_n + \omega - i\eta} \right\}. \end{aligned} \quad (2.63)$$

A positive infinitesimal η was added to the frequency ω in order to make the integrals converge in the limit $t \rightarrow \infty$ for the retarded correlation function. Similarly, the positive infinitesimal η was subtracted from the frequency ω for the advanced correlation function in order to make the integrals converge in the limit $t \rightarrow -\infty$. If $\hat{A} = \hat{B}^\dagger$ then it can be seen from the Lehmann representation that the two correlation functions are the complex conjugate of each other,

$$C_{AB}^A(\omega) = C_{AB}^R(\omega)^*. \quad (2.64)$$

The retarded and advanced correlation functions at non-zero temperature are most conveniently obtained in the imaginary time formalism where $\tau = it$. The Heisenberg picture in imaginary time is defined as follows:

$$\hat{A}(\tau)_H = e^{\tau \hat{H}} \hat{A} e^{-\tau \hat{H}}. \quad (2.65)$$

$\hat{A}(\tau)_H$ can always be distinguished from the ordinary Heisenberg picture $\hat{A}(t)_H$ due to the imaginary time argument. The imaginary time correlation function is defined as follows:

$$C_{AB}(\tau) = -\langle T_\tau \hat{A}(\tau)_H \hat{B} \rangle, \quad (2.66)$$

where T_τ is the imaginary time ordering operator:

$$T_\tau \hat{A}(\tau)_H \hat{B} = \begin{cases} \hat{A}(\tau)_H \hat{B} & \text{for } \tau > 0, \\ \pm \hat{B} \hat{A}(\tau)_H & \text{for } \tau < 0. \end{cases} \quad (2.67)$$

The sign change occurs whenever two fermionic operators are interchanged. Due to the symmetry relation $C_{AB}(\tau + \beta) = \pm C_{AB}(\tau)$ it is sufficient to introduce a discrete Fourier transform on the interval $0 < \tau < \beta$:

$$C_{AB}(i\omega_n) = \int_0^\beta d\tau e^{i\omega_n \tau} C_{AB}(\tau), \quad C_{AB}(\tau) = \frac{1}{\beta} \sum_n e^{-i\omega_n \tau} C_{AB}(i\omega_n), \quad (2.68)$$

where ω_n is denoted a Matsubara frequency:

$$\omega_n = \begin{cases} 2\pi n/\beta & \text{for } \hat{A}, \hat{B} \text{ bosonic,} \\ (2n+1)\pi/\beta & \text{for } \hat{A}, \hat{B} \text{ fermionic,} \end{cases} \quad (2.69)$$

and $n \in \mathbb{N}$. For bosons, $\exp(i\beta\omega_n) = +1$ while for fermions $\exp(i\beta\omega_n) = -1$. The Fourier transform of the imaginary time correlation function can be related to the retarded and advanced correlation functions by using the Lehmann representation again:

$$\begin{aligned} C_{AB}(i\omega_n) &= -\frac{1}{Z} \int_0^\beta d\tau e^{i\omega_n \tau} \text{Tr} e^{-\beta \hat{H}} e^{\hat{H} \tau} \hat{A} e^{-\hat{H} \tau} \hat{B} \\ &= -\frac{1}{Z} \int_0^\beta d\tau e^{i\omega_n \tau} \sum_{mm'} e^{-\beta E_m} e^{(E_m - E_{m'}) \tau} A_{mm'} B_{m'm} \\ &= -\frac{1}{Z} \sum_{mm'} e^{-\beta E_m} \frac{A_{mm'} B_{m'm}}{E_m - E_{m'} + i\omega_n} \left\{ e^{i\omega_n \beta} e^{\beta(E_m - E_{m'})} - 1 \right\} \\ &= -\frac{1}{Z} \sum_{mm'} \frac{A_{mm'} B_{m'm}}{E_m - E_{m'} + i\omega_n} \left\{ \pm e^{-\beta E_{m'}} - e^{-\beta E_m} \right\} \\ &= \sum_{mm'} \left\{ \rho_m \mp \rho_{m'} \right\} \frac{A_{mm'} B_{m'm}}{E_m - E_{m'} + i\omega_n} \\ &= \sum_{mm'} \rho_m \left\{ \frac{A_{mm'} B_{m'm}}{E_m - E_{m'} + i\omega_n} \mp \frac{B_{mm'} A_{m'm}}{E_{m'} - E_m + i\omega_n} \right\}. \end{aligned} \quad (2.70)$$

The Fourier transform of the imaginary time correlation function is analytic in the entire complex plane except for the real axis where it has a number of poles. Comparing the Lehmann representation of the imaginary time correlation function with Eq. (2.63) it can be seen that the retarded and advanced correlation functions can be obtained from $C_{AB}(i\omega)$ by performing the analytic continuation:

$$\begin{aligned} i\omega_n \rightarrow \omega + i\eta &\Rightarrow C_{AB}(i\omega_n) \rightarrow C_{AB}^R(\omega), \\ i\omega_n \rightarrow \omega - i\eta &\Rightarrow C_{AB}(i\omega_n) \rightarrow C_{AB}^A(\omega). \end{aligned} \quad (2.71)$$

Usually the eigenstates $\{|n\rangle\}$ of the Hamiltonian \hat{H} are not known. However, in our case it is feasible to decompose the Hamiltonian into a part \hat{H}_0 which can be solved and a perturbation \hat{V} ,

$$\hat{H} = \hat{H}_0 + \hat{V}. \quad (2.72)$$

In this case the imaginary time formalism allows for a solution of the correlation function by a systematic expansion in powers of \hat{V} . For this purpose one introduces the interaction picture in imaginary time,

$$\hat{A}(\tau)_I = e^{\tau\hat{H}_0} \hat{A} e^{-\tau\hat{H}_0}, \quad (2.73)$$

and the time evolution operator $\hat{U}(\tau, \tau')$:

$$\hat{U}(\tau, \tau') = e^{\tau\hat{H}_0} e^{-(\tau-\tau')\hat{H}} e^{-\tau'\hat{H}_0}. \quad (2.74)$$

We assume that $0 < \tau < \beta$. This assumption does not represent a restriction for practical calculations because it is the only case of interest for the Fourier transform in Eq. (2.68). Inserting a factor of unity at the appropriate places around the exponentials the correlation function can be written as a time ordered product of the operators \hat{A}, \hat{B} and the time evolution operator \hat{U} :

$$\begin{aligned} C_{AB}(\tau) &= -\frac{1}{Z} \text{Tr} e^{-\beta\hat{H}} e^{\tau\hat{H}} \hat{A} e^{-\tau\hat{H}} \hat{B} \\ &= -\frac{1}{Z} \text{Tr} \begin{matrix} \uparrow & & \uparrow & & \uparrow \\ e^{-\beta\hat{H}_0} & e^{(\beta-\tau)\hat{H}} & e^{\tau\hat{H}_0} & \hat{A} & e^{-\tau\hat{H}_0} & \hat{B} \\ \uparrow & & \uparrow & & \uparrow \end{matrix} \\ &= -\frac{1}{Z} \text{Tr} e^{-\beta\hat{H}_0} \hat{U}(\beta, \tau) \hat{A}(\tau)_I \hat{U}(\tau, 0) \hat{B}. \end{aligned} \quad (2.75)$$

Accordingly, the partition function may be expressed as

$$Z = \text{Tr} e^{-\beta\hat{H}} = \text{Tr} e^{-\beta\hat{H}_0} \hat{U}(\beta, 0). \quad (2.76)$$

It can be seen from Eq. (2.29) that in the framework of second quantization \hat{U} consists of an even number of creation and annihilation operators. Therefore no sign change occurs when we move \hat{U} to the right under the time ordering operator T_τ :

$$\hat{U}(\beta, \tau) \hat{A}(\tau)_I \hat{U}(\tau, 0) \hat{B} = T_\tau \hat{U}(\beta, \tau) \hat{U}(\tau, 0) \hat{A}(\tau)_I \hat{B} = T_\tau \hat{U}(\beta, 0) \hat{A}(\tau)_I \hat{B}. \quad (2.77)$$

If we combine these expressions it is possible to reformulate the imaginary time correlation function as an expectation value of the system without the perturbation \hat{V} ,

$$\begin{aligned} \langle \hat{A} \rangle_0 &= \text{Tr} \hat{\rho}_0 \hat{A} = \frac{1}{Z_0} \text{Tr} e^{-\beta\hat{H}_0} \hat{A}, \\ Z_0 &= \text{Tr} e^{-\beta\hat{H}_0}, \end{aligned} \quad (2.78)$$

namely

$$C_{AB}(\tau) = -\frac{\langle T_\tau \hat{U}(\beta, 0) \hat{A}(\tau)_I \hat{B} \rangle_0}{\langle T_\tau \hat{U}(\beta, 0) \rangle_0} = -\frac{\langle T_\tau \hat{S}(\beta) \hat{A}(\tau)_I \hat{B} \rangle_0}{\langle T_\tau \hat{S}(\beta) \rangle_0}, \quad (2.79)$$

where the $\hat{S}(\tau)$ -matrix is defined as

$$\hat{S}(\tau) \equiv \hat{U}(\tau, 0). \quad (2.80)$$

Thus, by means of the interaction picture we expressed the imaginary time correlation function as an expectation value $\langle \dots \rangle_0$ of the non-interacting system. Eq. (2.80) can be expanded in powers of \hat{V} if we

notice that \hat{S} obeys the differential equation

$$\partial_\tau \hat{S}(\tau) = \partial_\tau \hat{U}(\tau, 0) = \partial_\tau \left(e^{\tau \hat{H}_0} e^{-\tau \hat{H}} \right) = e^{\tau \hat{H}_0} (\hat{H}_0 - \hat{H}) e^{-\tau \hat{H}} = -\hat{V}(\tau)_I \hat{S}(\tau), \quad (2.81)$$

which is solved by integration and using $\hat{S}(0) = 1$:

$$\hat{S}(\tau) = 1 - \int_0^\tau d\tau' \hat{V}(\tau')_I \hat{S}(\tau'). \quad (2.82)$$

Iteration yields:

$$\begin{aligned} \hat{S}(\tau) &= 1 - \int_0^\tau d\tau_1 \hat{V}(\tau_1)_I + \int_0^\tau d\tau_1 \hat{V}(\tau_1)_I \int_0^{\tau_1} d\tau_2 \hat{V}(\tau_2)_I + \dots \\ &= \sum_{n=0}^{\infty} \frac{(-1)^n}{n!} \int_0^\tau d\tau_1 \dots \int_0^{\tau_{n-1}} d\tau_n T_\tau \hat{V}(\tau_1)_I \dots \hat{V}(\tau_n)_I, \end{aligned} \quad (2.83)$$

which can formally be written as

$$\hat{S}(\tau) = T_\tau \exp \left(- \int_0^\tau d\tau' \hat{V}(\tau')_I \right). \quad (2.84)$$

Inserting the \hat{S} matrix into Eq. (2.80) the correlation functions reads:

$$C_{AB}(\tau) = - \frac{\langle T_\tau e^{-\int_0^\beta d\tau' \hat{V}(\tau')_I} \hat{A}(\tau)_I \hat{B} \rangle_0}{\langle T_\tau e^{-\int_0^\beta d\tau \hat{V}(\tau)_I} \rangle_0}. \quad (2.85)$$

This expression is a very useful result. It shows that the imaginary time formalism allows for a systematic expansion of the correlation function in powers of \hat{V} .

2.3.1 Diagrammatic technique

In our case \hat{V} , \hat{A} and \hat{B} are single particle operators of the form:

$$\hat{V} = \sum_{nm} V_{nm} a_n^\dagger a_m, \quad \hat{A} = \sum_{nm} A_{nm} a_n^\dagger a_m, \quad \hat{B} = \sum_{nm} B_{nm} a_n^\dagger a_m. \quad (2.86)$$

When we insert these expressions into Eq. (2.85) it can be seen that we have to evaluate in the numerator and denominator terms like $\langle T_\tau \xi_1(\tau_1)_I \dots \xi_n(\tau_n)_I \rangle_0$, where $\xi(\tau)_I = e^{\tau \hat{H}_0} \xi e^{-\tau \hat{H}_0}$ and ξ is a creation or annihilation operator. Wick's theorem states that an expectation value of this type can be factorized into a product of single particle correlation functions [43]:

$$\langle T_\tau \xi_1(\tau_1)_I \dots \xi_n(\tau_n)_I \rangle_0 = \sum_{P_{i_n}} (\pm 1)^{P_{i_n}} \langle T_\tau \xi_{i_1}(\tau_{i_1})_I \xi_{i_2}(\tau_{i_2})_I \rangle_0 \dots \langle T_\tau \xi_{i_{n-1}}(\tau_{i_{n-1}})_I \xi_{i_n}(\tau_{i_n})_I \rangle_0, \quad (2.87)$$

where the sum runs over all permutations P_{i_n} of the indices i_n and P_{i_n} is the parity of the corresponding permutation. Since the pairing of the $\xi(\tau)$ is between the states of the non-interacting system, in which the particle number is conserved, only those single particle correlation functions on the right hand side of Eq. (2.87) are not zero which consist of a pair $\propto \langle a_n a_m^\dagger \rangle_0$ of creation and annihilation operators. According to Feynman we associate each such factor with a drawing:

$$-\langle T_\tau a_n(\tau)_I a_m^\dagger(\tau')_I \rangle_0 = \begin{array}{c} \tau' m \\ \longrightarrow \\ \tau n \end{array}. \quad (2.88)$$

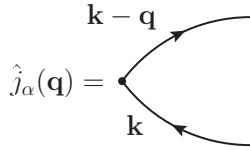
The very important linked cluster theorem states that when we apply Wick's theorem to Eq. (2.85) all the disconnected terms in the numerator and denominator cancel each other [44]. A drawing is said to be disconnected if it is not linked by a sequence of lines to the diagram itself. Moreover, for each diagram of order n in the potential \hat{V} there exist a number of topological identical diagrams which differ only in the labeling of internal indices. Sorting these contributions out one can show that

$$C_{AB}(\tau) = - \sum'_{n=0} (-1)^n \int_0^\beta d\tau_1 \cdots \int_0^\beta d\tau_n \langle T_\tau \hat{V}(\tau_1)_I \cdots \hat{V}(\tau_n)_I \hat{A}(\tau)_I \hat{B} \rangle_0, \quad (2.89)$$

where the dash on the sum symbol indicates that the sum runs over all topological different and connected diagrams exclusively [44]. For the calculation of the current-current correlation function from Eq. (2.54) in imaginary time the operators \hat{A} and \hat{B} have to be replaced with the current operator \hat{j} :

$$\Pi_{\alpha\beta}(\mathbf{q}, \tau) = - \sum'_{n=0} (-1)^n \int_0^\beta d\tau_1 \cdots \int_0^\beta d\tau_n \langle T_\tau \hat{V}(\tau_1)_I \cdots \hat{V}(\tau_n)_I \hat{j}_\alpha(\mathbf{q}, \tau)_I \hat{j}_\beta(-\mathbf{q}, 0) \rangle_0. \quad (2.90)$$


Besides Eq. (2.88) we need additional rules for the diagrammatical evaluation of $\Pi_{\alpha\beta}(\mathbf{q}, \tau)$, namely how to translate the current operator $\hat{j}_\mathbf{q}$ from Eq. (2.20) and the impurity potential \hat{V} from Eq. (2.27). We represent the current operator by the following vertex:



$$\hat{j}_\alpha(\mathbf{q}) =$$

$$\hat{j}_\mathbf{q} = \frac{e}{2m} \sum_{\mathbf{k}\sigma} (2\mathbf{k} - \mathbf{q}) a_{\mathbf{k}-\mathbf{q},\sigma}^\dagger a_{\mathbf{k}\sigma}, \quad (2.91)$$

and the impurity scattering by a scattering line:



$$\hat{V} = \sum_\sigma \sum_{\mathbf{k}\mathbf{q}} \sum_{j=1}^{N_i} e^{-i\mathbf{q}\cdot\mathbf{R}_j} v_\mathbf{q} a_{\mathbf{k}+\mathbf{q},\sigma}^\dagger a_{\mathbf{k}\sigma}. \quad (2.92)$$

If we insert the second quantization form for the operators into Eq. (2.90) and employ Wick's theorem, each term in the sum is just a product of functions of the type

$$g_{\mathbf{k}\sigma, \mathbf{k}'\sigma'}(\tau, \tau') = - \langle T_\tau a_{\mathbf{k}\sigma}(\tau)_I a_{\mathbf{k}'\sigma'}^\dagger(\tau')_I \rangle_0. \quad (2.93)$$

The expectation value $\langle \dots \rangle_0$ is evaluated with respect to the non-interacting Hamiltonian \hat{H}_0 from Eq. (2.29) which is diagonal in the basis $\{|\mathbf{k}\sigma\rangle\}$. For this reason we have in momentum representation $g_{\mathbf{k}\sigma, \mathbf{k}'\sigma'}(\tau, \tau') = g_{\mathbf{k}\sigma, \mathbf{k}\sigma}(\tau, \tau') \delta_{\mathbf{k}\mathbf{k}'} \delta_{\sigma\sigma'}$. Moreover, due to the cyclic invariance of the trace the function $g_{\mathbf{k}\sigma, \mathbf{k}\sigma}(\tau, \tau')$ is only a function of the imaginary time difference $\tau - \tau'$:

$$\begin{aligned} g_{\mathbf{k}\sigma, \mathbf{k}\sigma}(\tau, \tau') &= - \frac{1}{Z_0} \text{Tr} \left[e^{-\beta \hat{H}_0} e^{\tau \hat{H}_0} a_{\mathbf{k}\sigma} e^{-\tau \hat{H}_0} e^{\tau' \hat{H}_0} a_{\mathbf{k}\sigma}^\dagger e^{-\tau' \hat{H}_0} \right] \\ &= - \frac{1}{Z_0} \text{Tr} \left[e^{-\beta \hat{H}_0} e^{(\tau - \tau') \hat{H}_0} a_{\mathbf{k}\sigma} e^{-(\tau - \tau') \hat{H}_0} a_{\mathbf{k}\sigma}^\dagger \right] = g_{\mathbf{k}\sigma, \mathbf{k}\sigma}(\tau - \tau'). \end{aligned} \quad (2.94)$$

Since $g_{\mathbf{k}\sigma, \mathbf{k}\sigma}(\tau - \tau')$ depends only on a single time argument its Fourier transform can be defined as in the general case Eq. (2.68):

$$g_{\mathbf{k}\sigma, \mathbf{k}\sigma}(\tau - \tau') = \frac{1}{\beta} \sum_{i\omega_n} e^{-i\omega_n(\tau - \tau')} g_{\mathbf{k}\sigma, \mathbf{k}\sigma}(\omega_n), \quad g_{\mathbf{k}\sigma, \mathbf{k}\sigma}(\omega_n) = \int_0^\beta d\tau e^{i\omega_n \tau} g_{\mathbf{k}\sigma, \mathbf{k}\sigma}(\tau). \quad (2.95)$$

Remember that the difference $\omega_n - \omega_m$ of even or odd frequencies is always a bosonic frequency, hence

$\exp[i(\omega_n - \omega_m)\beta] = 1$ and the integrals over the internal time variables τ_i in Eq. (2.90) lead to a Kronecker- δ :

$$\frac{1}{\beta} \int_0^\beta d\tau e^{i(\omega_n - \omega_m)\tau} = \frac{1}{\beta} \left[e^{i(\omega_n - \omega_m)\tau} \frac{1}{i(\omega_n - \omega_m)} \right] \Big|_{\tau=0}^{\tau=\beta} = \delta_{\omega_n \omega_m}. \quad (2.96)$$

Eq. (2.96) means that energy conservation is secured at every vertex in the diagram. Since elastic scattering from impurities cannot change the momentum of the particles if we take the configurational average, momentum is also conserved in the diagram. This implies that every four momentum $(\mathbf{q}, i\omega_n)$ entering a diagram must also exit it. Thus, in frequency space the analogous equation of Eq. (2.90) for $\Pi_{\alpha\beta}(\mathbf{q}, i\omega_n)$ becomes just the sum of all topological different and connected diagrams that transfer the frequency $i\omega_n$ between two current vertices Eq. (2.91) and include any number of scattering events Eq. (2.92):

$$\begin{aligned} \Pi_{\alpha\beta}(\mathbf{q}, i\omega_n) = & \text{Diagram 1} + \text{Diagram 2} + \text{Diagram 3} + \text{Diagram 4} \\ & + \text{Diagram 5} + \text{Diagram 6} + \text{Diagram 7} + \text{Diagram 8} + \dots \end{aligned} \quad (2.97)$$

For clarity only the first diagram was labelled fully. The wiggly lines are only graphical tools that symbolize the external frequencies which are not summed over when evaluating the diagram.

2.3.2 Green's functions

The equilibrium Green's functions are defined as the single particle correlation functions

$$G(\tau) = -\langle T_\tau a_{\mathbf{k}\sigma}(\tau)_H a_{\mathbf{k}\sigma}^\dagger \rangle, \quad G_0(\tau) = -\langle T_\tau a_{\mathbf{k}\sigma}(\tau)_I a_{\mathbf{k}\sigma}^\dagger \rangle_0. \quad (2.98)$$

The Green's functions are very important quantities which we need to compute when we evaluate correlation functions using diagrammatic techniques. For example, the non-interacting or free Green's function $G_0(\tau)$ is just the sort of correlation function we encountered in the current-current correlation function above, $G_0(\tau) = g_{\mathbf{k}\sigma, \mathbf{k}\sigma}(\tau)$. Since we work with fermions, the creation and annihilation operators obey anti-commutation relations:

$$\{a_{\mathbf{k}\sigma}, a_{\mathbf{k}'\sigma'}^\dagger\} = \delta_{\mathbf{k}\mathbf{k}'} \delta_{\sigma\sigma'}, \quad \{a_{\mathbf{k}\sigma}, a_{\mathbf{k}'\sigma'}\} = 0, \quad \{a_{\mathbf{k}\sigma}^\dagger, a_{\mathbf{k}'\sigma'}^\dagger\} = 0. \quad (2.99)$$

Even in our simple model of non-interacting electrons in an impurity potential $G(\tau)$ is too difficult to compute. Consider the time derivative of the operator $a_{\mathbf{k}\sigma}(\tau)$:

$$\partial_\tau a_{\mathbf{k}\sigma}(\tau)_H = \partial_\tau \left(e^{\tau \hat{H}} a_{\mathbf{k}\sigma} e^{-\tau \hat{H}} \right) = e^{\tau \hat{H}} [\hat{H}, a_{\mathbf{k}\sigma}] e^{-\tau \hat{H}} = [\hat{H}, a_{\mathbf{k}\sigma}](\tau)_H. \quad (2.100)$$

Differentiating the single particle correlation function with respect to τ and using the the fact that the derivative of the step function is the δ -function yields the so-called equation of motion:

$$\begin{aligned} \partial_\tau G(\tau) = & -\partial_\tau \left[\Theta(\tau) \langle a_{\mathbf{k}\sigma}(\tau)_H a_{\mathbf{k}\sigma}^\dagger \rangle - \Theta(-\tau) \langle a_{\mathbf{k}\sigma}^\dagger a_{\mathbf{k}\sigma}(\tau)_H \rangle \right] \\ = & -\delta(\tau) \langle a_{\mathbf{k}\sigma} a_{\mathbf{k}\sigma}^\dagger + a_{\mathbf{k}\sigma}^\dagger a_{\mathbf{k}\sigma} \rangle - \langle T_\tau [\hat{H}, a_{\mathbf{k}\sigma}](\tau)_H a_{\mathbf{k}\sigma}^\dagger \rangle. \end{aligned} \quad (2.101)$$

If we evaluate the commutator $[\hat{H}, a_{\mathbf{k}\sigma}](\tau)_H$ we will just generate another Green's function. However, Eq. (2.101) can be used to calculate $G_0(\tau)$ which is obtained from the Hamiltonian $\hat{H}_0 = \sum_{\mathbf{k}\sigma} \varepsilon_{\mathbf{k}} a_{\mathbf{k}\sigma}^\dagger a_{\mathbf{k}\sigma}$. Using the identity

$$[\hat{A}\hat{B}, \hat{C}] = \hat{A}\hat{B}\hat{C} + \hat{A}\hat{C}\hat{B} - \hat{A}\hat{C}\hat{B} - \hat{C}\hat{A}\hat{B} = \hat{A}\{\hat{B}, \hat{C}\} - \{\hat{A}, \hat{C}\}\hat{B} \quad (2.102)$$

and the commutation relations Eq. (2.99) the commutator $[\hat{H}_0, a_{\mathbf{k}\sigma}] = -\varepsilon_{\mathbf{k}} a_{\mathbf{k}\sigma}$ is easy to evaluate and the equation of motion for $G_0(\tau)$ becomes

$$\partial_\tau G_0(\tau) = -\delta(\tau) - \varepsilon_{\mathbf{k}} G_0(\tau) \quad \Leftrightarrow \quad -i\omega_n G_0(i\omega_n) = -1 - \varepsilon_{\mathbf{k}} G_0(i\omega_n). \quad (2.103)$$

According to Eq. (2.71) the non-interacting retarded and advanced Green's function can be obtained from $G_0(i\omega_n)$ via analytic continuation:

$$G_0(i\omega_n) = \frac{1}{i\omega_n - \varepsilon_{\mathbf{k}}} \quad \Rightarrow \quad G_0^{R/A}(\omega) = \frac{1}{\omega - \varepsilon_{\mathbf{k}} \pm i\eta}. \quad (2.104)$$

Due to Wick's theorem any correlation function is equal to a sum of products of single particle correlation functions $G_0(\tau)$. The corresponding building blocks in the frequency domain are $G_0(i\omega)$.

2.4 Impurity averaging

We have already found out that the elastic scattering of electrons from N_i impurities at randomly distributed positions \mathbf{R}_j can be modeled by the potential Eq. (2.27):

$$\langle \mathbf{k}' | \hat{V} | \mathbf{k} \rangle = V(\mathbf{k}' - \mathbf{k}), \quad V(\mathbf{q}) = \sum_{j=1}^{N_i} e^{-i\mathbf{q}\cdot\mathbf{R}_j} v_{\mathbf{q}}. \quad (2.105)$$

We have to average over all possible positions of the impurities which are supposed to be uniformly distributed over the entire system. This averaging procedure is denoted the configurational average and will be indicated by an index $\langle \dots \rangle_c$. Any contribution to the Green's function of n -th order in \hat{V} contains n scattering events, but the scatterers need not necessarily be on n different scattering sites. All possible ways to scatter on p different impurities have to be considered where p is any number in the interval $1 \leq p \leq n$. The first order contribution is evaluated easily since we have only $p = 1$. For macroscopic systems the sum over impurity positions \mathbf{R}_j becomes the position average over the entire volume of the sample,

$$\left\langle \sum_{j=1}^{N_i} e^{-i\mathbf{q}\cdot\mathbf{R}_j} \right\rangle_c \equiv \frac{1}{\mathcal{V}} \int d^3 R_j \sum_{j=1}^{N_i} e^{-i\mathbf{q}\cdot\mathbf{R}_j} = N_i \delta_{\mathbf{q},0}. \quad (2.106)$$

The factor $\delta_{\mathbf{q}=0}$ means that the sum is zero unless $\mathbf{q} = 0$. Next we consider $n = 2$. If $p = 1$ the configurational average is the same as for $n = 1$ but for $p = 2$ we have to take into account that two different impurities cannot occupy the same impurity site. Hence, if the first impurity occupies any of the N_i impurity sites the second impurity can only occupy one of the $N_i - 1$ available sites:

$$\begin{aligned} \left\langle \sum_{i,j} e^{-i\mathbf{q}_1\cdot\mathbf{R}_i - i\mathbf{q}_2\cdot\mathbf{R}_j} \right\rangle_c &= \left\langle \sum_{i=j} e^{-i(\mathbf{q}_1+\mathbf{q}_2)\cdot\mathbf{R}_j} \right\rangle_c + \left\langle \sum_{i \neq j} e^{-i\mathbf{q}_1\cdot\mathbf{R}_i - i\mathbf{q}_2\cdot\mathbf{R}_j} \right\rangle_c \\ &= N_i \delta_{\mathbf{q}_1+\mathbf{q}_2=0} + N_i(N_i - 1) \delta_{\mathbf{q}_1,0} \delta_{\mathbf{q}_2,0}. \end{aligned} \quad (2.107)$$

However, since $N_i \gg 1$ we can write $N_i(N_i-1) \approx N_i^2$. The general result of the configurational averaging procedure of the n -th order term can be shown to be [45]

$$\left\langle \sum_{i_1, \dots, i_n} e^{-i \sum_{j=1}^n \mathbf{q}_j \cdot \mathbf{R}_{i_j}} \right\rangle_c \approx N_i \delta_{\Sigma_{\mathbf{q}}} + N_i^2 \delta_{\Sigma_{\mathbf{q}_1}} \delta_{\Sigma_{\mathbf{q}_2}} + N_i^3 \delta_{\Sigma_{\mathbf{q}_1}} \delta_{\Sigma_{\mathbf{q}_2}} \delta_{\Sigma_{\mathbf{q}_3}} + \dots, \quad (2.108)$$

where we have to make all possible combinations of distributing the \mathbf{q} -indices among the products of delta functions $\delta_{\Sigma_{\mathbf{q}}}$. For a Gaussian disorder model the single impurity potential is assumed to be short ranged and of the form $v(\mathbf{r}) = v_0 \delta(\mathbf{r})$. The Fourier transform of this potential is a constant, $v_{\mathbf{q}} = v_0/\mathcal{V}$, so that the configurational average of the first order contribution in the scattering potential yields

$$\langle V(\mathbf{q}) \rangle_c = n_i v_0 \delta_{\mathbf{q},0}. \quad (2.109)$$

In this expression, the number of impurities N_i per volume \mathcal{V} is the impurity concentration n_i . We will see below that $\langle V(\mathbf{q}) \rangle_c$ can be absorbed into the Hamiltonian and results in a simple shift of the energy levels. The first non trivial approximation stems from the second order contribution:

$$\langle V(\mathbf{q}_1)V(\mathbf{q}_2) \rangle_c = n_i^2 v_0^2 \delta_{\mathbf{q}_1,0} \delta_{\mathbf{q}_2,0} + n_i v_0^2 \delta_{\mathbf{q}_1+\mathbf{q}_2,0}. \quad (2.110)$$

2.4.1 Self-energy for Gaussian disorder

We expand the Green's function in powers of \hat{V} by means of the formula Eq. (2.89) with the replacement $\hat{A} = a_{\mathbf{k}\sigma}$ and $\hat{B} = a_{\mathbf{k}\sigma}^\dagger$. In frequency space we employ the same diagrammatic approach as reviewed for the calculation of the current-current correlation function at the end of Sec. (2.3.1) and establish the following additional rules:

- For each scattering event $n_i \delta_{\mathbf{q}=0}$ draw a vertex \otimes ,
- For each scattering amplitude v_0 draw a dashed line $-----$,
- For the Green's function $G(i\omega_n)$ draw a double line \Longrightarrow ,
- For the free Green's function $G_0(i\omega_n)$ draw a single line \longrightarrow ,
- Sum over all internal variables.

If we apply these rules to all the terms in the expansion of $G(i\omega_n)$ we end up with the following diagrammatic series:

$$\begin{aligned} \Longrightarrow &= \longrightarrow + \begin{array}{c} \otimes \\ | \\ \longrightarrow \end{array} + \begin{array}{c} \otimes \quad \otimes \\ | \quad | \\ \longrightarrow \quad \longrightarrow \end{array} + \begin{array}{c} \otimes \\ / \quad \backslash \\ \longrightarrow \quad \longrightarrow \end{array} \\ &+ \begin{array}{c} \otimes \quad \otimes \quad \otimes \\ | \quad | \quad | \\ \longrightarrow \quad \longrightarrow \quad \longrightarrow \end{array} + \begin{array}{c} \otimes \quad \otimes \\ | \quad | \\ \longrightarrow \quad \longrightarrow \end{array} + \begin{array}{c} \otimes \\ / \quad \backslash \\ \longrightarrow \quad \longrightarrow \end{array} + \begin{array}{c} \otimes \\ / \quad \backslash \\ \longrightarrow \quad \longrightarrow \end{array} + \dots \end{aligned} \quad (2.111)$$

All the infinitely many irreducible diagrams, i. e. those which have the G_0 lines removed at both ends and do not separate into two diagrams by cutting a single G_0 line, can be grouped into the so-called self-energy diagram $\Sigma(i\omega_n) = \sum_{i=1}^{\infty} \Sigma^{(i)}(i\omega_n)$:

$$\Sigma = \begin{array}{c} \otimes \\ | \\ \circlearrowleft \end{array} + \begin{array}{c} \otimes \\ / \quad \backslash \\ \longrightarrow \quad \longrightarrow \end{array} + \begin{array}{c} \otimes \\ / \quad \backslash \\ \longrightarrow \quad \longrightarrow \\ \otimes \\ | \\ \longrightarrow \end{array} + \begin{array}{c} \otimes \\ / \quad \backslash \\ \longrightarrow \quad \longrightarrow \\ \otimes \quad \otimes \\ | \quad | \\ \longrightarrow \quad \longrightarrow \end{array} + \dots \quad (2.112)$$

By virtue of the self-energy the series Eq. (2.111) can be recast into a closed form. First we collect all the terms of the form $G_0 \Sigma^{(i)} G_0$, then all the terms $G_0 \Sigma^{(i)} G_0 \Sigma^{(j)} G_0$ and so on. All combinations of indices i, j, \dots have to be considered [46]:

$$G = G_0 + G_0 \Sigma G_0 + G_0 \Sigma G_0 \Sigma G_0 + \dots = G_0 + G_0 \Sigma [G_0 + G_0 \Sigma G_0 + \dots] = G_0 + G_0 \Sigma G. \tag{2.113}$$

Eq. (2.113) is the so-called Dyson equation. In terms of diagrams it can be written as



$$\tag{2.114}$$

and leads to the solution:


$$G(i\omega_n) = \frac{1}{[G_0(i\omega_n)]^{-1} - \Sigma(i\omega_n)} = \frac{1}{i\omega_n - \varepsilon_{\mathbf{k}} - \Sigma(i\omega_n)}. \tag{2.115}$$

We see that from the exact self-energy the exact Green's function may be obtained. However, in practice it is only feasible to approximate the exact self-energy by a few diagrams from the series Eq. (2.112). The self-energy in the lowest order approximation is a constant factor:

$$\Sigma(i\omega_n) = \begin{matrix} \otimes \\ \vdots \\ \otimes \end{matrix} = n_i v_0. \tag{2.116}$$

The effect of this self-energy term is simply a shift of the energy levels. If we adjust our energy scale appropriately the self-energy term can be absorbed into the definition of the chemical potential in Eq. (2.60), $\varepsilon_{\mathbf{k}} \rightarrow \varepsilon_{\mathbf{k}} - n_i v_0$, and has no consequences at all:

$$G(i\omega_n) = \frac{1}{i\omega_n - (\varepsilon_{\mathbf{k}} + n_i v_0)} \rightarrow \frac{1}{i\omega_n - \varepsilon_{\mathbf{k}}}. \tag{2.117}$$

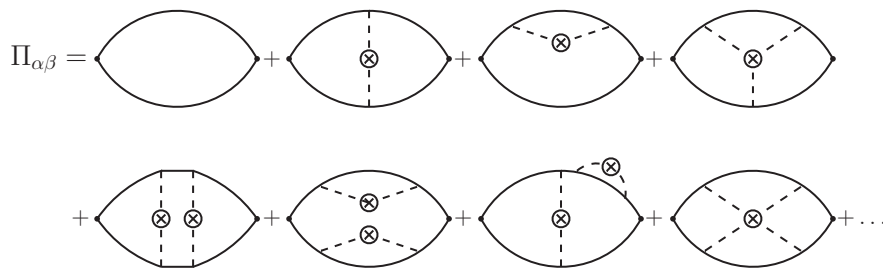
We only expect non-trivial effects to occur when we go to next higher order diagram  :

$$\Sigma(i\omega_n) = \frac{1}{\mathcal{V}} \sum_{\mathbf{k}} n_i v_0^2 G_0(i\omega_n) = \frac{1}{\mathcal{V}} \sum_{\mathbf{k}} \frac{n_i v_0^2}{i\omega_n - \varepsilon_{\mathbf{k}}}. \tag{2.118}$$

This approximation for the self-energy is known as the first order Born approximation.

2.5 Kubo-Středa formula

We now employ the diagrammatic technique to evaluate the current-current correlation function in frequency space, $\Pi_{\alpha\beta}(\mathbf{k}, i\omega_n)$. We have to draw all the diagrams that connect the two current vertices up to infinite order in the scattering potential \hat{V} , Eq. (2.97):



$$\tag{2.119}$$

A partial summation of these diagrams can be performed by replacing the free Green's functions $G_0(i\omega_n)$ with the full Green's functions $G(i\omega_n)$ which contain all the scattering events on the upper or lower fermion line respectively, e.g.

$$\text{Diagram} = \text{Diagram} + \text{Diagram} + \text{Diagram} + \text{Diagram} + \dots \quad (2.120)$$

When we replace the free Green's functions with the full Green's functions we are left with only those diagrams which connect the upper and lower fermion line:

$$\Pi_{\alpha\beta} = \text{Diagram} + \text{Diagram} + \text{Diagram} + \text{Diagram} + \dots \quad (2.121)$$

Next we collect the irreducible diagrams which contain all the possible ways to connect the upper and lower part of the conductivity bubble via an impurity scattering line in a diagram denoted \square :

$$\square = \text{Diagram} + \text{Diagram} + \text{Diagram} + \dots \quad (2.122)$$

We notice that in terms of \square the diagrammatic series Eq. (2.121) can be recast into the form

$$\Pi_{\alpha\beta} = \text{Diagram} + \text{Diagram} + \text{Diagram} + \dots \quad (2.123)$$

$$\equiv \text{Diagram}$$

In the last line the so-called vertex function was introduced. By definition it fulfills the self-consistent equation

$$\blacktriangleright = \bullet + \square \blacktriangleright, \quad (2.124)$$

where the unperturbed vertex \bullet is given by $e(2\mathbf{k} - \mathbf{q})/(2m)$, Eq. (2.91). However, as will be shown later, for an inversion symmetric system the vertex correction vanishes for the Gaussian disorder model.

In the limit $\mathbf{q} \rightarrow 0$, the current operators become $\hat{j}_\alpha(\mathbf{q}) \rightarrow e\hat{v}_\alpha$ according to Eq. (2.21) and the current-current correlation function can therefore be written as

$$\Pi_{\alpha\beta}(i\omega_n) = -e^2 \left\langle \text{Tr} \frac{1}{\beta} \sum_{ip_n} \hat{v}_\alpha G(ip_n) \hat{v}_\beta G(ip_n + i\omega_n) \right\rangle_c. \quad (2.125)$$

In this case the trace Tr stands for the summation over all states in the momentum space. The Green's function $G(z)$ is analytic for $z \notin \mathbb{R}$, but has poles along the real axis. In order to evaluate the frequency sum we define an auxiliary function

$$P(z, z + i\omega_n) = -e^2 \left\langle \text{Tr} \hat{v}_\alpha G(z) \hat{v}_\beta G(z + i\omega_n) \right\rangle_c, \quad (2.126)$$

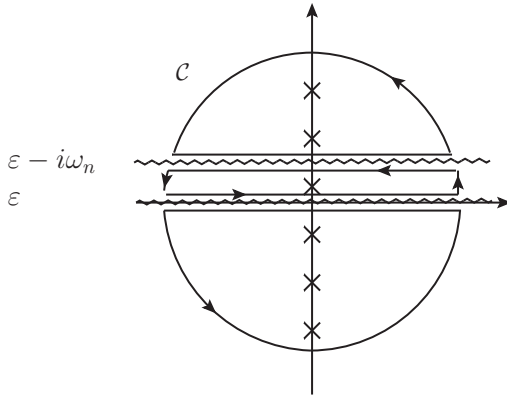


FIG. 2.1: Integration contour \mathcal{C} in the complex plane. The parts of the contour which are parallel to the real axis are shifted by an infinitesimal amount $i\eta$ away from $z = \varepsilon$ and $z = \varepsilon - i\omega_n$. All the poles of $f(z)$ lie on the imaginary axis.

in terms of which the current-current correlation function reads

$$\Pi_{\alpha\beta}(i\omega_n) = \frac{1}{\beta} \sum_{ip_n} P(ip_n, ip_n + i\omega_n). \quad (2.127)$$

$\Pi_{\alpha\beta}(z)$ is analytic in the entire complex plane except for $z = \varepsilon$ and $z = \varepsilon - i\omega_n$. To evaluate $\Pi_{\alpha\beta}(i\omega_n)$ we consider the integral

$$I = \int_{\mathcal{C}} dz f(z) P(z, z + i\omega_n), \quad f(z) = \frac{1}{e^{\beta z} + 1}, \quad (2.128)$$

where $f(z)$ is the Fermi function and the integration contour \mathcal{C} is depicted in Fig. (2.1). We shift the parts of the contour which are parallel to the real axis by an infinitesimal amount $\pm i\eta$ away from $z = \varepsilon$ and $z = \varepsilon - i\omega_n$, a procedure which leads to branch cuts in that region. The contour \mathcal{C} encloses all the poles $z = ip_n$ of the Fermi function along the imaginary axis but only regions where $P(z, z + i\omega_n)$ is analytic in z . Since the residue of $f(z)$ is given by $-1/\beta$, by means of the residue theorem the integral I can be evaluated as follows:

$$\begin{aligned} \int_{\mathcal{C}} dz f(z) P(z, z + i\omega_n) &= 2\pi i \sum_{ip_n} \text{Res} [f(z) P(z, z + i\omega_n), ip_n] \\ &= -\frac{2\pi i}{\beta} \sum_{ip_n} P(ip_n, ip_n + i\omega_n). \end{aligned} \quad (2.129)$$

Since the integrand vanishes in the limit $|z| \rightarrow \infty$ the semi-circles do not contribute to the integral if the contour is extended over the entire complex plane. Hence, we only have to consider the branch cuts which are shifted by an infinitesimal small distance $\pm i\eta$ away from $z = \varepsilon$ and $z = \varepsilon - i\omega_n$:

$$\begin{aligned} \Pi_{\alpha\beta}(i\omega_n) &= - \int \frac{d\varepsilon}{2\pi i} \text{Tr} \left\{ f(\varepsilon) [P(\varepsilon + i\eta, \varepsilon + i\omega_n) - P(\varepsilon - i\eta, \varepsilon + i\omega_n)] \right. \\ &\quad \left. + f(\varepsilon - i\omega_n) [P(\varepsilon - i\omega, \varepsilon + i\eta) - P(\varepsilon - i\omega, \varepsilon - i\eta)] \right\}. \end{aligned} \quad (2.130)$$

We have seen above that the retarded correlation function can be obtained from the imaginary time correlation function by the analytic continuation $i\omega_n \rightarrow \omega + i\eta$. Since $f(\varepsilon - i\omega_n) = f(\varepsilon)$ for bosonic frequencies ω_n we get

$$\begin{aligned} \Pi_{\alpha\beta}(\omega) &= e^2 \int \frac{d\varepsilon}{2\pi i} f(\varepsilon) \text{Tr} \left\{ \hat{v}_\alpha G^R(\varepsilon) \hat{v}_\beta G^R(\varepsilon + \omega) - \hat{v}_\alpha G^A(\varepsilon) \hat{v}_\beta G^R(\varepsilon + \omega) \right. \\ &\quad \left. + \hat{v}_\alpha G^A(\varepsilon - \omega) \hat{v}_\beta G^R(\varepsilon) - \hat{v}_\alpha G^A(\varepsilon - \omega) \hat{v}_\beta G^A(\varepsilon) \right\}_c. \end{aligned} \quad (2.131)$$

The dc conductivity $\sigma_{\alpha\beta}$ is a real quantity. According to Eq. (2.56) it can be calculated via

$$\sigma_{\alpha\beta} = \text{Re} \left[\lim_{\omega \rightarrow 0} \frac{-1}{i\omega} \Pi_{\alpha\beta}(\omega) \right] = - \lim_{\omega \rightarrow 0} \frac{1}{\omega} \text{Im} \Pi_{\alpha\beta}(\omega). \quad (2.132)$$

For small frequencies $\Pi_{\alpha\beta}(\omega)$ can be expanded into a Taylor series,

$$\Pi_{\alpha\beta}(\omega) \approx \Pi_{\alpha\beta}(0) + \left. \frac{\partial}{\partial \omega} \Pi_{\alpha\beta}(\omega) \right|_{\omega=0} \omega + \mathcal{O}(\omega^2). \quad (2.133)$$

Since $G^R(\varepsilon)$ and $G^A(\varepsilon)$ are the adjoint of each other the lowest order term of $\Pi_{\alpha\beta}(\omega)$ is entirely real and gives no contribution to the conductivity:

$$\Pi_{\alpha\beta}(0) \propto \int \frac{d\varepsilon}{2\pi i} f(\varepsilon) 2i \text{Im} G^R(\varepsilon) G^R(\varepsilon) \in \mathbb{R}. \quad (2.134)$$

On the other hand,

$$\begin{aligned} \left. \frac{\partial}{\partial \omega} \Pi_{\alpha\beta}(\omega) \right|_{\omega=0} &= e^2 \int \frac{d\varepsilon}{2\pi i} f(\varepsilon) \text{Tr} \left\langle \hat{v}_\alpha G^R(\varepsilon) \hat{v}_\beta \frac{\partial}{\partial \varepsilon} G^R(\varepsilon) - \hat{v}_\alpha G^A(\varepsilon) \hat{v}_\beta \frac{\partial}{\partial \varepsilon} G^R(\varepsilon) \right. \\ &\quad \left. - \hat{v}_\alpha \frac{\partial}{\partial \varepsilon} G^A(\varepsilon) \hat{v}_\beta G^R(\varepsilon) + \hat{v}_\alpha \frac{\partial}{\partial \varepsilon} G^A(\varepsilon) \hat{v}_\beta G^A(\varepsilon) \right\rangle_c, \end{aligned} \quad (2.135)$$

where the term in brackets is real since $\langle \dots \rangle^* = \langle \dots \rangle$. The expression $\langle \dots \rangle / (2\pi i)$ is therefore imaginary and yields using Eq. (2.132):

$$\begin{aligned} \sigma_{\alpha\beta} &= \frac{e^2}{2\pi\mathcal{V}} \int d\varepsilon f(\varepsilon) \text{Tr} \left\langle \hat{v}_\alpha G^R(\varepsilon) \hat{v}_\beta \partial_\varepsilon G^R(\varepsilon) - \hat{v}_\alpha G^A(\varepsilon) \hat{v}_\beta \partial_\varepsilon G^R(\varepsilon) \right. \\ &\quad \left. - \hat{v}_\alpha \partial_\varepsilon G^A(\varepsilon) \hat{v}_\beta G^R(\varepsilon) + \hat{v}_\alpha \partial_\varepsilon G^A(\varepsilon) \hat{v}_\beta G^A(\varepsilon) \right\rangle_c. \end{aligned} \quad (2.136)$$

This equation is the so-called Bastin formula, [47]. If one keeps only one half of this expression and performs an integration by parts on the other half, then several terms which contain a product of advanced and retarded Green's function cancel each other:

$$\begin{aligned} \sigma_{\alpha\beta} &= \frac{e^2}{4\pi\mathcal{V}} \int d\varepsilon f(\varepsilon) \text{Tr} \left\langle \hat{v}_\alpha G^R(\varepsilon) \hat{v}_\beta \partial_\varepsilon G^R(\varepsilon) - \hat{v}_\alpha G^A(\varepsilon) \hat{v}_\beta \partial_\varepsilon G^R(\varepsilon) \right. \\ &\quad \left. - \hat{v}_\alpha \partial_\varepsilon G^A(\varepsilon) \hat{v}_\beta G^R(\varepsilon) + \hat{v}_\alpha \partial_\varepsilon G^A(\varepsilon) \hat{v}_\beta G^A(\varepsilon) \right\rangle_c \\ &\quad - \frac{e^2}{4\pi\mathcal{V}} \int d\varepsilon f(\varepsilon) \text{Tr} \left\langle \hat{v}_\alpha \partial_\varepsilon G^R(\varepsilon) \hat{v}_\beta G^R(\varepsilon) - \hat{v}_\alpha \partial_\varepsilon G^A(\varepsilon) \hat{v}_\beta G^R(\varepsilon) \right. \\ &\quad \left. - \hat{v}_\alpha G^A(\varepsilon) \hat{v}_\beta \partial_\varepsilon G^R(\varepsilon) + \hat{v}_\alpha G^A(\varepsilon) \hat{v}_\beta \partial_\varepsilon G^A(\varepsilon) \right\rangle_c \\ &\quad - \frac{e^2}{4\pi\mathcal{V}} \int d\varepsilon \partial_\varepsilon f(\varepsilon) \text{Tr} \left\langle \hat{v}_\alpha G^R(\varepsilon) \hat{v}_\beta G^R(\varepsilon) - \hat{v}_\alpha G^A(\varepsilon) \hat{v}_\beta G^R(\varepsilon) \right. \\ &\quad \left. - \hat{v}_\alpha G^A(\varepsilon) \hat{v}_\beta G^R(\varepsilon) + \hat{v}_\alpha G^A(\varepsilon) \hat{v}_\beta G^A(\varepsilon) \right\rangle_c \\ &= - \frac{e^2}{4\pi\mathcal{V}} \int d\varepsilon f(\varepsilon) \text{Tr} \left\langle \hat{v}_\alpha \partial_\varepsilon G^R(\varepsilon) \hat{v}_\beta G^R(\varepsilon) - \hat{v}_\alpha G^R(\varepsilon) \hat{v}_\beta \partial_\varepsilon G^R(\varepsilon) \right. \\ &\quad \left. + \hat{v}_\alpha G^A(\varepsilon) \hat{v}_\beta \partial_\varepsilon G^A(\varepsilon) - \hat{v}_\alpha \partial_\varepsilon G^A(\varepsilon) \hat{v}_\beta G^A(\varepsilon) \right\rangle_c \\ &\quad - \frac{e^2}{4\pi\mathcal{V}} \int d\varepsilon \partial_\varepsilon f(\varepsilon) \text{Tr} \left\langle \hat{v}_\alpha G^R(\varepsilon) \hat{v}_\beta G^R(\varepsilon) + \hat{v}_\alpha G^A(\varepsilon) \hat{v}_\beta G^A(\varepsilon) \right\rangle_c \\ &\quad - \frac{e^2}{4\pi\mathcal{V}} \int d\varepsilon \partial_\varepsilon f(\varepsilon) \text{Tr} \left\langle -2\hat{v}_\alpha G^A(\varepsilon) \hat{v}_\beta G^R(\varepsilon) \right\rangle_c. \end{aligned} \quad (2.137)$$

Thus, the conductivity can be decomposed into three parts, [48]

$$\sigma_{\alpha\beta} = \sigma_{\alpha\beta}^{\text{Ia}} + \sigma_{\alpha\beta}^{\text{Ib}} + \sigma_{\alpha\beta}^{\text{II}}. \quad (2.138)$$

In the zero temperature limit, where $\partial_\varepsilon f(\varepsilon) = -\delta(\varepsilon - \varepsilon_F)$, the first two contributions read:

$$\begin{aligned} \sigma_{\alpha\beta}^{\text{Ia}} &= -\frac{e^2}{2\pi\mathcal{V}} \text{Tr}\langle \hat{v}_\alpha G^A(\varepsilon_F) \hat{v}_\beta G^R(\varepsilon_F) \rangle_c, \\ \sigma_{\alpha\beta}^{\text{Ib}} &= \frac{e^2}{4\pi\mathcal{V}} \text{Tr}\langle \hat{v}_\alpha G^R(\varepsilon_F) \hat{v}_\beta G^R(\varepsilon_F) + \text{h.c.} \rangle_c. \end{aligned} \quad (2.139)$$

$\sigma_{\alpha\beta}^{\text{Ia}}$ and $\sigma_{\alpha\beta}^{\text{Ib}}$ have to be evaluated at the Fermi level. The third contribution is a so-called Fermi sea integral:

$$\sigma_{\alpha\beta}^{\text{II}} = \frac{e^2}{4\pi\mathcal{V}} \int_{-\infty}^{\infty} d\varepsilon f(\varepsilon) \text{Tr}\langle \hat{v}_\alpha G^R(\varepsilon) \hat{v}_\beta \partial_\varepsilon G^R(\varepsilon) - \hat{v}_\alpha \partial_\varepsilon G^R(\varepsilon) \hat{v}_\beta G^R(\varepsilon) + \text{h.c.} \rangle_c. \quad (2.140)$$

These three equations constitute the Kubo-Středa formula. It is a formally exact equation and allows for a fully quantum mechanical calculation of the conductivity for the system of non-interacting particles interacting with an impurity potential. The only approximation has been that of linear response theory which is applicable to weak perturbing fields only. The drawback of the Kubo-Středa formula is that it is far from obvious to decide which parts in the decomposition Eq. (2.138) are important. Usually the part $\sigma_{\alpha\beta}^{\text{Ib}}$ is neglected [23], but we will see that for the AHE all parts have to be considered in general.

2.5.1 Weak disorder limit

For the calculation of the intrinsic- and the side jump contribution to the AHE we will consider only those terms in the Kubo-Středa formula which are of the lowest order in the impurity concentration n_i . For this purpose we will need the spectral density $A(\omega)$ which is defined as follows:

$$A(\omega) \equiv i[G^R(\omega) - G^A(\omega)] = -2 \text{Im} G^R(\omega) = -2 \text{Im} \frac{1}{\omega - \varepsilon_{\mathbf{k}} - \Sigma^R(\omega)}. \quad (2.141)$$

In the last term of the above equation we omitted the infinitesimal $i\eta$ since the self-energy $\Sigma^R(\omega)$ is already a complex quantity. In first order Born approximation the self-energy $\Sigma^R(\omega)$ is proportional to the impurity concentration n_i as can be explicitly seen in Eq. (2.118). Let us write $\Delta \equiv -\text{Im} \Sigma^R$ for the imaginary part of the self-energy. In the weak disorder limit where $n_i \rightarrow 0$ the imaginary part Δ vanishes and the spectral density becomes a delta function:

$$\begin{aligned} A(\omega) &= -2 \text{Im} \frac{1}{\omega - \varepsilon_{\mathbf{k}} - \text{Re} \Sigma^R(\omega) - i \text{Im} \Sigma^R(\omega)} \\ &= \frac{2\Delta}{(\omega - \varepsilon_{\mathbf{k}} - \text{Re} \Sigma^R(\omega))^2 + \Delta^2} \\ &\rightarrow 2\pi\delta(\omega - \varepsilon_{\mathbf{k}} - \text{Re} \Sigma^R(\omega)) \quad \text{for } \Delta \rightarrow 0. \end{aligned} \quad (2.142)$$

In the last line the real part of the self-energy can be absorbed into the definition of the energy level. Therefore, in the weak disorder limit we can replace the difference of the advanced and retarded Green's function with a δ -function,

$$A(\omega) = i[G^R(\omega) - G^A(\omega)] = 2\pi\delta(\omega - \varepsilon_{\mathbf{k}}). \quad (2.143)$$

2.5.2 Eigenstate representation

The Green's function in the basis $\{|\mathbf{k}\rangle\}$ is given by the expression Eq. (2.115),

$$G^R(\omega) = \frac{1}{\omega - \varepsilon_{\mathbf{k}} - \Sigma^R(\omega)}, \quad (2.144)$$

where $\varepsilon_{\mathbf{k}}$ is an eigenvalue of the Hamiltonian \hat{H}_0 . In a multi-band system each state is characterized by an additional quantum number, the band number n . The generalization of $G^R(\omega)$ to such a multi-band system in equilibrium is denoted with a subscript $_{\text{eq}}$. At each point \mathbf{k} in the Brillouin zone the matrix elements of the Hamiltonian in the basis $\{|n\mathbf{k}\rangle\}$ read $[H_0(\mathbf{k})]_{nm} = \langle n\mathbf{k}|\hat{H}_0|m\mathbf{k}\rangle$ and the Green's function assumes the matrix form

$$G_{\text{eq}}^R(\omega) = \frac{1}{\omega - H_0(\mathbf{k}) - \Sigma_{\text{eq}}^R(\omega)}. \quad (2.145)$$

The Hamiltonian is diagonalized by an unitary matrix U which consists of eigenvectors of H_0 :

$$\varepsilon_{\mathbf{k}} = U^\dagger(\mathbf{k})H_0(\mathbf{k})U(\mathbf{k}) = \begin{pmatrix} \varepsilon_{1\mathbf{k}} & & 0 \\ & \ddots & \\ 0 & & \varepsilon_{N\mathbf{k}} \end{pmatrix}. \quad (2.146)$$

$\varepsilon_{1\mathbf{k}}, \dots, \varepsilon_{N\mathbf{k}}$ are the eigenvalues of $\hat{H}_0(\mathbf{k})$. Any operator which is rotated into the basis of eigenstates of $\hat{H}_0(\mathbf{k})$ by the matrices U^\dagger and U is said to be in eigenstate representation. For example, consider the free Green's function in eigenstate representation:

$$G_{0,c}^R(\omega) = U^\dagger G_{0,\text{eq}}^R(\omega)U = \sum_n \frac{S_n}{\omega - \varepsilon_{n\mathbf{k}} + i\eta}, \quad (2.147)$$

where $[S_n]_{ij} = \delta_{ij}\delta_{in}$ is a diagonal matrix in the band indices. However, unlike the Hamiltonian and the free Green's function, an arbitrary operator will in general not assume diagonal form in eigenstate representation. For example, we decompose the self-energy into its diagonal part Σ_{d}^R and its off-diagonal part Σ_{nd}^R :

$$\Sigma_c^R(\omega) \equiv U^\dagger \Sigma_{\text{eq}}^R(\omega)U = \Sigma_{\text{d}}^R(\omega) + \Sigma_{\text{nd}}^R(\omega). \quad (2.148)$$

As usual the real part of the self-energy may be absorbed into the definition of the chemical potential, $\varepsilon_{n\mathbf{k}} \rightarrow \varepsilon_{n\mathbf{k}} + \text{Re} \Sigma_{\text{eq}}^R$. Hence, only the imaginary part needs to be considered. The formula Eq. (2.118) for the self-energy can readily be generalized to the multi-band system if we replace the free Green's function G_0^R with its correspondent function $G_{0,\text{eq}}^R$. Upon impurity averaging we obtain:

$$\begin{aligned} \Sigma_{\text{eq}}^R(\omega) &= i \text{Im} \Sigma_{\text{eq}}^R(\omega) = \frac{n_i v_0^2}{\mathcal{V}} \sum_{\mathbf{k}} \text{Im} G_{0,\text{eq}}^R(\omega) = \frac{n_i v_0^2}{\mathcal{V}} \sum_{\mathbf{k}} \text{Im} [UG_{0,c}^R(\omega)U^\dagger] \\ &= \frac{n_i v_0^2}{\mathcal{V}} \sum_{\mathbf{k}} \frac{1}{2i} [UG_{0,c}^R(\omega)U^\dagger - UG_{0,c}^A(\omega)U^\dagger] \\ &= \frac{n_i v_0^2}{\mathcal{V}} \sum_{\mathbf{k}} U \text{Im} [G_{0,c}^R(\omega)] U^\dagger. \end{aligned} \quad (2.149)$$

The imaginary part may be calculated by means of the Dirac identity:

$$\frac{1}{x \pm i\eta} = P\left(\frac{1}{x}\right) \mp i\pi\delta(x), \quad (2.150)$$

where $P\left(\frac{1}{x}\right)$ is the principal part. If we apply Dirac's identity to Eq. (2.147) we directly obtain

$$\Sigma_{\text{eq}}^R(\omega) = -i\pi \frac{n_i v_0^2}{\mathcal{V}} \sum_{n\mathbf{k}} U S_n U^\dagger \delta(\omega - \varepsilon_{n\mathbf{k}}), \quad \text{Im } \Sigma_{\text{eq}}^R(\omega) = -n_i v_0^2 \gamma(\omega). \quad (2.151)$$

It is important to note that the matrix $\gamma(\omega)$ does not depend on external parameters:

$$\gamma(\omega) = \frac{\pi}{\mathcal{V}} \sum_{n\mathbf{k}} U S_n U^\dagger \delta(\omega - \varepsilon_{n\mathbf{k}}). \quad (2.152)$$

Next, we define the diagonal Green's function according to

$$G_{\text{d}}^R(\omega) = \sum_n \frac{S_n}{\omega - \varepsilon_{n\mathbf{k}} - i \text{Im } \Sigma_{\text{d},n}^R(\omega)}, \quad \partial_\omega G_{\text{d}}^R(\omega) = \sum_n \frac{-S_n}{(\omega - \varepsilon_{n\mathbf{k}} - i \text{Im } \Sigma_{\text{d},n}^R(\omega))^2}, \quad (2.153)$$

where $\Sigma_{\text{d},n}^R = [\Sigma_{\text{d}}^R]_{nn}$. Using the relation $[AB]^{-1} = B^{-1}A^{-1}$ and the fact that U is unitary, the Green's function in eigenstate representation can be expanded in powers of G_{d}^R :

$$\begin{aligned} G_c^R(\omega) &= U^\dagger G_{\text{eq}}^R(\omega) U = [U^\dagger (\omega - \hat{H}_0(\mathbf{k}) - \Sigma_{\text{eq}}^R(\omega)) U]^{-1} = [\omega - \varepsilon_{\mathbf{k}} - \Sigma_c^R(\omega)]^{-1} \\ &= \left[(G_{\text{d}}^R(\omega))^{-1} - \Sigma_{\text{nd}}^R(\omega) \right]^{-1} = \left[(G_{\text{d}}^R(\omega))^{-1} [1 - G_{\text{d}}^R(\omega) \Sigma_{\text{nd}}^R(\omega)] \right]^{-1} \\ &= [1 - G_{\text{d}}^R(\omega) \Sigma_{\text{nd}}^R(\omega)]^{-1} G_{\text{d}}^R(\omega) \\ &= G_{\text{d}}^R(\omega) + G_{\text{d}}^R(\omega) \Sigma_{\text{nd}}^R(\omega) G_{\text{d}}^R(\omega) + \dots \end{aligned} \quad (2.154)$$

Eq. (2.154) is the Dyson equation for $G_c^R(\omega)$. For our calculations we will consider only those contributions up to the first order in $\Sigma_{\text{nd}}^R(\omega)$.

2.5.3 Derivation of intrinsic contribution

For the derivation of the intrinsic contribution, we directly start from the Bastin formula Eq. (2.136) and insert the impurity averaged Greens functions into it:

$$\begin{aligned} \sigma_{\alpha\beta}^{\text{int}} &= \frac{e^2}{2\pi\mathcal{V}} \sum_{\mathbf{k}} \int d\varepsilon f(\varepsilon) \text{Tr} \left\{ \hat{v}_\alpha [G_{\text{eq}}^R(\varepsilon) - G_{\text{eq}}^A(\varepsilon)] \hat{v}_\beta \partial_\varepsilon G_{\text{eq}}^R(\varepsilon) \right. \\ &\quad \left. - \hat{v}_\alpha \partial_\varepsilon G_{\text{eq}}^A(\varepsilon) \hat{v}_\beta [G_{\text{eq}}^R(\varepsilon) - G_{\text{eq}}^A(\varepsilon)] \right\}. \end{aligned} \quad (2.155)$$

For the intrinsic contribution we insert the lowest order approximation of the Green's function and rotate the velocity operator into eigenstate representation, $v_\alpha = U v_{c,\alpha} U^\dagger$:

$$G_{\text{eq}}^{R/A} = U G_c^{R/A} U^\dagger \approx U G_{\text{d}}^{R/A} U^\dagger + \mathcal{O}(\Sigma_{\text{nd}}^{R/A}). \quad (2.156)$$

Remember that the advanced and retarded Green's functions are complex conjugate of each other in frequency space. This yields:

$$\begin{aligned} \sigma_{\alpha\beta}^{\text{int}} &= \frac{e^2}{2\pi\mathcal{V}} \sum_{\mathbf{k}} \int d\varepsilon f(\varepsilon) 2 \text{Re} \text{Tr} \left\{ \hat{v}_{c,\alpha} [G_{\text{d}}^R(\varepsilon) - G_{\text{d}}^A(\varepsilon)] \hat{v}_{c,\beta} \partial_\varepsilon G_{\text{d}}^R(\varepsilon) \right\} \\ &= \frac{e^2}{2\pi\mathcal{V}} \sum_{\mathbf{k}} \int d\varepsilon f(\varepsilon) 2 \text{Re} \text{Tr} \left\{ \hat{v}_{c,\alpha} (-2\pi i) \sum_n S_n \delta(\varepsilon - \varepsilon_{n\mathbf{k}}) \hat{v}_{c,\beta} \partial_\varepsilon G_{\text{d}}^R(\varepsilon) \right\}. \end{aligned} \quad (2.157)$$

Using $\text{Re}(iz) = -\text{Im} z$ and Eq. (2.153) this expression can be written as:

$$\begin{aligned} & \text{Re Tr} \left\{ \hat{v}_{c,\alpha} (-2\pi i) \sum_n S_n \delta(\varepsilon - \varepsilon_{n\mathbf{k}}) \hat{v}_{c,\beta} \partial_\varepsilon G_d^R(\varepsilon) \right\} \\ &= 2\pi \text{Im Tr} \left\{ \hat{v}_{c,\alpha} \sum_n S_n \delta(\varepsilon - \varepsilon_{n\mathbf{k}}) \hat{v}_{c,\beta} \partial_\varepsilon G_d^R(\varepsilon) \right\} \\ &= -2\pi \text{Im Tr} \left\{ \hat{v}_{c,\alpha} \sum_n S_n \delta(\varepsilon - \varepsilon_{n\mathbf{k}}) \hat{v}_{c,\beta} \sum_m \frac{S_m}{(\varepsilon - \varepsilon_{m\mathbf{k}} - \Sigma_{d,m}^R(\varepsilon))^2} \right\} \end{aligned} \quad (2.158)$$

We keep only terms up to zero order in n_i :

$$\sigma_{\alpha\beta}^{\text{int}} = -2e^2 \text{Im} \frac{1}{\mathcal{V}} \sum_{\mathbf{k}} \sum_{nm} \text{Tr} \left\{ f(\varepsilon_{n\mathbf{k}}) \frac{\hat{v}_{c,\alpha} S_n \hat{v}_{c,\beta} S_m}{(\varepsilon_{n\mathbf{k}} - \varepsilon_{m\mathbf{k}})^2} \right\} \quad (2.159)$$

The trace can be evaluated as follows:

$$\begin{aligned} \text{Tr} \hat{v}_{c,\alpha} S_n \hat{v}_{c,\beta} S_m &= \sum_{a,b} \sum_{c,d} \langle a | \hat{v}_{c,\alpha} | b \rangle \langle b | S_n | c \rangle \langle c | \hat{v}_{c,\beta} | d \rangle \langle d | S_m | a \rangle \\ &= \sum_{a,b} \sum_{c,d} \langle a | \hat{v}_{c,\alpha} | b \rangle \delta_{bc} \delta_{bn} \langle c | \hat{v}_{c,\beta} | d \rangle \delta_{da} \delta_{dm} \\ &= \langle m | \hat{v}_{c,\alpha} | n \rangle \langle n | \hat{v}_{c,\beta} | m \rangle \end{aligned} \quad (2.160)$$

This yields:

$$\sigma_{\alpha\beta}^{\text{int}} = -2e^2 \text{Im} \frac{1}{\mathcal{V}} \sum_{\mathbf{k}} \sum_{nm} f(\varepsilon_{n\mathbf{k}}) \frac{\langle m | \hat{v}_{c,\alpha} | n \rangle \langle n | \hat{v}_{c,\beta} | m \rangle}{(\varepsilon_{n\mathbf{k}} - \varepsilon_{m\mathbf{k}})^2}. \quad (2.161)$$

For the zero temperature limit we consider the following reformulation:

$$\begin{aligned} \sigma_{\alpha\beta}^{\text{int}} &= -2e^2 \frac{1}{2i} \frac{1}{\mathcal{V}} \sum_{\mathbf{k}} \sum_{nm} f(\varepsilon_{n\mathbf{k}}) \frac{\langle m | \hat{v}_{c,\alpha} | n \rangle \langle n | \hat{v}_{c,\beta} | m \rangle - \langle m | \hat{v}_{c,\beta} | n \rangle \langle n | \hat{v}_{c,\alpha} | m \rangle}{(\varepsilon_{n\mathbf{k}} - \varepsilon_{m\mathbf{k}})^2} \\ &= -2e^2 \frac{1}{2i} \frac{1}{\mathcal{V}} \sum_{\mathbf{k}} \sum_{nm} [f(\varepsilon_{n\mathbf{k}}) - f(\varepsilon_{m\mathbf{k}})] \frac{\langle m | \hat{v}_{c,\alpha} | n \rangle \langle n | \hat{v}_{c,\beta} | m \rangle}{(\varepsilon_{n\mathbf{k}} - \varepsilon_{m\mathbf{k}})^2} \end{aligned} \quad (2.162)$$

In the limit of $T \rightarrow 0$ the valence band will be occupied and the conductance band is empty. Therefore, the difference $f(\varepsilon_{n\mathbf{k}}) - f(\varepsilon_{m\mathbf{k}})$ of Fermi functions will be equal to

$$f(\varepsilon_{n\mathbf{k}}) - f(\varepsilon_{m\mathbf{k}}) = \begin{cases} 1, & \text{if } n \in \text{valence band and } m \in \text{conductance band,} \\ -1, & \text{if } n \in \text{conductance band and } m \in \text{valence band,} \\ 0, & \text{else.} \end{cases} \quad (2.163)$$

After a few manipulations we obtain the form of σ^{int} in which it is usually written:

$$\begin{aligned} \sigma_{\alpha\beta}^{\text{int}} &= -2e^2 \frac{1}{2i} \frac{1}{\mathcal{V}} \sum_{\mathbf{k}} \left\{ \sum_n^{\text{occ}} \sum_m^{\text{emp}} \frac{\langle m | \hat{v}_{c,\alpha} | n \rangle \langle n | \hat{v}_{c,\beta} | m \rangle}{(\varepsilon_{n\mathbf{k}} - \varepsilon_{m\mathbf{k}})^2} - \sum_n^{\text{occ}} \sum_m^{\text{emp}} \frac{\langle m | \hat{v}_{c,\beta} | n \rangle \langle n | \hat{v}_{c,\alpha} | m \rangle}{(\varepsilon_{n\mathbf{k}} - \varepsilon_{m\mathbf{k}})^2} \right\} \\ &= -2e^2 \frac{1}{2i} \frac{1}{\mathcal{V}} \sum_{\mathbf{k}} \sum_n^{\text{occ}} \sum_m^{\text{emp}} \frac{\langle m | \hat{v}_{c,\alpha} | n \rangle \langle n | \hat{v}_{c,\beta} | m \rangle - \langle n | \hat{v}_{c,\alpha} | m \rangle \langle m | \hat{v}_{c,\beta} | n \rangle}{(\varepsilon_{n\mathbf{k}} - \varepsilon_{m\mathbf{k}})^2} \\ &= 2e^2 \text{Im} \frac{1}{\mathcal{V}} \sum_{\mathbf{k}} \sum_n^{\text{occ}} \sum_m^{\text{emp}} \frac{\langle n | \hat{v}_{c,\alpha} | m \rangle \langle m | \hat{v}_{c,\beta} | n \rangle}{(\varepsilon_{n\mathbf{k}} - \varepsilon_{m\mathbf{k}})^2}. \end{aligned} \quad (2.164)$$

2.5.4 Derivation of side jump contribution

For the side-jump conductivity take only the Fermi surface part of the Kubo-Středa formula:

$$\begin{aligned}\sigma_{\alpha\beta} &= \frac{e^2}{2\pi\mathcal{V}} \sum_{\mathbf{k}} \int d\varepsilon \partial_\varepsilon f(\varepsilon) \text{Tr} \left\{ \hat{v}_\alpha G_{\text{eq}}^A \hat{v}_\beta G_{\text{eq}}^R - \frac{1}{2} \left(\hat{v}_\alpha G_{\text{eq}}^R \hat{v}_\beta G_{\text{eq}}^R + \hat{v}_\alpha G_{\text{eq}}^A \hat{v}_\beta G_{\text{eq}}^A \hat{v}_\beta \right) \right\} \\ &= \frac{e^2}{2\pi\mathcal{V}} \sum_{\mathbf{k}} \int d\varepsilon \partial_\varepsilon f(\varepsilon) \text{Re Tr} \left\{ \hat{v}_\alpha G_{\text{eq}}^A \hat{v}_\beta G_{\text{eq}}^R - \hat{v}_\alpha G_{\text{eq}}^R \hat{v}_\beta G_{\text{eq}}^R \right\}\end{aligned}\quad (2.165)$$

Use eigenstate representation again. From the Dyson equation

$$G_c^{R/A} = G_d^{R/A} + G_d^{R/A} \Sigma_{\text{nd}}^{R/A} G_d^{R/A} + \dots \quad (2.166)$$

consider the terms containing the self-energy once:

$$\begin{aligned}\sigma_{\alpha\beta} &= \frac{e^2}{2\pi\mathcal{V}} \sum_{\mathbf{k}} \int d\varepsilon \partial_\varepsilon f(\varepsilon) \text{Re Tr} \left\{ \hat{v}_{c,\alpha} \left(G_d^A - G_d^R \right) \hat{v}_{c,\beta} G_d^R \Sigma_{\text{nd}}^R G_d^R \right\} \\ &= -\frac{e^2}{\mathcal{V}} \sum_{\mathbf{k}} \text{Re Tr} \left\{ i \hat{v}_{c,\alpha} \sum_n S_n \delta(\varepsilon_F - \varepsilon_{n\mathbf{k}}) \hat{v}_{c,\beta} G_d^R \Sigma_{\text{nd}}^R G_d^R \right\} = -\frac{e^2}{\mathcal{V}} \sum_{\mathbf{k}} \text{Re Tr} \Xi,\end{aligned}\quad (2.167)$$

where

$$\Xi = i \sum_n \sum_{mm'} \hat{v}_{c,\alpha} S_n \delta(\varepsilon_F - \varepsilon_{n\mathbf{k}}) \hat{v}_{c,\beta} \frac{S_m}{\varepsilon_{n\mathbf{k}} - \varepsilon_{m\mathbf{k}} - i \text{Im} \Sigma_{d,m}^R} \Sigma_{\text{nd}}^R \frac{S_{m'}}{\varepsilon_{n\mathbf{k}} - \varepsilon_{m'\mathbf{k}} - i \text{Im} \Sigma_{d,m'}^R} \quad (2.168)$$

Diagrammatically speaking, this contribution can be identified with the following diagrams:



$$(2.169)$$

Due to the special form of the S_n -matrices this expression can be simplified considerably. When evaluating the trace we have to sum over matrix elements of the form

$$[AS_n B]_{ij} = \sum_{ab} A_{ia} [S_n]_{ab} B_{bj} = \sum_{ab} A_{ia} B_{bj} \delta_{ab} \delta_{na} = A_{in} B_{nj}, \quad (2.170)$$

and likewise

$$[S_n A S_m]_{ij} = \sum_{ab} [S_n]_{ia} A_{ab} [S_m]_{bj} = \sum_{ab} \delta_{ia} \delta_{ni} A_{ab} \delta_{bj} \delta_{mb} = A_{ij} \delta_{in} \delta_{mj} = A_{nm} \delta_{in} \delta_{mj}. \quad (2.171)$$

We notice that the matrix S_n extracts the n -th row of a preceding matrix A and the n -th column of a subsequent matrix B in the above expressions. For the calculation of Ξ we have to evaluate the matrix elements of Σ_{nd}^R between S_m and $S_{m'}$,

$$[S_m \Sigma_{\text{nd}}^R S_{m'}]_{ij} = [\Sigma_{\text{nd}}^R]_{mm'} \delta_{im} \delta_{jm'}. \quad (2.172)$$

Since Σ_{nd}^R is an off-diagonal matrix, it follows that terms with $m = m'$ are identical to zero and do not give a contribution. For the calculation of the side-jump conductivity we are interested in those terms

which are of order $\mathcal{O}(n_i^0)$. Therefore, we consider in Ξ only the case where $n = m$ or $n = m'$. We will see that in the limit $n_i \rightarrow 0$ they do not depend on disorder:

$$\begin{aligned} \Xi &= i \sum_{n \neq m} \hat{v}_{c,\alpha} S_n \delta(\varepsilon_F - \varepsilon_{n\mathbf{k}}) \hat{v}_{c,\beta} \frac{S_n}{-i \operatorname{Im} \Sigma_{d,n}^R} \Sigma_{nd}^R \frac{S_m}{\varepsilon_{n\mathbf{k}} - \varepsilon_{m\mathbf{k}} - i \operatorname{Im} \Sigma_{d,m}^R} \\ &+ i \sum_{n \neq m} \hat{v}_{c,\alpha} S_n \delta(\varepsilon_F - \varepsilon_{n\mathbf{k}}) \hat{v}_{c,\beta} \frac{S_m}{\varepsilon_{n\mathbf{k}} - \varepsilon_{m\mathbf{k}} - i \operatorname{Im} \Sigma_{d,m}^R} \Sigma_{nd}^R \frac{S_n}{-i \operatorname{Im} \Sigma_{d,n}^R}. \end{aligned} \quad (2.173)$$

However, we want to replace the off-diagonal self-energy Σ_{nd}^R with the full self-energy Σ_c^R for which we know according to Eq. (2.148) and Eq. (2.151) that

$$\Sigma_c^R = U^\dagger \Sigma_{\text{eq}}^R U = iU^\dagger [\operatorname{Im} \Sigma_{\text{eq}}^R] U = -in_i v_0^2 U^\dagger \gamma U. \quad (2.174)$$

If we sum only over those indices with $n \neq m$ we can safely replace $[\Sigma_{nd}^R]_{nm}$ with $[\Sigma_c^R]_{nm}$, but if we let the sum over indices n and m run unrestricted we have to subtract the diagonal parts $[\Sigma_c^R]_{nn} = [\Sigma_d^R]_{nn}$,

$$\begin{aligned} [S_n \Sigma_{nd}^R S_m]_{ij} &= ([\Sigma_c^R]_{nm} - [\Sigma_d^R]_{nm} \delta_{nm}) \delta_{in} \delta_{jm} \\ &= [S_n \Sigma_c^R (1 - S_n) S_m]_{ij} = [S_n (1 - S_m) \Sigma_c^R S_m]_{ij}. \end{aligned} \quad (2.175)$$

This yields in the limit $n_i \rightarrow 0$:

$$\begin{aligned} \Xi &= \sum_{nm} \hat{v}_{c,\alpha} S_n \delta(\varepsilon_F - \varepsilon_{n\mathbf{k}}) \hat{v}_{c,\beta} \frac{-S_n \operatorname{Im} \Sigma_c^R}{-i \operatorname{Im} [\Sigma_c^R]_{nn}} \cdot \frac{(1 - S_n) S_m}{\varepsilon_{n\mathbf{k}} - \varepsilon_{m\mathbf{k}}} \\ &+ \sum_{nm} \hat{v}_{c,\alpha} S_n \delta(\varepsilon_F - \varepsilon_{n\mathbf{k}}) \hat{v}_{c,\beta} \frac{S_m (1 - S_n)}{\varepsilon_{n\mathbf{k}} - \varepsilon_{m\mathbf{k}}} \cdot \frac{-\operatorname{Im} \Sigma_c^R S_n}{-i \operatorname{Im} [\Sigma_c^R]_{nn}}. \end{aligned} \quad (2.176)$$

S_n is an idempotent matrix, i.e. $S_n S_n = S_n$. We will see in a later chapter that the diagonal elements of the velocity can be written as $\langle n | \hat{v}_{c,\alpha} | n \rangle = \partial_{k_\alpha} \varepsilon_{n\mathbf{k}}$. Therefore, the conductivity reads

$$\begin{aligned} \sigma_{\alpha\beta} &= \frac{e^2}{\mathcal{V}} \sum_{\mathbf{k}} \operatorname{Re} \operatorname{Tr} \sum_n \delta(\varepsilon_F - \varepsilon_{n\mathbf{k}}) S_n \partial_{k_\beta} \varepsilon_{n\mathbf{k}} \frac{\gamma_c}{[\gamma_c]_{nn}} (1 - S_n) i \sum_m \frac{S_m \hat{v}_{c,\alpha}}{\varepsilon_{n\mathbf{k}} - \varepsilon_{m\mathbf{k}}} \\ &- \frac{e^2}{\mathcal{V}} \sum_{\mathbf{k}} \operatorname{Re} \operatorname{Tr} \sum_n \delta(\varepsilon_F - \varepsilon_{n\mathbf{k}}) \partial_{k_\alpha} \varepsilon_{n\mathbf{k}} S_n i \sum_m \frac{\hat{v}_{c,\beta} S_m}{\varepsilon_{m\mathbf{k}} - \varepsilon_{n\mathbf{k}}} (1 - S_n) \frac{\gamma_c}{[\gamma_c]_{nn}}. \end{aligned} \quad (2.177)$$

We define the so-called Berry-connection matrix as follows:

$$[\mathcal{A}_\beta]_{ij} \equiv i \sum_m \frac{[\hat{v}_{c,\beta} S_m]_{ij}}{\varepsilon_{m\mathbf{k}} - \varepsilon_{i\mathbf{k}}} = i \sum_m \frac{[\hat{v}_{c,\beta}]_{im} \delta_{mj}}{\varepsilon_{m\mathbf{k}} - \varepsilon_{i\mathbf{k}}} = i \frac{[\hat{v}_{c,\beta}]_{ij}}{\varepsilon_{j\mathbf{k}} - \varepsilon_{i\mathbf{k}}}. \quad (2.178)$$

In terms of the Berry-connection matrix we can write:

$$\begin{aligned} \left[i S_n \sum_m \frac{\hat{v}_{c,\beta} S_m}{\varepsilon_{m\mathbf{k}} - \varepsilon_{n\mathbf{k}}} \right]_{ij} &= i \sum_m \frac{[\hat{v}_{c,\beta} S_m]_{nj}}{\varepsilon_{m\mathbf{k}} - \varepsilon_{n\mathbf{k}}} \delta_{in} = [S_n \mathcal{A}_\beta]_{ij}, \\ \left[i \sum_m \frac{S_m \hat{v}_{c,\alpha}}{\varepsilon_{n\mathbf{k}} - \varepsilon_{m\mathbf{k}}} S_n \right]_{ij} &= i \sum_m \frac{[S_m \hat{v}_{c,\alpha}]_{in}}{\varepsilon_{n\mathbf{k}} - \varepsilon_{m\mathbf{k}}} \delta_{nj} = i \sum_m \frac{[\hat{v}_{c,\alpha}]_{mn}}{\varepsilon_{n\mathbf{k}} - \varepsilon_{m\mathbf{k}}} \delta_{nj} \delta_{im} = i \frac{[\hat{v}_{c,\alpha}]_{in}}{\varepsilon_{n\mathbf{k}} - \varepsilon_{i\mathbf{k}}} \delta_{nj} \\ &= i \sum_m \frac{[\hat{v}_{c,\alpha}]_{im}}{\varepsilon_{m\mathbf{k}} - \varepsilon_{i\mathbf{k}}} \delta_{mn} \delta_{nj} = i \sum_m \frac{[\hat{v}_{c,\alpha} S_m]_{in}}{\varepsilon_{m\mathbf{k}} - \varepsilon_{i\mathbf{k}}} \delta_{nj} = [\mathcal{A}_\alpha S_n]_{ij}, \end{aligned} \quad (2.179)$$

and the conductivity simplifies to

$$\sigma_{\alpha\beta} = \frac{e^2}{\mathcal{V}} \sum_{n\mathbf{k}} \text{Re Tr} \delta(\varepsilon_F - \varepsilon_{n\mathbf{k}}) \left\{ \frac{\partial \varepsilon_{n\mathbf{k}}}{\partial k_\beta} \frac{\gamma_c}{[\gamma_c]_{nn}} (1 - S_n) \mathcal{A}_\alpha S_n - \frac{\partial \varepsilon_{n\mathbf{k}}}{\partial k_\alpha} S_n \mathcal{A}_\beta (1 - S_n) \frac{\gamma_c}{[\gamma_c]_{nn}} \right\}. \quad (2.180)$$

The conductivity does not contain diagonal elements of the Berry-connection matrix:

$$\begin{aligned} [(1 - S_n) \mathcal{A}_\alpha S_n]_{ij} &= [\mathcal{A}_\alpha]_{in} \delta_{nj} - \delta_{in} [\mathcal{A}_\alpha]_{nn} \delta_{nj} = [\mathcal{A}_\alpha]_{ij} \delta_{nj} (1 - \delta_{ij}), \\ [S_n \mathcal{A}_\beta (1 - S_n)]_{ij} &= [\mathcal{A}_\beta]_{nj} \delta_{in} - \delta_{in} [\mathcal{A}_\beta]_{nn} \delta_{nj} = [\mathcal{A}_\beta]_{ij} \delta_{in} (1 - \delta_{ij}). \end{aligned} \quad (2.181)$$

Since no non-diagonal elements occur, we can just as well set $[\mathcal{A}_\alpha]_{ii} = 0$ and avoid the singularities that occur in its original definition Eq. (2.178).

δ -function as a gradient

Consider the constant energy surface $S(\varepsilon_n)$ for each band and the unit vector \mathbf{n}_\perp perpendicular to the local surface element,

$$\mathbf{n}_\perp = \frac{\nabla_{\mathbf{k}} \varepsilon_n(\mathbf{k})}{|\nabla_{\mathbf{k}} \varepsilon_n(\mathbf{k})|}, \quad (2.182)$$

which allows to rewrite the \mathbf{k} -space volume element as

$$d^3 k = dS \mathbf{n}_\perp \cdot d\mathbf{k}_\perp = dS \frac{\nabla_{\mathbf{k}} \varepsilon_n(\mathbf{k})}{|\nabla_{\mathbf{k}} \varepsilon_n(\mathbf{k})|} \cdot d\mathbf{k}_\perp = dS \frac{1}{|\nabla_{\mathbf{k}} \varepsilon_n(\mathbf{k})|} d\varepsilon_n(\mathbf{k}). \quad (2.183)$$

It follows that the δ -function can be expressed as a gradient:

$$\int d^3 k \delta(E_F - \varepsilon_n(\mathbf{k})) = \int_{S(E_F)} \frac{dS}{|\nabla_{\mathbf{k}} \varepsilon_n(\mathbf{k})|}. \quad (2.184)$$

With this notation we can write the above formulae for the conductivity like in the paper of Kovalev *et al.* [17]. However, note that our expression for the side-jump is manifestly antisymmetric.

2.5.5 Vertex corrections

In this section we make up for the earlier claim that the vertex corrections vanish for an inversion symmetric system. For that purpose we make the approximation

$$\square \approx \otimes \quad (2.185)$$

In this approximation, the correct velocity \tilde{v}_α from the vertex diagram Eq. (2.5) can be written as the sum of the bare velocity \hat{v}_α and a correction $\delta\tilde{v}_\alpha$:

$$\triangleleft = \cdot + \otimes \triangleleft \quad (2.186)$$

$$\tilde{v}_\alpha = \hat{v}_\alpha + \delta\tilde{v}_\alpha, \quad (2.187)$$

where the corrections consist of a series of so-called ladder diagrams:

$$(2.188)$$

As usually, the ladder diagrams can be resummed to yield:

$$(2.189)$$

$$\delta\tilde{v}_\alpha(z, z') = \frac{n_i v_0^2}{\mathcal{V}} \sum_{\mathbf{k}} G(z) \hat{v}_\alpha G(z') + \frac{n_i v_0^2}{\mathcal{V}} \sum_{\mathbf{k}} G(z) \delta\tilde{v}_\alpha(z, z') G(z') \quad (2.190)$$

We replace the Green's functions by their eigenstate representation:

$$G_{\text{eq}}^{R/A} = U G_c^{R/A} U^\dagger, \quad G_c^{R/A} \approx G_d^{R/A} \quad (2.191)$$

This yields:

$$\begin{aligned} \frac{\delta\tilde{v}_\alpha}{n_i v_0^2} &= \sum_{\mathbf{k}} U G_d^R U^\dagger (\delta\tilde{v}_\alpha + \hat{v}_\alpha) U G_d^A U^\dagger \\ &= \frac{1}{\mathcal{V}} \sum_{nm} \sum_{\mathbf{k}} U \frac{S_n}{\omega_F - \omega_n - i[\text{Im} \Sigma_d^R]_{nn}} U^\dagger (\delta\tilde{v}_\alpha + \hat{v}_\alpha) U \frac{S_m}{\omega_F - \omega_m + i[\text{Im} \Sigma_d^R]_{mm}} U^\dagger \end{aligned} \quad (2.192)$$

The only way to get a contribution which diverges like $\mathcal{O}(1/(n_i v_0^2))$ is for $n = m$:

$$\begin{aligned} &\frac{1}{\omega_F - \omega_n - i[\text{Im} \Sigma_d^R]_{nn}} \cdot \frac{1}{\omega_F - \omega_n + i[\text{Im} \Sigma_d^R]_{nn}} = \\ &= \frac{1}{2 \text{Im}[\Sigma_d^R]_{nn}} \cdot \frac{2 \text{Im}[\Sigma_d^R]_{nn}}{(\omega_F - \omega_n)^2 + [\text{Im} \Sigma_d^R]_{nn}^2} \rightarrow \frac{\pi \delta(\omega_F - \omega_n)}{\text{Im}[\Sigma_d^R]_{nn}}, \end{aligned} \quad (2.193)$$

therefore

$$\begin{aligned} \frac{\delta\tilde{v}_\alpha}{n_i v_0^2} &= \sum_n \int \frac{d^3 k}{(2\pi)^3} U S_n U^\dagger \delta(\omega_F - \omega_n) (\delta\tilde{v}_\alpha + \hat{v}_\alpha) \frac{U S_n U^\dagger \pi}{n_i v_0^2 [\gamma_c]_{nn}} \\ &= \sum_n \int \frac{d^3 k}{(2\pi)^2} \frac{\delta(\varepsilon_n - \varepsilon_F) [U S_n U^\dagger \delta\tilde{v}_\alpha U S_n U^\dagger + U S_n U^\dagger \frac{\partial \varepsilon_n}{\partial k_\alpha}]}{2[\gamma_c]_{nn} n_i v_0^2} \end{aligned} \quad (2.194)$$

Vertex corrections $\delta\tilde{v}_\alpha$ vanish for an inversion-symmetric system in the Gaussian disorder model. This is because the inhomogeneity $\frac{\partial \varepsilon_n}{\partial k_\alpha}$ changes sign when \mathbf{k} is changed to $-\mathbf{k}$ and gives zero upon integration over \mathbf{k} . The only solution of the self-consistent equation Eq. (2.194) is then $\delta\tilde{v}_\alpha = 0$.

Ab initio methods

WE have seen that for the computation of the AHE conductivity we need at each point in the Brillouin zone the eigenvalues of the part of the Hamiltonian which describes the electrons. In other words, we need information about the electronic structure of the material. In this chapter it will be explained how the electronic structure of a bulk system can actually be calculated from *ab initio*, i.e. exclusively from the fundamental laws governing the physics of its basic constituents, the atoms. Our method of choice is density functional theory (DFT), which over the years has become the major tool for the calculation of ground-state properties of many-body systems. DFT usually provides the matrix elements of some operator in terms of Bloch functions. However, we will use these Bloch functions to construct a set of Wannier functions and employ the Wannier interpolation scheme to obtain the electronic structure at an arbitrary point in the Brillouin zone. Thus, by means of Wannier interpolation it is possible to calculate the AHE conductivity very accurately but at a relatively low computational cost.

3.1 Density functional theory

3.1.1 Kohn-Sham equations

In general, the many body Hamiltonian of a metallic system consists of five parts: The kinetic energy of the electrons and nuclei, the interaction between electrons and nuclei and the interaction of the electrons and nuclei among themselves. The interactions are caused by Coulomb repulsion and attraction. If there are N electrons and M nuclei with atomic number Z in the system, the Hamiltonian reads:

$$H_{\text{tot}} = \sum_{i=1}^N \frac{\mathbf{p}_i^2}{2m} + \sum_{I=1}^M \frac{\mathbf{p}_I^2}{2M_I} - \sum_{i=1}^N \sum_{I=1}^M \frac{Z_I e^2}{|\mathbf{r}_i - \mathbf{R}_I|} + \frac{1}{2} \sum_{i \neq j} \frac{e^2}{|\mathbf{r}_i - \mathbf{r}_j|} + \frac{1}{2} \sum_{I \neq J} \frac{Z_I Z_J e^2}{|\mathbf{R}_I - \mathbf{R}_J|}. \quad (3.1)$$

The corresponding wave function of the system is a function of the $N + M$ position coordinates \mathbf{r} for the electrons and \mathbf{R} for the nuclei. For real systems, the number of particles $N + M$ is of order $\mathcal{O}(10^{23})$ and the Schrödinger equation becomes way too difficult to solve. However, at this point the fact that the electrons are $\propto 10^4$ times lighter than the nuclei comes in handy. We can employ the Born-Oppenheimer approximation which states that due to the unequal masses of electrons and nuclei their motion is effectively decoupled, i.e. the motion of the nuclei is very inert and in comparison with the electron coordinates $\{\mathbf{r}_i\}$ the nuclei coordinates $\{\mathbf{R}_I\}$ can be considered as stationary. In this picture the kinetic energy of the nuclei is treated as a perturbation of the Hamiltonian for the electrons H and may be neglected in zero order approximation. H describes the motion of interacting electrons in the static potential of the M nuclei and the position coordinates $\{\mathbf{R}_I\}$ enter only as parameters:

$$\begin{aligned} H &= \sum_{i=1}^N \frac{\mathbf{p}_i^2}{2m} - \sum_{i=1}^N \sum_{I=1}^M \frac{Z_I e^2}{|\mathbf{r}_i - \mathbf{R}_I|} + \frac{1}{2} \sum_{i \neq j} \frac{e^2}{|\mathbf{r}_i - \mathbf{r}_j|} + \frac{1}{2} \sum_{I \neq J} \frac{Z_I Z_J e^2}{|\mathbf{R}_I - \mathbf{R}_J|} \\ &= \sum_{i=1}^N T_i + \sum_{i=1}^N V(\mathbf{r}_i) + \frac{1}{2} \sum_{i \neq j} W(\mathbf{r}_i, \mathbf{r}_j) + C. \end{aligned} \quad (3.2)$$

For a given set of parameters $\{\mathbf{R}_I\}$ a further simplification can be achieved if we try to solve for the electron density $n(\mathbf{r})$ rather than the electron wave function $\Psi(\mathbf{r}_1, \dots, \mathbf{r}_N)$. This is the key idea of DFT. Whereas the wave function depends on all the position coordinates of the N electrons, the density does not scale with the particle number and is a scalar function only,

$$\begin{aligned} n(\mathbf{r}) &= \langle \Psi | \sum_i \delta(\mathbf{r} - \mathbf{r}_i) | \Psi \rangle \\ &= \int d^3r_1 \dots \int d^3r_N \Psi^*(\mathbf{r}_1, \dots, \mathbf{r}_N) \sum_i \delta(\mathbf{r} - \mathbf{r}_i) \Psi(\mathbf{r}_1, \dots, \mathbf{r}_N). \end{aligned} \quad (3.3)$$

An important theorem by Hohenberg and Kohn states that the ground state energy of the system is a functional of the density alone and can be obtained by minimizing the energy with respect to $n(\mathbf{r})$, [49]. The energy functional $E\{n(\mathbf{r})\}$ can be decomposed into the three parts which arise from the kinetic energy of the electrons, their potential energy and their interaction energy:

$$E\{n(\mathbf{r})\} = \langle \Psi | H | \Psi \rangle = T\{n(\mathbf{r})\} + V\{n(\mathbf{r})\} + W\{n(\mathbf{r})\} + C. \quad (3.4)$$

For a given set of parameters $\{\mathbf{R}_I\}$ the interaction energy C among the nuclei is only a constant, but it is usually left in the energy functional to describe relaxation and structure optimization. Although the functional of the potential energy is simply

$$V\{n(\mathbf{r})\} = \sum_i \langle \Psi | V(\mathbf{r}_i) | \Psi \rangle = \int d^3r \sum_{i=1}^N V(\mathbf{r}) \langle \Psi | \delta(\mathbf{r} - \mathbf{r}_i) | \Psi \rangle = \int d^3r V(\mathbf{r}) n(\mathbf{r}), \quad (3.5)$$

the explicit dependency of the functionals $T\{n(\mathbf{r})\}$ and $W\{n(\mathbf{r})\}$ on the density $n(\mathbf{r})$ is not known. For the functional of the potential energy $W\{n(\mathbf{r})\}$ the usual approach to this problem consists in separating the so-called Hartree term $W_H\{n(\mathbf{r})\}$ from the other quantum contributions $W_{\#}\{n(\mathbf{r})\}$. The Hartree term has the form of the classical electrostatic interaction energy of a charge distribution with density $en(\mathbf{r})$:

$$\begin{aligned} W\{n(\mathbf{r})\} &= \frac{1}{2} \sum_{i \neq j} \langle \Psi | W(\mathbf{r}_i, \mathbf{r}_j) | \Psi \rangle = W_H\{n(\mathbf{r})\} + W_{\#}\{n(\mathbf{r})\} \\ &= \frac{e^2}{2} \int d^3r \int d^3r' \frac{n(\mathbf{r})n(\mathbf{r}')}{|\mathbf{r} - \mathbf{r}'|} + W_{\#}\{n(\mathbf{r})\}. \end{aligned} \quad (3.6)$$

A solution for the ground state energy can be found if we assume that the density $n(\mathbf{r})$ is simultaneously the ground state density of a hypothetical non-interacting electronic system which fulfills the Schrödinger equation

$$\left(-\frac{1}{2m} \nabla^2 + V_s(\mathbf{r}) \right) \psi_i(\mathbf{r}) = \varepsilon_i \psi_i(\mathbf{r}). \quad (3.7)$$

In terms of the wave functions $\psi_i(\mathbf{r})$ of the non-interacting system the complicated expression Eq. (3.3) for the density at position \mathbf{r} is simply the sum of the single particle densities $|\psi_i(\mathbf{r})|^2$,

$$n(\mathbf{r}) = \sum_{i=1}^N |\psi_i(\mathbf{r})|^2. \quad (3.8)$$

The functional of the kinetic energy becomes

$$T_s\{n(\mathbf{r})\} = -\frac{1}{2m} \sum_{i=1}^N \int d^3r \psi_i^*(\mathbf{r}) \nabla^2 \psi_i(\mathbf{r}). \quad (3.9)$$

Although the explicit dependency of the functional $T_s\{n(\mathbf{r})\}$ on the density is still not known it can be used as a suitable ansatz for the functional of the kinetic energy in Eq. (3.4). For this purpose we introduce the exchange-correlation functional $E_x\{n(\mathbf{r})\}$, which contains the corrections to the Hartree term for $W\{n(\mathbf{r})\}$ and the corrections to the kinetic energy $T_s\{n(\mathbf{r})\}$ for $T\{n(\mathbf{r})\}$:

$$E_x\{n(\mathbf{r})\} = [T\{n(\mathbf{r})\} - T_s\{n(\mathbf{r})\}] + [W\{n(\mathbf{r})\} - W_H\{n(\mathbf{r})\}]. \quad (3.10)$$

This leads us to the following exact equation:

$$E\{n(\mathbf{r})\} = -\frac{1}{2m} \sum_{i=1}^N \int d^3r \psi_i^*(\mathbf{r}) \nabla^2 \psi_i(\mathbf{r}) + \int d^3r V(\mathbf{r}) n(\mathbf{r}) + \frac{1}{2} \sum_{I \neq J} \frac{Z_I Z_J e^2}{|\mathbf{R}_I - \mathbf{R}_J|} + \frac{e^2}{2} \int d^3r \int d^3r' \frac{n(\mathbf{r}) n(\mathbf{r}')}{|\mathbf{r} - \mathbf{r}'|} + E_x\{n(\mathbf{r})\}. \quad (3.11)$$

For the ground state density $E\{n(\mathbf{r})\}$ has to be minimized as a functional of $n(\mathbf{r})$. Likewise we can minimize with respect to the function ψ_i^* under the constraint that it should be normalized. The method of Lagrange multipliers leads to the expression

$$\delta_{\psi_i^*} \left[E\{n(\mathbf{r})\} - \sum_{j=1}^N \varepsilon_j \left(\int d^3r |\psi_j|^2 - 1 \right) \right] = 0. \quad (3.12)$$

If we perform the functional derivative and use Eq. (3.8) this leads to a differential equation for the wave functions $\psi_i(\mathbf{r})$ [50]:

$$\left[-\frac{1}{2m} \nabla^2 + V(\mathbf{r}) + \int d^3r' \frac{e^2}{|\mathbf{r} - \mathbf{r}'|} n(\mathbf{r}') + \frac{\delta E_x\{n(\mathbf{r})\}}{\delta n(\mathbf{r})} \right] \psi_i(\mathbf{r}) = \varepsilon_i \psi_i(\mathbf{r}). \quad (3.13)$$

These equations are known as the Kohn-Sham equations. It can be seen by comparison with Eq. (3.7) that the wave functions $\psi_i(\mathbf{r})$ of the non-interacting system obey a single-particle Schrödinger equation in the presence of the effective potential

$$V_s(\mathbf{r}) = V(\mathbf{r}) + \int d^3r' \frac{e^2}{|\mathbf{r} - \mathbf{r}'|} n(\mathbf{r}') + \frac{\delta E_x\{n(\mathbf{r})\}}{\delta n(\mathbf{r})}. \quad (3.14)$$

The potential $V_s(\mathbf{r})$ contains not only the periodic potential due to the nuclei but also the interaction effects of the electrons. For the calculation of $V_s(\mathbf{r})$ we need the density $n(\mathbf{r})$ which depends on $\psi_i(\mathbf{r})$. Thus, to know the potential $V_s(\mathbf{r})$ we must know the wave functions $\psi_i(\mathbf{r})$. Since we need the potential $V_s(\mathbf{r})$ to know the wave functions the Kohn-Sham equations have to be solved self-consistently:

- We start from a suitable guess for the density $n(\mathbf{r})$ and calculate the corresponding effective potential from Eq. (3.14). The superposition of atomic densities may provide a suitable starting density at the very beginning of the self-consistency cycle.
- Then we solve Eq. (3.13) for the wave functions $\psi_i(\mathbf{r})$ and energies ε_i .
- From the $\psi_i(\mathbf{r})$ we calculate a new density $\tilde{n}(\mathbf{r}) = \sum_i |\psi_i(\mathbf{r})|^2$.
- If the densities $n(\mathbf{r})$ and $\tilde{n}(\mathbf{r})$ do not coincide we set $n(\mathbf{r}) \rightarrow \tilde{n}(\mathbf{r})$ as a new guess for the ground state density and repeat the above steps until self-consistency is achieved. Then we know the ground state density $n_0(\mathbf{r}) = n(\mathbf{r})$ and the ground state energy $E\{n_0(\mathbf{r})\}$.

In general, the Kohn-Sham eigenvalues ε_i and eigenstates $\psi_i(\mathbf{r})$ are not the true eigenvalues and eigenstates of the solid but only a tool for the calculation of the density $n(\mathbf{r})$. However, it is common practice to interpret the ε_i as one-electron states and obtain the electronic structure from them. This is often a

very good approximation and in fine agreement with experiment; if not, one has to go beyond standard DFT techniques.

3.1.2 Plane-wave basis set

We have seen that within the Kohn-Sham scheme the system of interacting electrons can be mapped onto a system of non-interacting electrons subject to the effective potential $V_s(\mathbf{r})$. To keep the notation simple, we drop the index s :

$$\left(-\frac{1}{2m}\nabla^2 + V(\mathbf{r})\right)\psi(\mathbf{r}) = \varepsilon\psi(\mathbf{r}). \quad (3.15)$$

In principle, this equation is exact and allows for a rigorous calculation of the ground state properties of the system. In a crystal $V(\mathbf{r})$ is a periodic function with the same periodicity as the Bravais lattice, i.e., for every lattice vector \mathbf{R} we have $V(\mathbf{r} + \mathbf{R}) = V(\mathbf{r})$. Due to the periodicity of $V_s(\mathbf{r})$ its Fourier transform can be written as a sum over the set of reciprocal lattice vectors \mathbf{G} that fulfill the equation $\exp(i\mathbf{G} \cdot \mathbf{R}) = 1$,

$$\begin{aligned} V(\mathbf{r}) &= \sum_{\mathbf{G}} e^{i\mathbf{G}\cdot\mathbf{r}} V_{\mathbf{G}}, \\ V_{\mathbf{G}} &= \frac{1}{\mathcal{V}} \int d^3r e^{-i\mathbf{G}\cdot\mathbf{r}} V(\mathbf{r}). \end{aligned} \quad (3.16)$$

We impose periodic boundary conditions on the system. The concrete choice of boundary conditions is immaterial in the limit $\mathcal{V} \rightarrow \infty$. Important is the fact that any function obeying the boundary conditions can be expanded in terms of plane waves [51],

$$\psi(\mathbf{r}) = \sum_{\mathbf{k}} c_{\mathbf{k}} e^{i\mathbf{k}\cdot\mathbf{r}}. \quad (3.17)$$

Inserting these expressions into Eq. (3.15) leads to the Schrödinger equation in Fourier space. The kinetic energy part becomes

$$-\frac{1}{2m}\nabla^2\psi(\mathbf{r}) = \sum_{\mathbf{k}} \frac{k^2}{2m} c_{\mathbf{k}} e^{i\mathbf{k}\cdot\mathbf{r}}, \quad (3.18)$$

and for the potential term we obtain

$$V(\mathbf{r})\psi(\mathbf{r}) = \sum_{\mathbf{G}} \sum_{\mathbf{k}} e^{i(\mathbf{G}+\mathbf{k})\cdot\mathbf{r}} V_{\mathbf{G}} c_{\mathbf{k}} = \sum_{\mathbf{G}} \sum_{\mathbf{q}} e^{i\mathbf{q}\cdot\mathbf{r}} V_{\mathbf{G}} c_{\mathbf{q}-\mathbf{G}}. \quad (3.19)$$

In the last term we change the summation index from \mathbf{q} to \mathbf{k} again so that the Schrödinger equation becomes

$$\sum_{\mathbf{k}} \frac{k^2}{2m} c_{\mathbf{k}} e^{i\mathbf{k}\cdot\mathbf{r}} + \sum_{\mathbf{G}} \sum_{\mathbf{k}} e^{i\mathbf{k}\cdot\mathbf{r}} V_{\mathbf{G}} c_{\mathbf{k}-\mathbf{G}} = \sum_{\mathbf{k}} \varepsilon c_{\mathbf{k}} e^{i\mathbf{k}\cdot\mathbf{r}}. \quad (3.20)$$

Finally we multiply this equation with $e^{-i\mathbf{k}'\cdot\mathbf{r}}$ from both sides and integrate over the volume \mathcal{V} of the crystal, a procedure which produces a $\delta_{\mathbf{k},\mathbf{k}'}$ so that the summation over the wave vectors yields the Schrödinger equation in momentum space:

$$\frac{k^2}{2m} c_{\mathbf{k}} + \sum_{\mathbf{G}} V_{\mathbf{G}} c_{\mathbf{k}-\mathbf{G}} = \varepsilon c_{\mathbf{k}}. \quad (3.21)$$

For fixed \mathbf{k} in the first Brillouin zone the set of equations for all reciprocal lattice vectors \mathbf{G} couples only those coefficients whose wave vectors differ by a reciprocal lattice vector. Therefore, for each \mathbf{k} the solution is a superposition of plane waves containing only \mathbf{k} and the wave vectors which differ from \mathbf{k} by a reciprocal wave vector. For a given \mathbf{k} the infinitely many solutions to the set of equations Eq. (3.21) are labelled with a band index n . Putting this information back into the ansatz of the wave function ψ we can write

$$\psi_{n\mathbf{k}}(\mathbf{r}) = \sum_{\mathbf{G}} c_{\mathbf{k}-\mathbf{G}} e^{i(\mathbf{k}-\mathbf{G})\cdot\mathbf{r}} = e^{i\mathbf{k}\cdot\mathbf{r}} u_{n\mathbf{k}}(\mathbf{r}), \quad (3.22)$$

with

$$u_{n\mathbf{k}}(\mathbf{r}) = \sum_{\mathbf{G}} c_{n,\mathbf{k}-\mathbf{G}} e^{-i\mathbf{G}\cdot\mathbf{r}}. \quad (3.23)$$

The $u_{n\mathbf{k}}(\mathbf{r})$ are clearly periodic functions because of $\exp(i\mathbf{G}\cdot\mathbf{R}) = 1$,

$$u_{n\mathbf{k}}(\mathbf{r} + \mathbf{R}) = \sum_{\mathbf{G}} c_{n,\mathbf{k}-\mathbf{G}} e^{-i\mathbf{G}(\mathbf{r}+\mathbf{R})} = \sum_{\mathbf{G}} c_{n,\mathbf{k}-\mathbf{G}} e^{-i\mathbf{G}\mathbf{r}} = u_{n\mathbf{k}}(\mathbf{r}). \quad (3.24)$$

Since the plane wave energy is $\propto (\mathbf{k} + \mathbf{G})^2$ the expansion series can be truncated after a few terms. The number of terms can be limited to the number of plane waves with energy lower than an energy cut-off E_{\max} ,

$$(\mathbf{k} + \mathbf{G})^2 \leq E_{\max}. \quad (3.25)$$

The correct choice of E_{\max} is determined by the desired accuracy of the calculation. A too large energy cut-off costs a lot of computing time while a too small energy cut-off leads to considerable errors for the quantities we wish to compute.

3.1.3 FLAPW method

In general, the wave function $\psi_{n\mathbf{k}}(\mathbf{r})$ with Bloch vector \mathbf{k} and band index n that solves the Kohn-Sham equation is sought of as a linear combination of suitable basis functions $\phi_m(\mathbf{k}, \mathbf{r})$,

$$\psi_{n\mathbf{k}}(\mathbf{r}) = \sum_m c_{nm}(\mathbf{k}) \phi_m(\mathbf{k}, \mathbf{r}). \quad (3.26)$$

The coefficients c_{nm} uniquely determine the wave function $\psi_{n\mathbf{k}}(\mathbf{r})$. The expansion of the wave function into plane waves $\phi_m(\mathbf{k}, \mathbf{r}) = \exp[i(\mathbf{k} + \mathbf{G}_m) \cdot \mathbf{r}]$ is one out of several possibilities to choose from. In some respect the choice of plane waves as a basis set is the most natural one. Plane waves are orthogonal to each other, easy to implement and using Fourier transform it is possible to work with the plane-wave basis set in momentum space. In particular, the part of the Hamiltonian describing the kinetic energy becomes diagonal in momentum space and can be computed very efficiently.

However, it turns out that a large number of plane waves is necessary to describe Bloch states accurately. The electrons must have high kinetic energies in the vicinity of the nucleus in order to compensate for the Coulomb attraction. Consequently, the wave functions oscillate rapidly in these regions and are not smooth, i.e., terms of higher order in the plane-wave expansion have to be considered and the energy cut-off has to be large. The sizable number of basis functions that is required makes the diagonalization of the Hamiltonian in terms of plane waves computationally demanding for most materials.

An alternative method consists in choosing so-called linear augmented plane-waves as basis set. In this approach the plane waves are replaced by a linear combination of radial functions and their energy derivatives in a region near the nuclei. The boundaries where the basis functions have different repre-

representations are defined by spheres, which are centered at each atom site. Their radius is often chosen to be nearly half the distance between nearest neighbor atoms, so that the spheres fill the greatest possible space that is available without overlap. The regions within the spheres are the so-called muffin-tins (MTs), while the remaining space is the so-called interstitial region. Accordingly, the basis functions $\phi_m(\mathbf{k}, \mathbf{r})$ for the expansion of the wave functions $\psi_{n\mathbf{k}}$ assume the form

$$\phi_{m'}(\mathbf{k}, \mathbf{r}) = \begin{cases} e^{i(\mathbf{k}+\mathbf{G}_{m'})\cdot\mathbf{r}}, & \text{interstitial region,} \\ \sum_{lm} [A_{lm}^{m'}(\mathbf{k})\varphi_l(\mathbf{r}) + B_{lm}^{m'}(\mathbf{k})\dot{\varphi}_l(\mathbf{r})] Y_{lm}(\tilde{\mathbf{r}}), & \text{muffin-tin sphere.} \end{cases} \quad (3.27)$$

In this equation $Y_{lm}(\tilde{\mathbf{r}})$ is a spherical harmonic with $\tilde{\mathbf{r}} = \mathbf{r}/r$. The function $\dot{\varphi}_l(r)$ is the energy derivative of $\varphi_l(r)$ that is a solution of the radial Schrödinger equation to the energy parameter ε_l [52]:

$$\left\{ -\frac{1}{2m} \nabla^2 + \frac{1}{2m} \frac{l(l+1)}{r^2} + V(r) - \varepsilon_l \right\} r\varphi_l(r) = 0, \quad (3.28)$$

and $V(r)$ is the radial component of the potential $V(\mathbf{r})$. The appropriate coefficients $A_{lm}^{m'}$ and $B_{lm}^{m'}$ in Eq. (3.27) are determined by the continuity of $\varphi_m(\mathbf{k}, \mathbf{r})$ and $\nabla\varphi_m(\mathbf{k}, \mathbf{r})$ at the boundary of the muffin-tin sphere. This way of dealing with the expansion of the wave functions $\psi_{n\mathbf{k}}$ is known as the full-potential linearized augmented plane-wave (FLAPW) method.

By common consensus the FLAPW method is regarded as the most accurate DFT method since no approximations for the wave functions or the potential are performed [53]. For the computation of the AHE conductivity we profit from the high accuracy since the ground state properties of transition metals like Fe, Co and Ni depend very sensitively on small energy differences due to spin-orbit coupling and magnetic order.

3.2 Basis sets

3.2.1 Bloch functions

According to Eq. (3.22), in Dirac notation the Bloch functions provided by DFT can be written as the product of a plane wave times a factor $|u_{n\mathbf{k}}\rangle$ that possesses the same periodicity as the Bravais lattice,

$$|\psi_{n\mathbf{k}}\rangle = e^{i\mathbf{k}\cdot\hat{\mathbf{r}}}|u_{n\mathbf{k}}\rangle. \quad (3.29)$$

We require the Bloch functions to be normalized with respect to the crystal volume \mathcal{V} :

$$\langle\psi_{n\mathbf{k}}|\psi_{n\mathbf{k}}\rangle \equiv \int_{\mathcal{V}} d^3r \psi_{n\mathbf{k}}^*(\mathbf{r})\psi_{n\mathbf{k}}(\mathbf{r}) = 1. \quad (3.30)$$

Then the Bloch functions obey the following orthogonality and completeness relations:

$$\langle\psi_{n\mathbf{k}}|\psi_{m\mathbf{k}'}\rangle = \delta_{nm}\delta_{\mathbf{k}\mathbf{k}'}, \quad 1 = \sum_{n\mathbf{k}} |\psi_{n\mathbf{k}}\rangle\langle\psi_{n\mathbf{k}}|. \quad (3.31)$$

It follows that at each \mathbf{k} the periodic part of the Bloch functions is also orthogonal:

$$\langle\psi_{n\mathbf{k}}|\psi_{m\mathbf{k}}\rangle = \langle u_{n\mathbf{k}}|u_{m\mathbf{k}}\rangle \stackrel{!}{=} \delta_{nm}\delta_{\mathbf{k}\mathbf{k}} \quad \Rightarrow \quad \langle u_{n\mathbf{k}}|u_{m\mathbf{k}}\rangle = \delta_{nm}. \quad (3.32)$$

However, in general we need not require the periodic part of the Bloch functions to be orthogonal at different points in the Brillouin zone,

$$\langle u_{n\mathbf{k}} | u_{m\mathbf{k}'} \rangle \neq \delta_{\mathbf{k}\mathbf{k}'} \delta_{nm}. \quad (3.33)$$

We have seen that for an eigenstate specified by band index n and wave vector \mathbf{k} the Kohn-Sham equation takes the form of a single-particle Schrödinger equation which reads

$$\hat{H}|\psi_{n\mathbf{k}}\rangle = \varepsilon_{n\mathbf{k}}|\psi_{n\mathbf{k}}\rangle, \quad \hat{H} = \frac{\hat{\mathbf{p}}^2}{2m} + V(\hat{\mathbf{r}}) = -\frac{1}{2m}\nabla^2 + V(\hat{\mathbf{r}}). \quad (3.34)$$

Instead of the equation for the $|\psi_{n\mathbf{k}}\rangle$ we can reformulate the equation for the $|u_{n\mathbf{k}}\rangle$:

$$e^{-i\mathbf{k}\cdot\hat{\mathbf{r}}}\hat{H}e^{i\mathbf{k}\cdot\hat{\mathbf{r}}}|u_{n\mathbf{k}}\rangle = \varepsilon_{n\mathbf{k}}|u_{n\mathbf{k}}\rangle. \quad (3.35)$$

We define for every operator $\hat{O}(\mathbf{k}) \equiv e^{-i\mathbf{k}\cdot\hat{\mathbf{r}}}\hat{O}e^{i\mathbf{k}\cdot\hat{\mathbf{r}}}$. The periodic part of the Bloch functions obeys a Schrödinger equation with the same eigenvalues $\varepsilon_{n\mathbf{k}}$, but a modified Hamiltonian $\hat{H}(\mathbf{k})$ which can be recast into the form:

$$\begin{aligned} \hat{H}(\mathbf{k}) &= e^{-i\mathbf{k}\cdot\hat{\mathbf{r}}}\hat{H}e^{i\mathbf{k}\cdot\hat{\mathbf{r}}} = -\frac{1}{2m}e^{-i\mathbf{k}\cdot\hat{\mathbf{r}}}\nabla\left(i\mathbf{k}e^{i\mathbf{k}\cdot\hat{\mathbf{r}}} + e^{i\mathbf{k}\cdot\hat{\mathbf{r}}}\nabla\right) + V(\hat{\mathbf{r}}) \\ &= -\frac{1}{2m}e^{-i\mathbf{k}\cdot\hat{\mathbf{r}}}\left(-k^2e^{i\mathbf{k}\cdot\hat{\mathbf{r}}} + 2i\mathbf{k}e^{i\mathbf{k}\cdot\hat{\mathbf{r}}}\nabla + e^{i\mathbf{k}\cdot\hat{\mathbf{r}}}\nabla^2\right) + V(\hat{\mathbf{r}}) = \frac{k^2}{2m} + \mathbf{k}\cdot\hat{\mathbf{v}} + \hat{H}. \end{aligned} \quad (3.36)$$

Here the velocity is given by $\hat{\mathbf{v}} = \hat{\mathbf{p}}/m = -i\nabla/m$. In the same way we obtain [13]:

$$\hat{\mathbf{v}}(\mathbf{k}) = e^{-i\mathbf{k}\cdot\hat{\mathbf{r}}}\frac{1}{mi}\nabla e^{i\mathbf{k}\cdot\hat{\mathbf{r}}} = e^{-i\mathbf{k}\cdot\hat{\mathbf{r}}}\frac{1}{mi}\left(i\mathbf{k}e^{i\mathbf{k}\cdot\hat{\mathbf{r}}} + e^{i\mathbf{k}\cdot\hat{\mathbf{r}}}\nabla\right) = \frac{\mathbf{k}}{m} + \hat{\mathbf{v}} = \nabla_{\mathbf{k}}\hat{H}(\mathbf{k}). \quad (3.37)$$

The last expression allows us to express the matrix elements of the velocity operator as matrix elements of the gradient of the Hamiltonian:

$$v_{nm,\alpha} \equiv \langle \psi_{n\mathbf{k}} | \hat{v}_\alpha | \psi_{m\mathbf{k}} \rangle = \langle u_{n\mathbf{k}} | \hat{v}_\alpha(\mathbf{k}) | u_{m\mathbf{k}} \rangle = \langle u_{n\mathbf{k}} | \nabla_{k_\alpha} \hat{H}(\mathbf{k}) | u_{m\mathbf{k}} \rangle. \quad (3.38)$$

We use the orthogonality of the periodic part of the Bloch functions at identical \mathbf{k} ,

$$\nabla_{\mathbf{k}}\varepsilon_{n\mathbf{k}} = \nabla_{\mathbf{k}}\langle u_{n\mathbf{k}} | \hat{H}(\mathbf{k}) | u_{n\mathbf{k}} \rangle = \langle u_{n\mathbf{k}} | \nabla_{\mathbf{k}}\hat{H}(\mathbf{k}) | u_{n\mathbf{k}} \rangle + \varepsilon_{n\mathbf{k}} \underbrace{\nabla_{\mathbf{k}}\langle u_{n\mathbf{k}} | u_{n\mathbf{k}} \rangle}_{=0}. \quad (3.39)$$

Therefore, the diagonal elements of the velocity operator in the basis $\{|u_{n\mathbf{k}}\rangle\}$ can be written as the gradient of the *ab initio* energies $\varepsilon_{n\mathbf{k}}$, i.e., $v_{nn,\alpha} = \nabla_{k_\alpha}\varepsilon_{n\mathbf{k}}$.

3.2.2 Wannier functions

Bloch functions are inspired by the idea that crystal electrons can be described in terms of plane waves. This is the nearly free electron picture. A complementary view can be obtained by taking the Fourier transform of Bloch functions as basis set. Since the Bloch functions are periodic in the reciprocal lattice, $\psi_{n\mathbf{k}}$ can be written as a Fourier series with wave vectors in the direct lattice [51]:

$$|W_{n\mathbf{R}}\rangle = \frac{1}{\sqrt{N}} \sum_{\mathbf{k}} e^{-i\mathbf{k}\cdot\mathbf{R}} |\psi_{n\mathbf{k}}\rangle. \quad (3.40)$$

The sum runs over a set of N vectors \mathbf{k} . $|W_{n\mathbf{R}}\rangle$ is the so-called Wannier function at position \mathbf{R} and can be defined for every band n .

The N vectors \mathbf{R} are chosen distributed evenly in the Wigner-Seitz cell around $\mathbf{R} = \mathbf{0}$, which is the most isotropic choice possible.

Due to their similarity in form to tight binding functions one hopes that the Wannier functions are localized, i.e., the overlap matrix element $\langle W_{n\mathbf{R}}|W_{m\mathbf{R}'}\rangle$ of Wannier functions at neighboring lattice positions is assumed to be small Fig. (4.3). It is easy to show that Wannier functions at different sites or with different band indices are orthogonal to each other:

$$\langle W_{n\mathbf{R}}|W_{m\mathbf{R}'}\rangle = \frac{1}{N} \sum_{\mathbf{k}\mathbf{k}'} e^{i\mathbf{k}\cdot\mathbf{R}} e^{-i\mathbf{k}'\cdot\mathbf{R}'} \langle \psi_{n\mathbf{k}}|\psi_{m\mathbf{k}'}\rangle = \delta_{nm} \frac{1}{N} \sum_{\mathbf{k}} e^{i\mathbf{k}\cdot(\mathbf{R}-\mathbf{R}')} = \delta_{nm} \delta_{\mathbf{R}\mathbf{R}'}. \quad (3.41)$$

The problem with Wannier functions is that the Fourier transform does not define them uniquely because the Bloch functions are only determined up to a phase factor $\exp[i\varphi(\mathbf{k})]$, i.e., the physical properties of the system, which are governed by the electronic structure, are invariant under a gauge transformation

$$|\psi_{n\mathbf{k}}\rangle \rightarrow e^{i\varphi(\mathbf{k})} |\psi_{n\mathbf{k}}\rangle. \quad (3.42)$$

While the transformation Eq. (3.42) preserves the electronic structure $\varepsilon_{n\mathbf{k}} = \langle \psi_{n\mathbf{k}}|\hat{H}|\psi_{n\mathbf{k}}\rangle$, it significantly changes the spatial spread Ω of the Wannier functions which is defined as

$$\Omega \equiv \sum_n \langle W_{n\mathbf{0}}|\hat{r}^2|W_{n\mathbf{0}}\rangle - \langle W_{n\mathbf{0}}|\hat{\mathbf{r}}|W_{n\mathbf{0}}\rangle^2. \quad (3.43)$$

A further problem for the construction of Wannier functions is the necessity to deal with the mixing of bands at band crossings or at a degeneracy. In general, for a composite set of bands they may be mixed at each \mathbf{k} via a transformation

$$|\psi_{n\mathbf{k}}\rangle \rightarrow \sum_m \mathcal{U}_{mn}(\mathbf{k}) |\psi_{m\mathbf{k}}\rangle. \quad (3.44)$$

If the matrix $\mathcal{U}(\mathbf{k})$ is chosen to be diagonal, the gauge transformation Eq. (3.42) can be regarded as a special case of Eq. (3.44).

Wannier functions have not attracted much interest in practical calculations until recently when a method was devised which minimizes their spatial spread Ω . The constraint of maximal localization eliminates the non-uniqueness of the Wannier functions and determines the matrices $\mathcal{U}(\mathbf{k})$ up to a global phase [54]. Originally, maximally localized Wannier functions could be constructed for the case of isolated bands only, i.e., for a number of bands that are separated from the others by a finite energy gap. However, the method was successfully generalized to the case of entangled energy bands that lie within a specified energy window [55]. The additional input needed for the disentanglement procedure consists in the overlap matrices $\langle u_{n\mathbf{k}}|u_{m,\mathbf{k}+\mathbf{b}}\rangle$ of the periodic part of the Bloch functions at neighboring points \mathbf{k} and $\mathbf{k} + \mathbf{b}$.

In the present work a set of M maximally localized Wannier functions was constructed using the program `Wannier90` and the interface between `FLEUR` and `Wannier90` [56, 57]. Following the approach of Ref. [58] in the first step a energy window $E_{\min} < \varepsilon_F < E_{\max}$ was specified which encloses the bands of interest. E_{\min} is the lowest energy eigenvalue in the system and the value of E_{\max} is chosen to be clearly above the Fermi energy level ε_F , typically $E_{\max} \approx \varepsilon_F + 10$ eV. The disentanglement procedure then finds the optimally connected M -dimensional subspace in which the maximally localized Wannier functions are finally constructed. To a certain extent the number M of Wannier functions can be chosen arbitrarily, the only requirement being that $M \geq N_{\mathbf{k}}$, where $N_{\mathbf{k}}$ is the number of states in the energy window at position \mathbf{k} .

The Wannier functions allow for a very efficient interpolation scheme that will be explained in the next chapter. However, this Wannier interpolation procedure requires having well localized Wannier func-

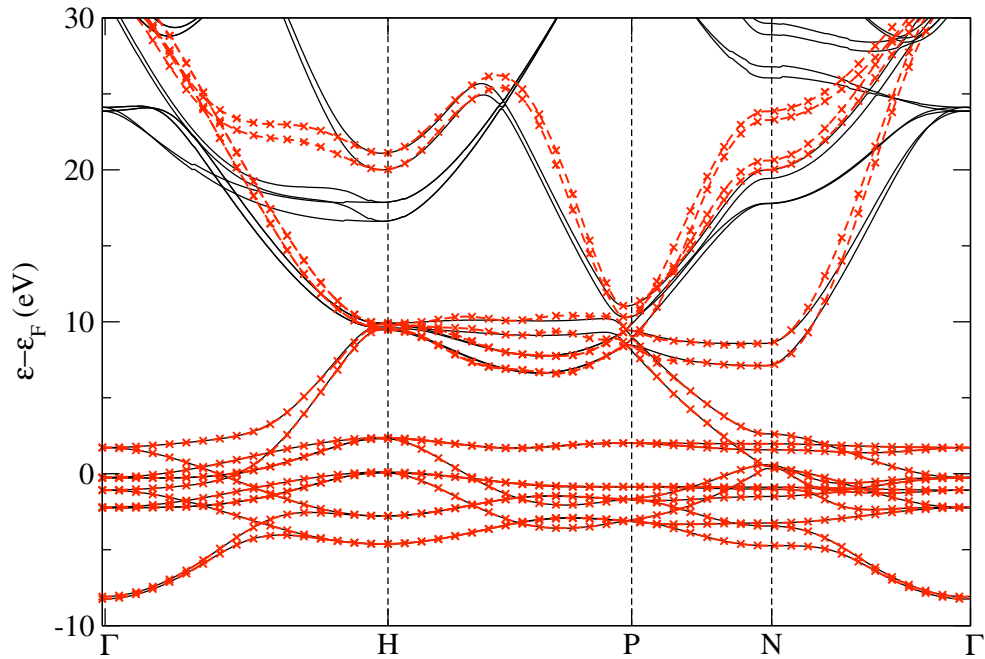


FIG. 3.1: Comparison of interpolated electronic structure (red) with *ab initio* calculation (black) for bcc Fe. Compare with [59].

tions rather than maximally localized ones. In Fig. (3.1) the interpolation of the electronic structure for bcc Fe is depicted. The energy window for disentanglement was chosen to range from the lowest energy value up to 10 eV above the Fermi energy level. It can be seen that the interpolated values agree perfectly well with the *ab initio* calculation in this window.

The great advantage of the Wannier interpolation scheme is that it does not require the full *ab initio* calculation for every \mathbf{k} -point. For Fe and Ni a set of 18 Wannier functions was constructed each, for Co and the ferromagnetic alloys FePt and FePd the number $M = 36$ was chosen since there are two atoms per unit cell. The interpolation technique is then pretty fast, because only operations on small $M \times M$ matrices are required once the hopping matrix elements $t_{nm}(\mathbf{R})$ are known. As in Ref. [59], a $8 \times 8 \times 8$ Monkhorst-Pack \mathbf{k} -mesh was used for the initial *ab initio* calculations, because this was found to provide the best tradeoff between interpolation accuracy and computational cost.

Implementation

IN the previous chapters the formulae of the intrinsic- and side-jump contribution to the AHE conductivity have been derived. In this chapter it will be explained how these formulae can actually be evaluated using first principles techniques. Additionally, the problems concerning the convergence of the Brillouin zone integration and degeneracies are addressed.

4.1 Required quantities

Recall that the expressions for the intrinsic- and side-jump conductivity are given by the equations

$$\begin{aligned}\sigma_{\alpha\beta}^{\text{int}} &= 2e^2 \text{Im} \frac{1}{\mathcal{V}} \sum_{\mathbf{k}} \sum_n^{\text{occ.}} \sum_m^{\text{emp.}} \frac{\langle n | \hat{v}_{c,\alpha} | m \rangle \langle m | \hat{v}_{c,\beta} | n \rangle}{(\varepsilon_{n\mathbf{k}} - \varepsilon_{m\mathbf{k}})^2}, \\ \sigma_{\alpha\beta}^{\text{sj}} &= \frac{e^2}{\mathcal{V}} \sum_{n\mathbf{k}} \text{Re} \text{Tr} \left\{ \delta(\varepsilon_F - \varepsilon_{n\mathbf{k}}) \left[\frac{\partial \varepsilon_{n\mathbf{k}}}{\partial k_\beta} \frac{\gamma_c}{[\gamma_c]_{nn}} (1 - S_n) \mathcal{A}_\alpha S_n - (\alpha \leftrightarrow \beta) \right] \right\}.\end{aligned}\quad (4.1)$$

In these expressions, the indices n and m run over all bands. For the side-jump contribution, the imaginary part of the self-energy is taken to be in eigenstate representation, $\gamma_c = U^\dagger \gamma U$, where

$$\gamma(\omega) = \frac{\pi}{\mathcal{V}} \sum_{n\mathbf{k}} U S_n U^\dagger \delta(\omega - \varepsilon_{n\mathbf{k}}), \quad (4.2)$$

U is the unitary matrix that diagonalizes the Hamiltonian,

$$[U^\dagger H(\mathbf{k}) U]_{nm} = \varepsilon_{n\mathbf{k}} \delta_{nm}, \quad (4.3)$$

S_n is a matrix that is diagonal in the band indices, $[S_n]_{ij} = \delta_{ij} \delta_{in}$, the Berry connection matrix is defined by

$$[\mathcal{A}_\alpha]_{ij} = i \frac{[\hat{v}_{c,\beta}]_{ij}}{\varepsilon_{j\mathbf{k}} - \varepsilon_{i\mathbf{k}}}, \quad (4.4)$$

and $[v_{c,\alpha}]_{nm} = [U^\dagger v_\alpha U]_{nm}$ are the matrix elements of the velocity operator $\hat{v}_\alpha = \nabla_{k_\alpha} \hat{H}$ in eigenstate representation. The evaluation of these expressions requires the knowledge of the energy eigenvalues $\varepsilon_{n\mathbf{k}}$ at each point \mathbf{k} in the Brillouin zone. Since a very fine \mathbf{k} -grid is necessary to converge the values for σ^{int} and σ^{sj} , it would be very cumbersome and time consuming if a full-blown *ab initio* calculation had to be performed to obtain these energy values $\varepsilon_{n\mathbf{k}}$. Moreover, since the information about the connectivity of the band structure gets lost near degeneracies or avoided crossings, it is not so clear how the required \mathbf{k} -derivatives can be evaluated on a discrete grid.

In this work, the Wannier interpolation scheme has been used to overcome these difficulties. By construction, the Wannier functions exactly reproduce the band structure that has been calculated with *ab initio* methods within a specified energy window, so that all the states in this window are properly

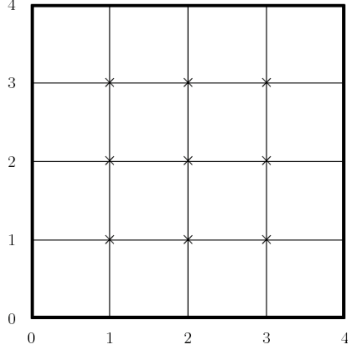


FIG. 4.1: Coarse mesh $\{\mathbf{q}\}$ for *ab initio* calculation.

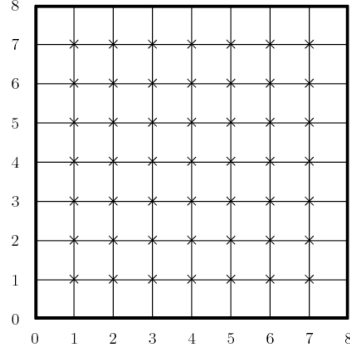


FIG. 4.2: Dense mesh $\{\mathbf{k}\}$ for Wannier interpolation.

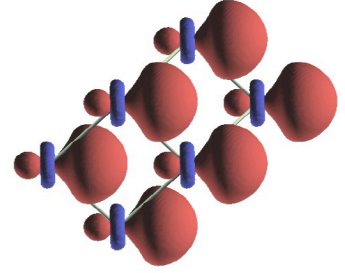


FIG. 4.3: Schematic plot of Wannier functions.

described. The only input needed are the matrix elements of the Hamiltonian in the basis of the Wannier functions. The band energies and their derivatives with respect to \mathbf{k} can then be evaluated at low computational cost.

4.2 Wannier interpolation scheme

The Wannier functions allow for a very efficient interpolation scheme of matrix elements of an operator \hat{O} , evaluated on a coarse mesh of N uniformly distributed points \mathbf{q} in the Brillouin zone Fig. (4.1),

$$\langle \psi_{n\mathbf{q}} | \hat{O} | \psi_{m\mathbf{q}} \rangle = \langle u_{n\mathbf{q}} | e^{-i\mathbf{q}\cdot\hat{\mathbf{r}}} \hat{O} e^{i\mathbf{q}\cdot\hat{\mathbf{r}}} | u_{m\mathbf{q}} \rangle = \langle u_{n\mathbf{q}} | \hat{O}(\mathbf{q}) | u_{m\mathbf{q}} \rangle, \quad (4.5)$$

to another point \mathbf{k} on a much denser mesh Fig. (4.2). The starting point are the matrix elements of the Hamiltonian in the basis of Bloch eigenstates, which are provided from first principles calculations by FLEUR:

$$H_{nm}(\mathbf{q}) = \langle \psi_{\mathbf{q}n} | \hat{H} | \psi_{\mathbf{q}m} \rangle = \langle u_{\mathbf{q}n} | \hat{H}(\mathbf{q}) | u_{\mathbf{q}m} \rangle = \varepsilon_{n\mathbf{q}} \delta_{nm}, \quad (4.6)$$

Here the electronic structure governed by the eigenvalues $\varepsilon_{n\mathbf{q}}$ is that of a real material and not that of a simple model Hamiltonian. Taking into account Eq. (3.44) the Wannier functions are constructed from the Bloch like states $|\psi_{n\mathbf{q}}^{(W)}\rangle$,

$$|\psi_{n\mathbf{q}}^{(W)}\rangle = \sum_m \mathcal{U}_{mn}(\mathbf{q}) |\psi_{m\mathbf{q}}\rangle, \quad (4.7)$$

from which the multi-band generalized Wannier functions are constructed according to Eq. (3.40),

$$|W_{n\mathbf{R}}\rangle = \frac{1}{\sqrt{N}} \sum_{\mathbf{q}} e^{-i\mathbf{q}\cdot\mathbf{R}} |\psi_{n\mathbf{q}}^{(W)}\rangle. \quad (4.8)$$

In the basis of the Bloch like states the Hamiltonian has the matrix elements

$$\begin{aligned} H_{nm}^{(W)}(\mathbf{q}) &= \langle u_{\mathbf{q}n}^{(W)} | \hat{H}(\mathbf{q}) | u_{\mathbf{q}m}^{(W)} \rangle = \sum_{m'm''} \mathcal{U}_{m'n}^*(\mathbf{q}) \langle \psi_{m'\mathbf{q}} | \hat{H} | \psi_{m''\mathbf{q}} \rangle \mathcal{U}_{m''m}(\mathbf{q}) \\ &= [\mathcal{U}(\mathbf{q})^\dagger H(\mathbf{q}) \mathcal{U}(\mathbf{q})]_{nm}. \end{aligned} \quad (4.9)$$

The idea of Wannier interpolation is to begin with the hopping elements $t_{nm}(\mathbf{R}) \equiv \langle W_{0n} | \hat{H} | W_{m\mathbf{R}} \rangle$,

which are obtained from the above equation via Fourier transform,

$$\begin{aligned}
H_{nm}^{(W)}(\mathbf{R}) &= \frac{1}{N} \sum_{\mathbf{q}} e^{-i\mathbf{q}\cdot\mathbf{R}} H_{nm}^{(W)}(\mathbf{q}) = \frac{1}{N} \sum_{\mathbf{q}} e^{-i\mathbf{q}\cdot\mathbf{R}} \langle u_{n\mathbf{q}}^{(W)} | \hat{H}(\mathbf{q}) | u_{m\mathbf{q}}^{(W)} \rangle \\
&= \frac{1}{N^2} \sum_{\mathbf{q}} \sum_{\mathbf{R}'} \sum_{\mathbf{R}''} e^{-i\mathbf{q}\cdot\mathbf{R}} e^{-i\mathbf{q}\cdot(\mathbf{R}'-\mathbf{R}'')} \langle W_{n\mathbf{R}'} | e^{i\mathbf{q}\hat{\mathbf{r}}} e^{-i\mathbf{q}\hat{\mathbf{r}}} \hat{H} e^{i\mathbf{q}\hat{\mathbf{r}}} e^{-i\mathbf{q}\hat{\mathbf{r}}} | W_{m\mathbf{R}''} \rangle \\
&= \frac{1}{N} \sum_{\mathbf{R}'} \sum_{\mathbf{R}''} \delta_{\mathbf{R}+\mathbf{R}'-\mathbf{R}'',0} \langle W_{n\mathbf{R}'} | \hat{H} | W_{m\mathbf{R}''} \rangle \\
&= \frac{1}{N} \sum_{\mathbf{R}'} \langle W_{n\mathbf{R}'} | \hat{H} | W_{m,\mathbf{R}'+\mathbf{R}} \rangle = \frac{1}{N} \langle W_{n0} | \hat{H} | W_{m\mathbf{R}} \rangle \sum_{\mathbf{R}'} 1 = \langle W_{n0} | \hat{H} | W_{m\mathbf{R}} \rangle,
\end{aligned} \tag{4.10}$$

and then to interpolate the Hamiltonian from a point \mathbf{q} on the *ab initio* mesh to an arbitrary point \mathbf{k} via the inverse Fourier transform :

$$H_{nm}^{(W)}(\mathbf{k}) = \sum_{\mathbf{R}} e^{i\mathbf{k}\cdot\mathbf{R}} H_{nm}^{(W)}(\mathbf{R}) = \sum_{\mathbf{R}} e^{i\mathbf{k}\cdot\mathbf{R}} t_{nm}(\mathbf{R}). \tag{4.11}$$

The same steps can be repeated for a general operator \hat{O} to obtain it in Wannier basis:

$$O_{nm}^{(W)}(\mathbf{k}) = \sum_{\mathbf{R}} e^{i\mathbf{k}\cdot\mathbf{R}} O_{nm}^{(W)}(\mathbf{R}) \tag{4.12}$$

Furthermore, diagonalizing the Hamiltonian $H^{(W)}(\mathbf{k})$ by finding for each \mathbf{k} an $M \times M$ unitary matrix U such that

$$H_{nm}^{(H)}(\mathbf{k}) \equiv [U^\dagger(\mathbf{k}) H^{(W)}(\mathbf{k}) U(\mathbf{k})]_{nm} = \varepsilon_{n\mathbf{k}}^{(H)} \delta_{nm} \tag{4.13}$$

allows for a direct calculation of the matrix elements of \hat{O} in the original Bloch representation by unrotating with U :

$$O_{nm}^{(H)}(\mathbf{k}) = [U^\dagger(\mathbf{k}) O^{(W)}(\mathbf{k}) U(\mathbf{k})]_{nm}, \quad O_{nm}^{(H)}(\mathbf{q}) = \langle \psi_{n\mathbf{q}} | \hat{O} | \psi_{m\mathbf{q}} \rangle. \tag{4.14}$$

The energy values $\varepsilon_{n\mathbf{k}}^{(H)}$ correspond to true eigenstates $\varepsilon_{n\mathbf{q}}^{(H)}$ on the *ab initio* mesh. Due to the spatial localization of the Wannier functions, away from that grid the interpolation error remains extremely small [59].

4.2.1 Interpolation of Hamiltonian

As mentioned earlier, in contrast to conventional interpolation schemes, where the information about the connectivity of the band structure gets lost, the Wannier interpolation technique allows to recover this information. The ingredients required are the Fourier transform of the matrix elements of the Hamiltonian in the basis of the Wannier functions:

$$H_{nm}^{(W)}(\mathbf{k}) = \sum_{\mathbf{R}} e^{i\mathbf{k}\cdot\mathbf{R}} \langle W_{n0} | \hat{H} | W_{m\mathbf{R}} \rangle. \tag{4.15}$$

This is the actual form of the Hamiltonian as implemented in our approach. The matrix elements may be conveniently computed with FLEUR. It is then an easy exercise to obtain the derivative of $H_{nm}^{(W)}(\mathbf{k})$ analytically,

$$\partial_{k_\alpha} H_{nm}^{(W)}(\mathbf{k}) = \sum_{\mathbf{R}} iR_\alpha e^{i\mathbf{k}\cdot\mathbf{R}} \langle W_{n0} | \hat{H} | W_{m\mathbf{R}} \rangle. \tag{4.16}$$

4.2.2 Interpolation of velocity

For the interpolation of the velocity operator, we replace the velocity in eigenstate representation with the corresponding quantity in the basis of the eigenfunctions:

$$[v_{c,\alpha}]_{nm} \rightarrow [U^\dagger \partial_\alpha H^{(W)} U]_{nm} = \bar{H}_{nm,\alpha}^{(H)}, \quad (4.17)$$

where we have introduced the notation $\bar{O}^{(H)} = U^\dagger O^{(W)} U$. Strictly speaking, one makes a small mistake, because when the velocity operator $\hat{v}_\alpha = \partial_{k_\alpha} \hat{H}$ is rotated the derivative should also act on the \mathbf{k} -dependent basis functions $\{|u_{n\mathbf{k}}\rangle\}$ and the matrix elements $U_{nm}(\mathbf{k}) = \langle u_{n\mathbf{k}}^{(W)} | u_{m\mathbf{k}}^{(H)} \rangle$ respectively. In Ref. [59] the correct transformation was found to be

$$v_{nm,\alpha}^{(H)} = \bar{H}_{nm,\alpha}^{(H)} - i \left(\varepsilon_m^{(H)} - \varepsilon_n^{(H)} \right) \bar{A}_{nm,\alpha}^{(H)}, \quad (4.18)$$

where $A_{nm,\alpha}^{(W)}(\mathbf{k}) = i \langle u_{n\mathbf{k}}^{(W)} | \partial_\alpha u_{m\mathbf{k}}^{(W)} \rangle$. However, the corrections of the velocity which are due to this additional term are negligible small. Moreover, further approximations would be inevitably needed for their evaluation.

4.3 Adaptive broadening

In practical calculations, the δ -function which appears in the expression for the side-jump conductivity is replaced with a Gaussian function of nonzero width w :

$$f(\varepsilon) = \frac{1}{\sqrt{2\pi w^2}} e^{-\frac{(\varepsilon - \varepsilon_F)^2}{2w^2}} \quad (4.19)$$

For a given grid spacing Δk the width of the Gaussian should be comparable with the level spacing $\Delta \varepsilon_{n\mathbf{k}}$. In this work, an adaptive broadening scheme is employed which assigns to each state an individual broadening width:

$$\Delta \varepsilon_{n\mathbf{k}} \approx \left| \frac{\partial \varepsilon_{n\mathbf{k}}}{\partial \mathbf{k}} \right| \Delta k, \quad w_{n\mathbf{k}} = c_w \left| \frac{\partial \varepsilon_{n\mathbf{k}}}{\partial \mathbf{k}} \right| \Delta k, \quad (4.20)$$

where c_w is a constant of the order of unity. By virtue of the adaptive broadening scheme, spurious oscillations of the calculated quantities are avoided which occur for a fixed broadening scheme whenever the level spacing becomes larger than a preliminary specified Gaussian width [58].

As a test of the broadening schemes, in Tab. (I) the values of the side-jump conductivity in Fe with magnetization into [001] direction are shown for several choices of the parameter w within a fixed broadening and for c_w within an adaptive broadening scheme. It appears that a small choice of w leads to a fast convergence when the number of \mathbf{k} -points in the grid is increased. The adaptive broadening scheme leads to a more uniform convergence. In particular, the values of the calculated conductivity do not depend on the choice of c_w for a sufficiently dense grid.

In Tab. (II) the share of the number of points in the Fermi surface on the total number of \mathbf{k} -points in the Brillouin zone calculated with a adaptive broadening scheme is presented. This quantity is closely related to the density of states (DOS) at the Fermi level. Given a function $f(\varepsilon_{n\mathbf{k}})$, the DOS $D_n(\varepsilon)$ is defined via

$$\frac{1}{\mathcal{V}} \sum_{\mathbf{k}} f(\varepsilon_{n\mathbf{k}}) \rightarrow \frac{1}{(2\pi)^3} \int d^3 k f(\varepsilon_{n\mathbf{k}}) \stackrel{!}{=} \int d\varepsilon D_n(\varepsilon) f(\varepsilon). \quad (4.21)$$

TABLE I: Fixed broadening scheme with width w and adaptive broadening scheme with parameter c_w for the calculation of the side-jump contribution in Fe [001]. Values are in S/cm.

Grid	w [eV]			c_w		
	0.01	0.05	0.1	0.8	1	1.2
100^3	366	371	266	277	259	247
200^3	137	144	144	147	144	142
300^3	111	118	126	122	122	121
400^3	110	113	121	115	115	115
500^3	110	110	121	112	112	112
600^3	110	110	120	111	111	111

TABLE II: Share of the number of points in Fermi surface on the total number of points in %

Grid	Fe [001]	Ni [001]	Co [001]	FePd [001]	FePt [001]
200^3	1.3281	2.2922	1.2121	0.7423	0.6944
300^3	1.3289	2.2922	1.2125	0.7423	0.6947
400^3	1.3293	2.2916	1.2126	0.7423	0.6948
500^3	1.3295	2.2914	1.2127		
600^3	1.3295	2.2914			

If we set $f(\varepsilon_{n\mathbf{k}}) = \delta(\varepsilon_{n\mathbf{k}} - \varepsilon_F)$ and sum over all bands, we get the number of states in the Fermi surface. This number is proportional to the total density of states at the Fermi energy level:

$$\frac{1}{V} \sum_{n\mathbf{k}} \delta(\varepsilon_F - \varepsilon_{n\mathbf{k}}) = \sum_n \int d\varepsilon D_n(\varepsilon) \delta(\varepsilon_F - \varepsilon) = \sum_n D_n(\varepsilon_F). \quad (4.22)$$

It can be seen that the share of the number of points in the Fermi surface converges far more quickly than the side-jump contribution. In Ref. [63] the DOS at the Fermi level for Fe, Co and Ni was found to be ≈ 1.1 [1/eV], ≈ 1.1 [1/eV] and ≈ 1.9 [1/eV], respectively. As it should be, the ratio of these values to each other corresponds to that of the values in Tab. (II). This is a further test that the broadening scheme has been implemented correctly.

Application and results

IN this chapter the results of the calculation of the scattering independent contribution to the AHE are presented. The techniques outlined earlier in this work were applied to the ferromagnetic materials Fe, Co and Ni and the ferromagnetic alloys FePd and FePt. The calculated values for the intrinsic- and side-jump conductivity are compared to experimental values for the AHE conductivity, from which the skew-scattering contribution was either explicitly subtracted or safely ignored at higher temperatures. It is found that the side-jump contribution constitutes a significant proportion to the AHE in most materials and shows a distinctive anisotropy with respect to the magnetization direction. Furthermore, this chapter provides an analysis of the Fermi-surface properties of the side-jump contribution in comparison to the intrinsic contribution.

5.1 Iron and Cobalt

In Tab. (I) the results of the calculations of the intrinsic conductivity σ^{int} and side-jump conductivity σ^{sj} for Fe and Co for different high-symmetry orientations of the magnetization in the crystal are shown. As it should be, the values for σ^{int} in Fe and Co agree perfectly well with previous calculations. The new feature is the calculation of σ^{sj} .

In Fe, taking the side-jump contribution into account significantly improves upon the the prediction of the AHE, i.e., the sum $\sigma^{\text{int}} + \sigma^{\text{sj}}$ is very close to the experimental value for all magnetization directions. For example in Fe [001], the side-jump conductivity together with the intrinsic conductivity account for about 85% of the measured AHE. The inclusion of σ^{sj} improves the agreement between theory and experiment by 10% in comparison to σ^{int} alone. For polycrystalline iron, the experimental value should be understood as the average over crystals with different magnetization directions. It is clear from the values in Tab. (I) that this average value lies somewhere in the interval from 880 S/cm to 1020 S/cm, which increases the accordance between experiment and theory still a bit.

TABLE I: Anomalous Hall conductivities for bcc Fe and hcp Co in units of S/cm for selected high-symmetry orientations of the magnetization. σ^{int} , σ^{sj} and $\sigma^{\text{int}} + \sigma^{\text{sj}}$ stand for the intrinsic contribution, side-jump contribution and their sum, respectively. The experimental values are for the scattering-independent conductivity, the previous calculated values for the intrinsic contribution only.

Fe	[001]	[111]	[110]	Co	<i>c</i> axis	<i>ab</i> plane
Prev. [15]	751			Prev. [35]	481	116
σ^{int}	767	842	810	σ^{int}	477	100
σ^{sj}	111	178	141	σ^{sj}	217	-30
$\sigma^{\text{int}} + \sigma^{\text{sj}}$	878	1020	951	$\sigma^{\text{int}} + \sigma^{\text{sj}}$	694	70
Exp. [34]	1032			Exp. [36]	813	150

TABLE II: Anomalous Hall conductivities for L1₀ FePd and FePt in units of S/cm for selected high-symmetry orientations of the magnetization. σ^{int} , σ^{sj} and $\sigma^{\text{int}} + \sigma^{\text{sj}}$ stand for the intrinsic contribution, side-jump contribution and their sum, respectively. The experimental values are for the scattering-independent conductivity, the previous calculated values for the intrinsic contribution only.

FePd	[001]	[110]	FePt	[001]	[110]
Prev. [26]	133		Prev. [26]	818	
σ^{int}	120	280	σ^{int}	833	409
σ^{sj}	263	280	σ^{sj}	128	220
$\sigma^{\text{int}} + \sigma^{\text{sj}}$	383	560	$\sigma^{\text{int}} + \sigma^{\text{sj}}$	961	629
Exp. [26]	806		Exp. [26, 60]	900-1267	

In Co, with an value of 217 S/cm the side-jump conductivity along the c axis is almost half as large as σ^{int} , and the scattering independent contribution to the AHE conductivity agrees within 85% to the experimental value like in Fe. On the contrary, in the basal ab plane σ^{sj} is small and negative, even changing the agreement with experiment to the worse compared to σ^{int} alone. It should be noted, however, that the experimental values for the conductivity from Ref. [36] are available at room temperature only. This disadvantage clearly limits the comparison with the calculated scattering independent contribution.

The values presented in Tab. (I) demonstrate that the intrinsic- and side-jump contribution change their magnitude with magnetization direction. This phenomenon is the manifestation of the magneto-crystalline anisotropy. In Fe, σ^{int} varies from 842 S/cm to 767 S/cm for different magnetization directions, which makes a difference of about 10 %. Interestingly, σ^{sj} appears to be considerably more anisotropic, since its rate of change with the magnetization direction is nearly four times larger. The anisotropy of σ^{sj} is even more pronounced in Co, where it changes sign when the magnetization is switched from the c axis to the basal ab plane. However, it is not surprising that the anisotropy in Co is more distinct than in Fe, since the hcp crystal structure of Co is uniaxial, as opposed to Fe.

5.2 Ferromagnetic alloys FePd and FePt

Even in the more complex case of the L1₀ ordered ferromagnetic alloys FePd and FePt the inclusion of the side-jump contribution improves systematically on the theoretical prediction of the AHE. As follows from Tab. (II), the calculated values for the intrinsic contribution are again in good agreement with previous known results. With regard to the comparison of $\sigma^{\text{int}} + \sigma^{\text{sj}}$ to experiments, including the side-jump contribution in FePd improves the prediction of the AHE by 30%. However, provided that the experimental value of 806 S/cm can be assumed to be exact, a certain discrepancy between theory and experiment remains. By all means, the universal side-jump contribution is not the only scattering independent contribution to the AHE and in FePd one might fail to describe it with a Gaussian disorder model alone. On the other hand for FePt, adding the calculated side-jump contribution to the intrinsic contribution brings the total AHE conductivity within the range of experimentally observed values for samples of thin [001]-magnetized L1₀ films of FePt. For a high degree of ordering and different sample thicknesses, values between 900 S/cm and 1276 S/cm for the AHE conductivity were obtained in recent experiments [26, 60], which perfectly match the theoretical prediction of 961 S/cm. In these experiments, measurements of the AHE were performed by explicitly taking a temperature varying saturation magnetization M_s into account.

It appears that the side-jump mechanism is especially important in FePd. For magnetization along [001] direction, σ^{sj} is twice as large as the intrinsic contribution, while for magnetization along [110] direction,

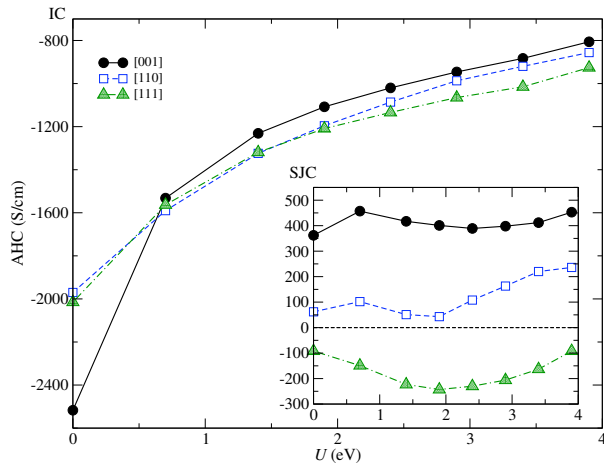


FIG. 5.1: U -dependence of the AHE conductivity in Ni calculated with GGA+ U .

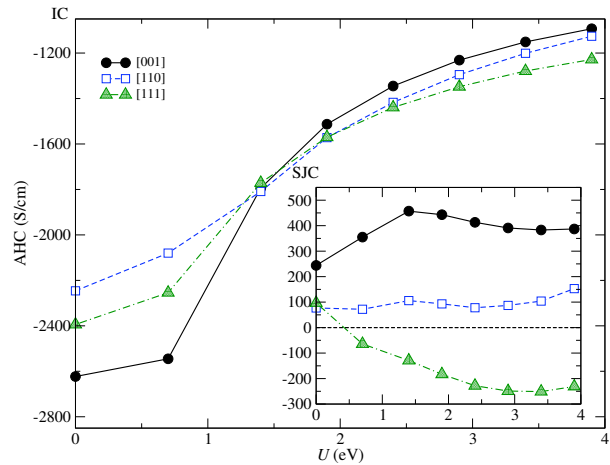


FIG. 5.2: U -dependence of the AHE conductivity in Ni calculated with LDA+ U .

σ^{sj} is of equal strength as σ^{int} . These findings reinforce the earlier indirect prediction of Ref. [26], where the side-jump contribution was obtained from measuring the AHE conductivity and subtracting the calculated value for σ^{int} . In doing so the authors of Ref. [26] concluded that σ^{sj} dominates the AHE in FePd, which is verified by its explicit calculation in the present work.

While the AHE in FePd is mainly due to the side-jump contribution, in ferromagnetic FePt alloys the situation is just the other way round. According to Tab. (II), for FePt the intrinsic contribution is much larger than in FePd and for FePt with magnetization along [001] direction, σ^{sj} is only half the value of that in FePd. This is again in agreement to Ref. [26], in which such a crossover between the intrinsic and side-jump conductivity in the two materials was explained by the different spin-orbit interaction strength of atomic Pd and Pt.

The $L1_0$ structure can be viewed as a tetragonal distortion of the fcc lattice, with less symmetry than a genuine fcc lattice. Therefore, the AHE conductivity $\sigma^{\text{int}} + \sigma^{\text{sj}}$ in FePd and FePt is supposed to be more anisotropic than in Fe. Indeed, the change of the AHE conductivity with respect to magnetization direction is around 30% for FePd and FePt, a value that is larger than in Fe ($\approx 10\%$), but smaller than in hcp Co ($\approx 90\%$). While the value of σ^{sj} for FePd [001] increases only a little when the magnetization is changed into [110] direction, the value of σ^{int} in FePd [110] is more than twice as large as in FePd [001] and then amounts to 50% of the total AHE. This behavior is in sharp contrast to FePt, where σ^{int} is roughly cut in half when the magnetization is changed from [001] direction to [110]. Additionally, σ^{sj} does not remain constant but is nearly twice as large in FePt [110] than in FePt [001].

5.3 Nickel

The calculation of the AHE conductivity in fcc Ni is especially difficult, since it is a transition metal in which the correlation effects between $3d$ electrons become important. Although these correlation effects are only moderate in strength, their accurate description plays a vital role in many phenomena which are caused by spin-orbit interaction (SOI). Unfortunately, standard DFT methods with the generalized gradient approximation (GGA) or the the local density approximation (LDA) do not treat the $3d$ electron-electron interaction correctly and yield inaccurate values for SOI-induced quantities in some transition metals. For example, it is well known that LDA fails to predict the magnetocrystalline anisotropy energy and the correct easy axis in Ni [61]. In the present work, the value of the intrinsic AHE conductivity, which is also caused by SOI, is much larger than the experimental value would suggest, implying a sizable side-jump contribution which is much larger than the calculated σ^{sj} . In the following, the results

of GGA+ U /LDA+ U calculations are presented, which indicate that the $3d$ correlation effects should be properly dealt with in order to get suitable values for σ^{int} .

5.3.1 GGA+ U /LDA+ U approach

The correlation effects which are not captured by standard DFT methods in Ni are incorporated into the calculation of the AHE by taking the so-called intra-atomic repulsion U and the intra-atomic exchange J into account [64, 65]. The computation of these quantities has already been implemented within DFT and the FLAPW method by identifying atomic like orbitals in which interactions of electrons are treated in a non-LDA manner [66].

In and Tab. (III) the calculated conductivities σ^{int} and σ^{sj} in Ni within the GGA+ U approach are shown. In line with the method of Ref. [61] for several values of the parameter U in the interval from 0 eV up to 4 eV the parameter J was chosen in such a way that the magnetic moment in Ni stays roughly constant. For $U = 0$ eV and $J = 0$ eV the GGA+ U approach gives values for the intrinsic contribution which lie between -2500 S/cm for Ni with magnetization along [001] direction and -2000 S/cm for the other magnetization directions are obtained. These results are in good agreement with previous results published in Ref. [37], where σ^{int} was stated to be -2073 S/cm for [111] magnetized Ni and a value of -2203 S/cm was calculated with an alternative method originally suggested by Haldane [67]. However, the experimental value for the scattering independent AHE in Ni is much smaller and amounts to only -637 S/cm [30]. The calculated values for the side-jump contribution are much smaller than σ^{int} and even negative in sign for Ni [111]. Therefore, taking the side-jump contribution into account only within standard GGA cannot explain the large discrepancy between theory and experiment in fcc Ni but correlation effects have to be included.

As can be seen from our calculations, presented in Tab. (III) and Fig. (5.1), the values of the intrinsic contribution change drastically with U . For all magnetization directions, the absolute value of σ^{int} reduces significantly with increasing U and approach a value of -800 S/cm for $U = 3.9$ eV. Recently, this observation was confirmed in another GGA+ U study by Fuh and Guo [68]. On the other hand, the values of the side-jump contribution show a completely different course as can be seen in Tab. (III) and the inset of Fig. (5.1). For magnetization into [001] direction σ^{sj} does almost not change and shows a non-monotonous behavior within the range of 100 S/cm up to 300 S/cm in the absolute value as a function of U for the two other magnetization directions.

In previous works, intricate properties of Ni such as the magnetocrystalline anisotropy energy and easy axis, among others, were correctly predicted within LDA+ U for $U = 1.9$ eV and $J = 1.2$ eV [61]. In practice, precisely this pair of parameters for U and J is often treated as an empirical value that improves the Fermi surface of Ni without changing the magnetic moment too much [63]. In the present work, it was found that a slightly smaller value of $J = 1.1$ eV is even better adapted to GGA+ U . Indeed, for $U = 1.9$ eV and $J = 1.1$ the computed conductivity $\sigma^{\text{int}} + \sigma^{\text{sj}} = -707$ S/cm for magnetization in [001] direction agrees with the experimental value within 35%.

Although still consistent with experiment, it turns out that the magnetic moments in Ni calculated with GGA+ U are a bit too large, being consistently larger than the experimental value of $0.60 \mu_B$ [62]. Therefore, additional calculations of the AHE conductivity using LDA+ U and the MJW functional were performed as well. As Tab. (IV) shows, without the additional parameters U and J , i.e., for $U = 0$ eV and $J = 0$ eV, the LDA succeeds in predicting the correct magnetic moment for Ni straight away. However, the absolute value of σ^{int} obtained in LDA is again very large, even exceeding the values of GGA by 250 S/cm on average. For magnetization in [111] direction, σ^{sj} is less than 5% of the calculated AHE conductivity and of opposite sign with regard to the corresponding value in GGA.

As U increases, the magnetic moment increases as well. In particular, for the above mentioned pair of parameters $U = 1.9$ eV and $J = 1.2$ eV, the magnetic moment is in perfect agreement to previous

TABLE III: AHE conductivity for fcc Ni in units of S/cm for selected high-symmetry orientations of the magnetization using GGA+ U and the PBE functional. The values of U and J were chosen in such a way that the magnetic moment (MM) is kept roughly constant.

U [eV]	J [eV]	MM [μ_B]	σ^{int}			σ^{sj}		
			[001]	[110]	[111]	[001]	[110]	[111]
0.0	0.0	0.6317	-2517	-1970	-2015	362.0	61.7	-92.0
0.7	0.3	0.6532	-1532	-1590	-1563	456.6	102.4	-149.0
1.4	0.7	0.6674	-1231	-1324	-1319	417.2	50.8	-223.1
1.9	1.1	0.6755	-1108	-1196	-1209	400.6	42.7	-243.3
2.4	1.9	0.6755	-1020	-1086	-1134	389.1	108.2	-229.8
2.9	2.2	0.6880	-946	-987	-1065	397.5	162.9	-205.5
3.4	2.5	0.7044	-883	-920	-1015	412.3	220.0	-163.2
3.9	2.6	0.7327	-806	-856	-926	452.8	236.0	-92.3

Experimental value for the scattering-independent conductivity: -1100 S/cm [31] \div -637 S/cm [30]

Previously calculated value of intrinsic contribution: -2073 S/cm \div -2203 S/cm [37]

TABLE IV: The same as in Tab. (III) using LDA+ U and the MJW functional.

U [eV]	J [eV]	MM [μ_B]	σ^{int}			σ^{sj}		
			[001]	[110]	[111]	[001]	[110]	[111]
0.0	0.0	0.6059	-2623	-2246	-2394	243.8	77.3	96.6
0.7	0.3	0.6247	-2545	-2080	-2254	355.3	72.2	-63.7
1.4	0.9	0.6334	-1794	-1809	-1771	456.7	105.6	-128.8
1.9	1.2	0.6469	-1513	-1572	-1570	442.9	93.0	-183.0
2.4	1.7	0.6529	-1345	-1417	-1439	413.2	77.6	-227.8
2.9	2.2	0.6594	-1231	-1295	-1348	390.6	87.0	-249.4
3.4	2.5	0.6705	-1151	-1201	-1279	382.9	103.7	-251.1
3.9	2.8	0.6823	-1093	-1126	-1228	386.9	153.1	-230.5

Exp. MM. [62]: $0.60 \mu_B$

Ref. [63]: $0.61 \mu_B$ for LDA

Ref. [63]: $0.65 \mu_B$ for $U=1.9$ eV, $J=1.2$ eV

TABLE V: AHE conductivity for bcc Fe in units of S/cm using GGA+ U and the PBE functional. The values of U and J were chosen as in Ref. [61]. The experimental value of the conductivity stands for the scattering-independent contribution only.

U [eV]	J [eV]	MM [μ_B]	σ^{int}			σ^{sj}		
			[001]	[110]	[111]	[001]	[110]	[111]
0.0	0.0	2.2295	767	811	842	115	141	178
1.2	0.8	2.1988	822	875	902	147	187	209

Exp. MM. [62]: $2.2 \mu_B$

Exp. [34]: 1032 S/cm

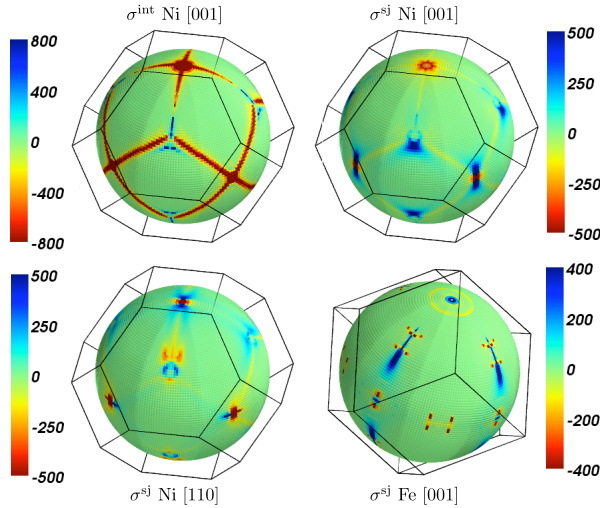
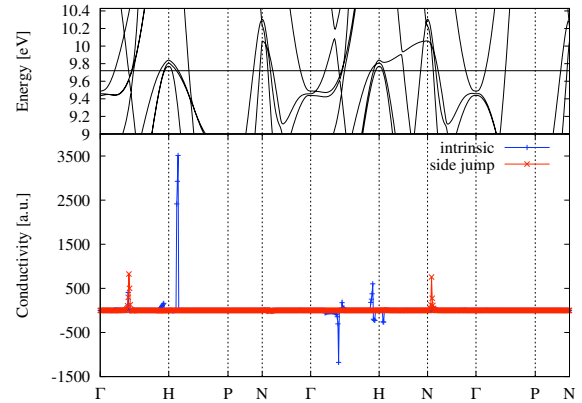


FIG. 5.3: (right) Intrinsic conductivity vs side-jump conductivity along high symmetry lines in atomic units in Fe [001]. The upper panel shows the calculated electronic structure near the Fermi energy. Compare with [15].

FIG. 5.4: (left) Angle-resolved conductivity $d\sigma/d\Omega$ in units of S/cm as a function of direction in the Brillouin zone. The value of $d\sigma/d\Omega$ corresponds to the sum of all contributions to the conductivity from inside the inner sphere in the Brillouin zone within the solid angle element $d\Omega$. The outside frame is the boundary of the Brillouin zone.



LDA+ U calculations [63]. Most interesting is the fact that for this choice of U and J the total AHE conductivity $\sigma^{\text{int}} + \sigma^{\text{sj}} = -1070$ S/cm coincides with the experimental value of -1100 S/cm measured at low temperatures [31]. This suggests that the main reason for the discrepancy between the values of the AHE conductivity obtained from DFT and experiment might lie in the improper description of electronic structure from first principles, which is corrected by taking correlation effects into account.

Within LDA+ U , the side-jump conductivity depends more sensitively on the intra-atomic repulsion U than within GGA+ U , even exhibiting a sign change for magnetization into [111] direction. However, comparing Fig. (5.1) with Fig. (5.2) it can be observed that GGA+ U and LDA+ U calculations share the same feature that the intrinsic contribution appears to approach a common value for all magnetization directions with increasing U , albeit this common value is somewhat lower in LDA+ U than in GGA+ U . On the contrary, σ^{sj} remains anisotropic when U increases, with distinct values for distinct magnetization directions.

GGA+ U approach for Fe

For comparison, GGA+ U calculations were also performed for Fe using $U = 1.2$ and $J = 0.8$ as empirical parameters [61]. Applying the GGA+ U approach reduces the magnetic moment a bit, just below the experimental value of $2.2 \mu_B$ [62]. However, for Fe the AHE conductivity does not change as drastically as in Ni. Rather, the intrinsic contribution and side-jump contribution are shifted evenly by up to approximately 60 S/cm and 30 S/cm, respectively, for all magnetization directions, bringing thus the total value of the calculated AHE conductivity even closer to experiment, see Tab. (V).

5.4 Fermi surface properties

In this section it shall be explained why σ^{int} and σ^{sj} exhibit such a different behavior in Fe and Ni within the GGA+ U /LDA+ U approach. To begin with, in Fig. (5.4) the angle-resolved conductivities for the

TABLE VI: AHE conductivity for Ni [001] with M_{fee} parameter -0.3 eV.

	σ^{int}			σ^{sj}		
	[001]	[110]	[111]	[001]	[110]	[111]
GGA	-1971	-1772	-1781	349	114	-36
LDA	-2311	-2071	-2259	270	118	116

intrinsic contribution and side-jump contribution in the Brillouin zone are depicted. For that purpose, all the contributions to the conductivity over all bands and all sheets of the Fermi surface are summed over. The color of each surface point in Fig. (5.4) corresponds to the sum of all the contributions from the center of the Brillouin zone, the Γ -point, until the surface of the sphere is reached. The sum goes along the direction indicated by the position of each particular surface point and the conductivity is weighted with the solid angle $d\Omega$ each point occupies.

It is known from previous works that the intrinsic conductivity has large contributions along the hot loops in the Brillouin zone, which are situated in the vicinity of the intersections between different sheets of bands [69]. Away from these regions there is a smooth, albeit small background of σ^{int} that is also significant and fills nearly the entire Brillouin zone [59]. This feature can be indirectly observed in Fig. (5.4) as well, since the negative intrinsic contribution for [001] magnetized Ni covers most of the sphere.

On the contrary, Fig. (5.4) illustrates that the main contributions to the side-jump conductivity in Ni and Fe come from isolated dots in the Brillouin zone. These dots are rather sparsely scattered over the Fermi sphere, and σ^{sj} decays very quickly with the distance from such dots. However, the position of the dots is not random. Rather, large and significant contributions to the side-jump conductivity occur in the same regions where the absolute value of σ^{int} is large as well. For Ni [001], the sign of σ^{sj} in the dot at the pole of the sphere coincides with that σ^{int} , whereas σ^{sj} in the dots that appear around the equator of the sphere are mainly opposite in sign to the corresponding value of σ^{int} . Since the dots change their position and magnitude with magnetization direction, as can be seen by comparing the angular distribution of σ^{sj} for Ni [001] and Ni [110] in Fig. (5.4), the anisotropy of the side-jump conductivity can be intuitively understood.

The difference in the distribution of the side-jump conductivity and intrinsic conductivity on the Fermi Surface arises from the effective magnetic monopole nature of the intrinsic contribution near avoided band crossings [70], whereas the side-jump does not contain such singularities near those crossings. This view is supported by Fig. (5.3), where σ^{int} and σ^{sj} for Fe are shown. The path in the Brillouin zone was chosen as in Ref. [15], and the intrinsic contribution shows the same behavior as in that work. For example, σ^{int} has sharp peaks near the high-symmetry point H, where the Fermi level lies within a gap of two spin-orbit coupled bands, while σ^{sj} does not peak in this regions. On the other hand, the same behavior as for the angular distribution of σ^{int} and σ^{sj} in Ni [001] in Fig. (5.4) can be observed again, namely that whenever σ^{sj} is large, σ^{int} is large as well and in the special case of Fe [001] of equal sign.

5.4.1 Exchange splitting

It turns out from the values presented in Tab. (IV) above that the magnetic moment for Ni calculated within LDA is in fine agreement with experiment. Likewise, the electronic structure of the *sp*-bands calculated within LDA is consistent with data obtained from photoemission spectroscopy. However, the predicted width of the occupied 3*d*-bands is about 30% too large [71]. Moreover, the density of states (DOS) at the Fermi level and the exchange splitting are also not correctly reproduced. While experiments show that the exchange splitting in Ni is small and highly anisotropic with values from 0.2 eV to 0.3 eV, the

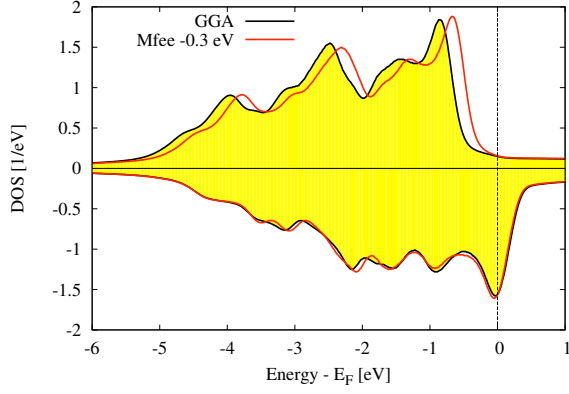


FIG. 5.5: Change of DOS in Ni by Mfee calculation. Positive and negative values of DOS refer to majority and minority spin electrons respectively.

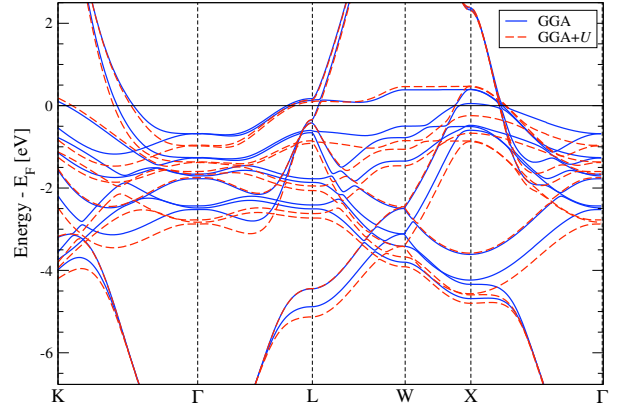


FIG. 5.6: Band structure of Ni calculated with GGA and GGA+ U with Coulomb repulsion parameter $U = 1.9$ eV and exchange parameter $J = 1.1$ eV.

LDA yields a rather large and almost isotropic splitting of 0.6 eV (see Ref. [63] and references therein).

It was found out that the inclusion of correlation effects within LDA+ U enhances the anisotropy, but on the other hand the LDA+ U scheme is associated with an increase of the average exchange splitting as well, depending on the choice of the values of the parameters U and J [63]. As far as the computation of the AHE conductivity is concerned, it is hard to tell from the outset whether the corrections of the Fermi surface by LDA+ U or this scaling of the exchange splitting is the reason for the improvement of the prediction of σ^{int} within LDA+ U .

For this purpose, supplementary calculations of the AHE conductivity were performed in which the exchange splitting was adjusted by hand using the so-called Mfee feature in FLEUR. In these Mfee calculations the potentials for spin up and spin down energy bands were shifted with respect to each other such that the exchange splitting was reduced by 0.3 eV, a value that gave good results in a previous work on the computation of magnetic excitations in Ni [63]. As can be seen in Fig. (5.5), the reduction of the exchange splitting leads to a somewhat larger DOS around the Fermi energy level.

In Tab. (VI) the calculated values for σ^{int} and σ^{sj} within the Mfee approach are shown. Like in GGA+ U /LDA+ U calculations, the magnitude of σ^{int} decreases, which resembles the desired behavior of bringing the theoretical prediction of the AHE conductivity closer to the experimental value. The side-jump contribution appears to be less affected by the scaling of the exchange splitting than by the choice of U . In particular, the sign of σ^{sj} for Ni [111] remains positive within LDA, while it is negative for both LDA+ U and GGA+ U even for small U . However, the agreement to experiment is worse than it is in the case for GGA+ U /LDA+ U calculations with $U=1.9$ eV. Presumably both the Fermi surface and the exchange splitting have to be adjusted to get an even better value of the AHE conductivity in Ni.

5.4.2 Energy dependence

In Fig. (5.6) the calculated band structure of fcc Ni using GGA and GGA+ U is displayed. It can be seen that within GGA the eighth band of Ni touches the Fermi level from below, giving rise to very small pockets on the Fermi surface at the X points in the Brillouin zone [37]. However, these so-called X_2 pockets cannot be observed in experiments [72]. When taking correlation effects into account by adopting GGA+ U , the main effect is that the energy of the d -dominated energy bands is decreased. As a result, the eighth band is shifted entirely under the Fermi energy level, in accordance to experiment and to other GGA+ U studies [68]. A band-by-band analysis revealed that band eight gives only a very small contribution to the intrinsic contribution and including the X_2 pocket or not affects the value of

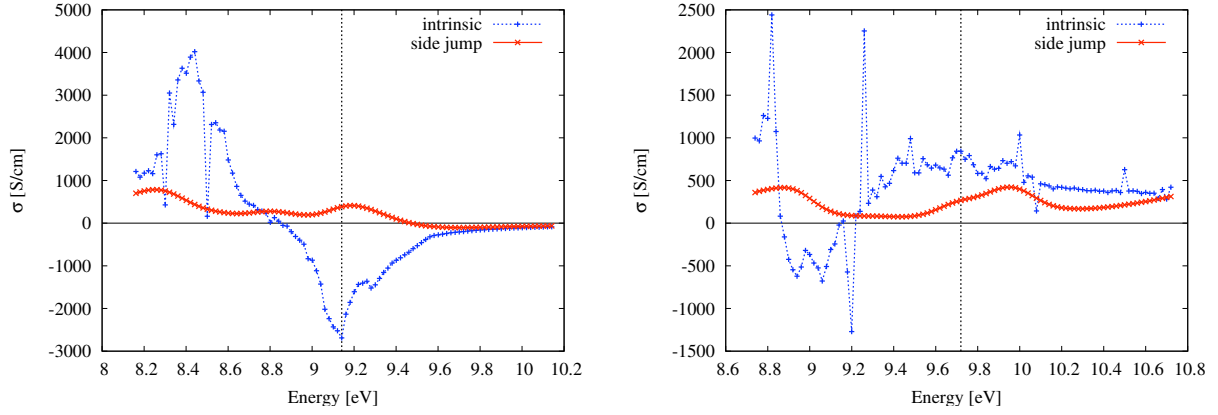


FIG. 5.7: Change of the AHE conductivity in Ni [001] (left) and in Fe [001] (right) as the Fermi energy level is altered by hand. The vertical lines indicate the position of the true Fermi energy level.

σ^{int} very little [59]. The data presented in Sec. 5.3.1 suggests that this observation also applies to the case of σ^{sj} , because the side-jump contribution does not change much in GGA+ U , when the X_2 pocket is absent, compared to pure GGA, when the X_2 pocket is present.

In Fig. (5.7) the dependence of σ^{int} and σ^{sj} in Ni and in Fe on the Fermi energy level is shown. The step oscillations of the intrinsic conductivity, which are especially visible in Fe, are spurious and result from numerical instabilities in the program code that was written in the context of the present work. More precisely, the numerical instabilities are due to the limited resolution of the step function $\Theta(\varepsilon_{n\mathbf{k}} - \varepsilon_F)$ that needs to be evaluated for the calculation of σ^{int} to decide whether a state with energy $\varepsilon_{n\mathbf{k}}$ is occupied or not. These oscillations do not occur for σ^{sj} because in this case the sharp step function is generically replaced by a smoother function that allows for partial occupancies at the Fermi energy level ε_F .

For Ni, the intrinsic conductivity has a pronounced minimum at the true Fermi energy level with a value of -2600 S/cm. Its magnitude becomes very small when ε_F is manually raised by 0.5 eV. On the other hand, if the Fermi energy is lowered, σ^{int} changes its sign around 8.84 eV and then rapidly increases to the huge value of 4000 S/cm at 8.44 eV. If the Fermi energy level is further lowered, σ^{int} decreases again. It should be pointed out, however, that all these findings were obtained within GGA and are in qualitative agreement to Ref. [68], where the GGA+ U approach with parameters $U = 1.9$ eV and $J = 1.2$ eV was adopted. In Fe, σ^{int} resides in the interval from 600 S/cm up to 800 S/cm around ε_F . The sign change of σ^{int} occurs in Fe as well, albeit at a considerably lower energy below the true Fermi energy level compared to Ni.

For Ni and Fe, the side-jump contribution appears to depend much less sensitively on ε_F than the intrinsic contribution, which again is a result of the singular behavior of σ^{int} near avoided band crossings. Within the rigid band approximation, adding or subtracting an electron to Ni changes the position of the Fermi energy level only. Of course this is a very crude approximation, but interestingly it was found out in Ref. [68] that shifting the position of the Fermi energy level by -0.71 eV to 8.43 eV or by -1.02 eV to 8.12 eV in Ni involves that the number of valence electrons is changed from 10.0 to 9.0 like in Co or to 8.0 like in Fe respectively. As can be read off from Fig. (5.7), σ^{int} is predicted to be positive for both energy values, in accordance to the experimental and theoretical findings in these materials.

5.4.3 Band resolved conductivity

In Fig. (5.8) the side-jump conductivity is plotted as the color-code on the Fermi surface of Fe [001], Co [001], Ni [001] and Ni [110]. For each material, the Fermi surface has been decomposed into its constituent Fermi sheets which are defined as the set of \mathbf{k} -points in the Brillouin zone at which $\varepsilon_{n\mathbf{k}} = \varepsilon_F$

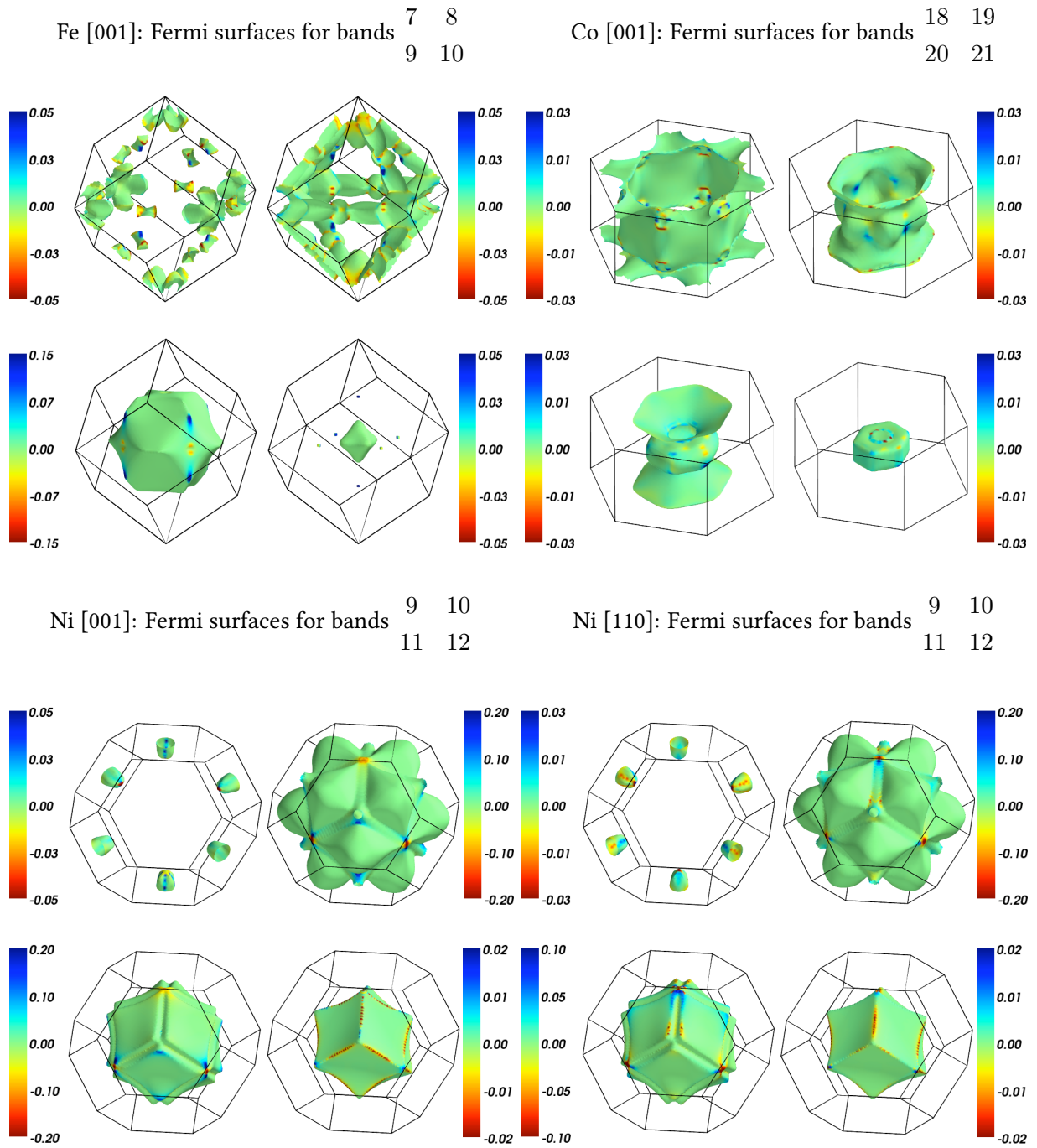


FIG. 5.8: Side-jump contribution to the AHE conductivity plotted on the Fermi surfaces for Fe [001] (upper left), Co [001] (upper right), Ni [001] (lower left) and Ni [110] (lower right) in arbitrary units. The outside frame is the boundary of the Brillouin zone.

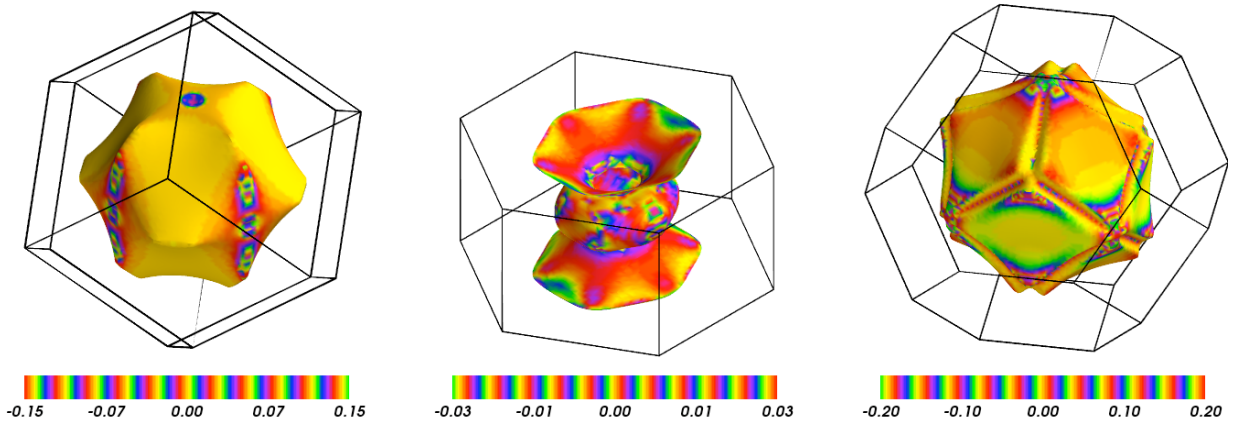


FIG. 5.9: The same as in Fig. (5.8) for the Fermi surfaces of band 9 in Fe (left), band 20 in Co (middle) and band 11 in Ni (right) using a different color code.

is satisfied for a particular band n . However, as explained in Ref. [37], in some cases the Fermi sheets are rather small and for convenience only the largest ones are shown in Fig. (5.8).

As in Ref. [37], the shape of the Fermi sheets in Ni is rather spherical, while in Fe their surfaces are non-trivially connected and reveal a complex structure. Like in Fig. (5.4), the side-jump contribution shows itself as isolated dots on the Fermi sheets and rapidly goes to zero everywhere else. Moreover, such dots are always distributed symmetrically in the Brillouin zone. In some cases, especially for Ni, regions in which σ^{sj} is of opposite sign are surprisingly close together and lead to large but mutually canceling contributions to the total side-jump conductivity. As the magnetization direction changes, the alteration of the Fermi sheets is very small and one cannot distinguish between the Fermi surface of Ni [001] and Ni [110] in Fig. (5.8). However, the distribution of the dots changes and with it the contribution of each Fermi sheet to the side-jump conductivity.

In order to illustrate the singular behavior of σ^{sj} , in Fig. (5.9) a finer color grading was chosen for some selected bands. Clearly the value of σ^{sj} is nearly constant at the flat areas of the Fermi sheets, but varies at their edges that occur whenever two or more Fermi sheets intersect each other. This might be a hint why the GGA+ U /LDA+ U approach has no great effect on the calculated value of σ^{sj} , because the Fermi surface is presumably modified at those positions in the Brillouin zone where the side-jump conductivity is small in any case.

Conclusions

This work¹ explains how a self-contained theory of the AHE can be derived that accounts for all the scattering independent contributions to the AHE conductivity. In previous works, solely the intrinsic contribution has been calculated and values for the side-jump contribution were available for simple model Hamiltonians only or were obtained indirectly by extrapolating to the zero disorder limit in disordered alloys. On the contrary, the new approach presented in this work allows for a direct calculation of the side-jump conductivity for the wide class of real materials which can be accessed via DFT.

By taking the side-jump contribution into account, this work shows that one succeeds in predicting a scattering independent part of the AHE conductivity which agrees with experiment to a level that has been unprecedented so far. For materials such as Fe, Co and FePt, σ^{sj} brings the calculated σ^{int} consistently nearer to the experimental value. Moreover, it could be demonstrated that the side-jump contribution shows a distinct anisotropy with respect to magnetization direction and shows itself as isolated dots on the Fermi sphere. This behavior is in sharp contrast to σ^{int} .

In practice, the AHE conductivity can be computed using the Wannier interpolation scheme, which makes the computation fast. Nevertheless, it turns out that a high number of \mathbf{k} points is needed to converge the value of σ^{sj} . The only input required is the electronic structure of the material which is to be investigated, and besides the Gaussian disorder model no assumptions about the scattering strength or impurity content have to be made.

In some materials, such as FePd, one fails to describe the side-jump contribution within the Gaussian disorder alone. In these cases, the deviations of the calculated values $\sigma^{\text{int}} + \sigma^{\text{sj}}$ from the experimental ones are larger. It would then be desirable to go beyond Gaussian disorder and apply a more realistic model of scattering processes, for example by taking scattering universality classes into account [73].

Especially in Ni, some of the disagreement between theory and experiment seems to be due to the lack of accuracy of common DFT functionals. However, adopting a GGA+ U /LDA+ U approach one obtains the correct AHE conductivity.

In summary, calculating the side-jump contribution provides valuable insights into the physics of the AHE. For future applications, the findings of this work might perhaps help to turn the AHE into a probing tool of complex electronic structures [74].

¹See also Ref. [74]

Appendix: Lattices

A.1 Internal coordinates

When performing a Brillouin-zone integration one usually does not want to bother about the concrete shape of the Brillouin-zone. It can be a rather complicated shape in general. It is therefore convenient to introduce the concept of internal coordinates. They are defined as follows:

$$\begin{aligned} \mathbf{r} &= A\mathbf{R}, \\ \mathbf{k} &= B\mathbf{K}. \end{aligned} \tag{A.1}$$

The matrix $A = (\mathbf{p}_1, \mathbf{p}_2, \mathbf{p}_3)$ contains the primitive translation vectors as columns. Due to

$$B^T = 2\pi A^{-1} \tag{A.2}$$

one can thus write:

$$\mathbf{k} \cdot \mathbf{r} = (B\mathbf{K})^T (A\mathbf{R}) = \mathbf{K}^T B^T A\mathbf{R} = 2\pi\mathbf{K} \cdot \mathbf{R} \tag{A.3}$$

A.2 Brillouin Zones

TABLE I: Position of neighbor \mathbf{k} -points and critical points in the Brillouin zone of the fcc lattice in units of $2\pi/a$.

n	x	y	z		x	y	z
1	-1	-1	-1	P			
2	1	-1	-1	Γ	0	0	0
3	-1	1	-1	X	1	0	0
4	1	1	-1	L	1/2	1/2	1/2
5	-1	-1	1	W	1/2	1	0
6	1	-1	1	K	3/4	3/4	0
7	-1	1	1	U	1	1/4	1/4
8	1	1	1				

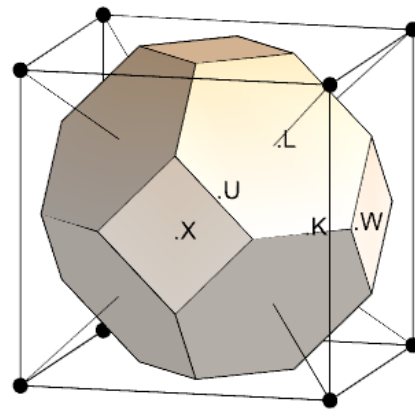


FIG. A.1: Brillouin zone of fcc lattice

TABLE II: Position of neighbor k-points and critical points in the Brillouin zone of the bcc lattice in units of $2\pi/a$.

n	x	y	z
1	-1	0	-1
2	1	0	-1
3	0	-1	-1
4	0	-1	1
5	-1	-1	0
6	-1	1	0
7	-1	0	1
8	1	0	1
9	0	1	-1
10	0	1	1
11	1	-1	0
12	1	1	0

P	x	y	z
Γ	0	0	0
H	0	1	0
N	1/2	1/2	0
P	1/2	1/2	1/2

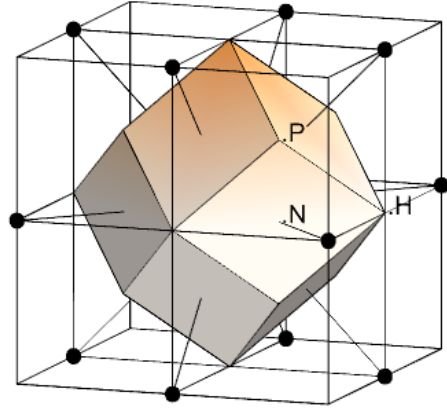


FIG. A.2: Brillouin zone of bcc lattice

TABLE III: Position of neighbor k-points and critical points in the Brillouin zone of the hcp lattice in units of $2\pi/(a\sqrt{3})$ (Basal and height parameters. Ideal: $c/a = \sqrt{8/3} \approx 1.633$).

n	x	y	z
1	$\sqrt{3}$	-1	0
2	$\sqrt{3}$	1	0
3	0	2	0
4	$-\sqrt{3}$	1	0
5	$-\sqrt{3}$	-1	0
6	0	-2	0
7	0	0	$\sqrt{3} \cdot a/c$
8	0	0	$-\sqrt{3} \cdot a/c$

P	x	y	z
Γ	0	0	0
A	0	0	$1/2 \cdot \sqrt{3} \cdot a/c$
H	$2/3 \cdot \sqrt{3}$	0	$1/2 \cdot \sqrt{3} \cdot a/c$
K	$2/3 \cdot \sqrt{3}$	0	0
L	$1/2 \cdot \sqrt{3}$	1/2	$1/2 \cdot \sqrt{3} \cdot a/c$
M	$1/2 \cdot \sqrt{3}$	1/2	0

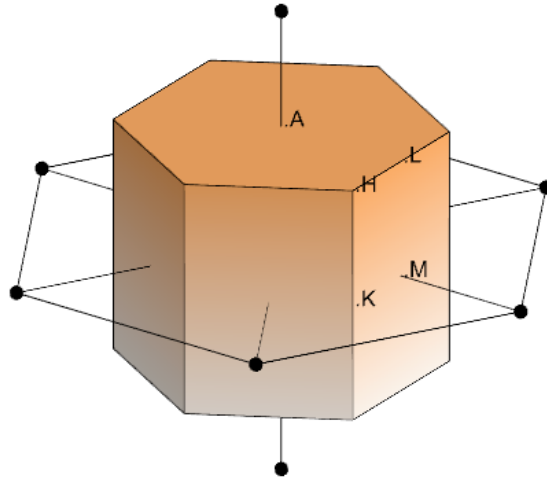


FIG. A.3: Brillouin zone of hcp lattice

Bibliography

- [1] E. Hall, *Philos. Mag. Series 5* **12**, 157 (1881).
- [2] E. M. Pugh, *Phys. Rev.* **36**, 1503 (1930).
- [3] E. M. Pugh and T. W. Lippert, *Phys. Rev.* **42**, 709 (1932).
- [4] I. A. Tsoukalas, *phys. stat. sol. (a)* **23**, K41 (1974).
- [5] N. Volkenshtein and G. Fedorov, *Soviet Phys. JETP* **11**, 48 (1960).
- [6] A. W. Smith and R. W. Sears, *Phys. Rev.* **34**, 1466 (1929).
- [7] R. Karplus and J. M. Luttinger, *Phys. Rev.* **95**, 1154 (1954).
- [8] J. Smit, *Physica* **21**, 877 (1955).
- [9] J. Smit, *Physica* **24**, 39 (1958).
- [10] J. M. Luttinger, *Phys. Rev.* **112**, 739 (1958).
- [11] L. Berger, *Phys. Rev. B* **2**, 4559 (1970).
- [12] E. Adams and E. Blount, *J. Phys. Chem. Solids* **10**, 286 (1959).
- [13] E. I. Blount, *Solid State Phys.* **13**, 305 (1962).
- [14] M. Onoda and N. Nagaosa, *J. Phys. Soc. Jpn.* **71**, 19 (2002).
- [15] Y. Yao, L. Kleinman, A. H. MacDonald, J. Sinova, T. Jungwirth, D.-s. Wang, E. Wang, and Q. Niu, *Phys. Rev. Lett.* **92**, 037204 (2004).
- [16] N. A. Sinitsyn, A. H. MacDonald, T. Jungwirth, V. K. Dugaev, and J. Sinova, *Phys. Rev. B* **75**, 045315 (2007).
- [17] A. A. Kovalev, J. Sinova, and Y. Tserkovnyak, *Phys. Rev. Lett.* **105**, 036601 (2010).
- [18] M. V. Berry, *Proc. R. Soc. Lond. A.* **392**, 45 (1984).
- [19] G. Sundaram and Q. Niu, *Phys. Rev. B* **59**, 14915 (1999).
- [20] N. A. Sinitsyn, *J. Phys.: Condens. Matter* **20**, 023201 (2008).
- [21] N. A. Sinitsyn, Q. Niu, and A. H. MacDonald, *Phys. Rev. B* **73**, 075318 (2006).
- [22] N. A. Sinitsyn, Q. Niu, J. Sinova, and K. Nomura, *Phys. Rev. B* **72**, 045346 (2005).
- [23] N. Nagaosa, J. Sinova, S. Onoda, A. H. MacDonald, and N. P. Ong, *Rev. Mod. Phys.* **82**, 1539 (2010).
- [24] N. Nagaosa, *J. Phys. Soc. Jpn.* **75**, 042001 (2006).
- [25] T. Jungwirth, Q. Niu, and A. H. MacDonald, *Phys. Rev. Lett.* **88**, 207208 (2002).
- [26] K. M. Seemann, Y. Mokrousov, A. Aziz, J. Miguel, F. Kronast, W. Kuch, M. G. Blamire, A. T. Hindmarch, B. J. Hickey, I. Souza, and C. H. Marrows, *Phys. Rev. Lett.* **104**, 076402 (2010).
- [27] C. Kooi, *Phys. Rev.* **95**, 843 (1954).
- [28] T. Miyasato, N. Abe, T. Fujii, A. Asamitsu, S. Onoda, Y. Onose, N. Nagaosa, and Y. Tokura, *Phys. Rev. Lett.* **99**, 086602 (2007).
- [29] W. Jellinghaus and M. P. de Andrés, *Ann. Physik* **462**, 149 (1961).
- [30] J. M. Lavine, *Phys. Rev.* **123**, 1273 (1961).
- [31] L. Ye, Y. Tian, D. Xiao, and X. Jin, *ArXiv e-prints* (2011), arXiv:1105.5664 [cond-mat.mtrl-sci].
- [32] P. Mavropoulos and N. Papanikolaou, *Computational Nanoscience: Do It Yourself!*, edited by J. Grotendorst, S. Blügel, and D. Marx, NIC serie, Vol. 31 (Forschungszentrum Jülich, 2006) pp. 131--158.
- [33] S. Lowitzer, D. Ködderitzsch, and H. Ebert, *Phys. Rev. Lett.* **105**, 266604 (2010).
- [34] P. N. Dheer, *Phys. Rev.* **156**, 637 (1967).

- [35] E. Roman, Y. Mokrousov, and I. Souza, *Phys. Rev. Lett.* **103**, 097203 (2009).
- [36] N. Volkenshtein, G. Fedorov, and V. Shirokovskii, *Phys. Met. Metall.* **11**, 151 (1961).
- [37] X. Wang, D. Vanderbilt, J. R. Yates, and I. Souza, *Phys. Rev. B* **76**, 195109 (2007).
- [38] J. Rammer and H. Smith, *Rev. Mod. Phys.* **58**, 323 (1986).
- [39] A. A. Kovalev, Y. Tserkovnyak, K. Výborný, and J. Sinova, *Phys. Rev. B* **79**, 195129 (2009).
- [40] S. Onoda, N. Sugimoto, and N. Nagaosa, *Prog. Theor. Phys.* **116**, 61 (2006).
- [41] S. Onoda, N. Sugimoto, and N. Nagaosa, *Phys. Rev. B* **77**, 165103 (2008).
- [42] H. Bruus and K. Flensberg, *Many-Body Quantum Theory in Condensed Matter Physics* (Oxford University Press, 2004).
- [43] A. L. Fetter and J. D. Walecka, *Quantum Theory of Many-Particle Systems* (McGraw-Hill, 1971).
- [44] G. D. Mahan, *Many-Particle Physics*, 3rd ed. (Kluwer Academic / Plenum Publishers, 2010).
- [45] W. Kohn and J. M. Luttinger, *Phys. Rev.* **108**, 590 (1957).
- [46] S. Doniach and E. H. Sondheimer, *Green's Functions for Solid State Physicists* (Imperial College Press, 1998).
- [47] A. Bastin, C. Lewiner, O. Betbeder-matibet, and P. Nozieres, *J. Phys. Chem. Solids* **32**, 1811 (1971).
- [48] P. Středa and L. Smrčka, *phys. stat. sol. (b)* **70**, 537 (1975).
- [49] P. Hohenberg and W. Kohn, *Phys. Rev.* **136**, B864 (1964).
- [50] G. Czycholl, *Theoretische Festkörperphysik* (Springer, 2008).
- [51] N. W. Ashcroft and D. N. Mermin, *Solid State Physics* (Saunders College Publishing, 1988).
- [52] S. Blügel and G. Bihlmayer, *Computational Nanoscience: Do It Yourself!*, edited by J. Groten-dorst, S. Blügel, and D. Marx, NIC serie, Vol. 31 (Forschungszentrum Jülich, 2006) pp. 85--129.
- [53] R. M. Martin, *Electronic Structure* (Cambridge University Press, 2010).
- [54] N. Marzari and D. Vanderbilt, *Phys. Rev. B* **56**, 12847 (1997).
- [55] I. Souza, N. Marzari, and D. Vanderbilt, *Phys. Rev. B* **65**, 035109 (2001).
- [56] A. A. Mostofi, J. R. Yates, Y.-S. Lee, I. Souza, D. Vanderbilt, and N. Marzari, *Comput. Phys. Comm.* **178**, 685 (2008).
- [57] F. Freimuth, Y. Mokrousov, D. Wortmann, S. Heinze, and S. Blügel, *Phys. Rev. B* **78**, 035120 (2008).
- [58] J. R. Yates, X. Wang, D. Vanderbilt, and I. Souza, *Phys. Rev. B* **75**, 195121 (2007).
- [59] X. Wang, J. R. Yates, I. Souza, and D. Vanderbilt, *Phys. Rev. B* **74**, 195118 (2006).
- [60] M. Chen, Z. Shi, W. J. Xu, X. X. Zhang, J. Du, and S. M. Zhou, *Appl. Phys. Lett.* **98** (2011).
- [61] I. Yang, S. Y. Savrasov, and G. Kotliar, *Phys. Rev. Lett.* **87**, 216405 (2001).
- [62] V. Iota, J. Klepeis, C. Yoo, J. Lang, D. Haskel, and G. Srajer, *Appl. Phys. Lett.* **90**, 042505 (2007).
- [63] E. Şaşıoğlu, A. Schindlmayr, C. Friedrich, F. Freimuth, and S. Blügel, *Phys. Rev. B* **81**, 054434 (2010).
- [64] V. I. Anisimov, F. Aryasetiawan, and A. I. Liechtenstein, *J. Phys.: Condens. Matter* **9**, 767 (1997).
- [65] A. I. Liechtenstein, V. I. Anisimov, and J. Zaanen, *Phys. Rev. B* **52**, R5467 (1995).
- [66] A. B. Shick, A. I. Liechtenstein, and W. E. Pickett, *Phys. Rev. B* **60**, 10763 (1999).
- [67] F. D. M. Haldane, *Phys. Rev. Lett.* **93**, 206602 (2004).
- [68] H. R. Fuh and G. Y. Guo, *ArXiv e-prints* (2011), arXiv:1107.3242 [cond-mat.str-el] .

- [69] H. Zhang, F. Freimuth, S. Blügel, Y. Mokrousov, and I. Souza, *Phys. Rev. Lett.* **106**, 117202 (2011).
- [70] Z. Fang, N. Nagaosa, K. S. Takahashi, A. Asamitsu, R. Mathieu, T. Ogasawara, H. Yamada, M. Kawasaki, Y. Tokura, and K. Terakura, *Science* **302**, 92 (2003).
- [71] W. Eberhardt and E. W. Plummer, *Phys. Rev. B* **21**, 3245 (1980).
- [72] F. Weling and J. Callaway, *Phys. Rev. B* **26**, 710 (1982).
- [73] S. A. Yang, H. Pan, Y. Yao, and Q. Niu, *Phys. Rev. B* **83**, 125122 (2011).
- [74] J. Weischenberg, F. Freimuth, J. Sinova, S. Blügel, and Y. Mokrousov, *Phys. Rev. Lett.* **107**, 106601 (2011).

Acknowledgements

I am especially thankful to my supervisor, Prof. Dr. Blügel, who has offered me the opportunity to write this thesis at his institute, and to Prof. Dr. Mokrousov, who kindly accepted to prepare the second opinion on my thesis and supported me wonderfully in any respect of my work.

I would also like to thank Dr. Frank Freimuth, for the fruitful discussions and his valuable insight into the subject. I am also indebted to the other members of the institute for their great helpfulness towards me right from the first day.

Lastly, I am also grateful for the support that I have received from my family during the course of my studies in Aachen and Jülich.

Selbstständigkeitserklärung

Ich versichere, dass ich die Arbeit selbstständig verfasst und keine anderen als die angegebenen Quellen und Hilfsmittel benutzt sowie Zitate kenntlich gemacht habe.

Jülich, November 2011

Jürgen Weischenberg